8-1-2013

Computational Biomechanical Modeling of the Human Knee During Kneeling

Tariq R. Abo-Alhol
University of Denver

COMPUTATIONAL BIOMECHANICAL MODELING OF THE HUMAN KNEE DURING KNEELING

A Dissertation

Presented to

The Faculty of Engineering and Computer Science

University of Denver

In Partial Fulfillment

of the Requirements for the Degree

Doctor of Philosophy

---

by

Tariq R Abo-Alhol

August 2013

Advisor: Peter J. Laz

Author: Tariq R. Abo-Alhol
Title: COMPUTATIONAL BIOMECHANICAL MODELING OF THE HUMAN KNEE DURING KNEELING
Advisor: Peter J. Laz
Degree date: August, 2013

Abstract

Total knee replacement benefits patients who suffer from severe knee pain or joint stiffness and other joint related illnesses that limit everyday activities. There has been an increase in the number of procedures performed each year and a need to evaluate the performance of these implants during specialized activities such as kneeling. Most computational studies lack insight into inter-patient variability and the results do not apply to large population. This study developed: (1) three-dimensional explicit finite element (FE) models to investigate natural and implanted knee joint kinematics and bone strain and (2) a platform to enable population-based evaluation by combining statistical model and joint function. Verification of a finite element model confirmed a strong agreement between model predicted and *in-vitro* kinematics of specimen-specific patellofemoral (PF) joints of four cadaveric knees in simulated kneeling. Three different commonly used PF implants were employed in an additional broader patellar bone strain study to assess the relative performance of these implants during highly demanding activities. This study predicted that the medialized dome design achieves the optimal balance of sufficient congruency between PF articular surfaces while still facilitating sagittal plane tilt to reduce isolated loading of the distal nose of the patella. A combined statistical shape model and FE method were utilized to successfully identify the most

important shape characteristics affecting joint performance during kneeling. Scaling in the knee joint has minimal effect on PF joint kinematics but greatly affects joint contact mechanics. Knee soft tissue dimensions alter the kinematics. The patellar bone strain model described here provides a novel platform for further implant performance analyses. The statistical shape-function model is a tool for population based studies to help predict the clinical outcome of joint replacement.

Acknowledgements

Completing of my doctoral degree was possible with the support of several people. First and foremost, I would like to give greatest thanks to my supervisor, Dr. Peter Laz, for his support, encouragement, expert advice, understanding, and coordination of my research. Thanks to Dr. Paul Rullkoetter for his unique and extensive knowledge in the fields of engineering and computational biomechanics. I owe a great deal of thanks to Dr. Clare Fitzpatrick, her insightful feedback and comments influenced my research tremendously. I would like, also, to express my gratitude to Dr. Yun Bo Yi, the member of my supervisory committee. I would like also to thank the Libyan Ministry of Higher Education and Scholarship Program for funding my PhD study.

I am thankful to work with a talented team of researchers at the Computational Biomechanics Lab, University of Denver; Milind Rao, James Deacy, Chadd Clary, Chandreshwar Rao, Azhar Ali, Lowell Smoger, Sean Smith, Chelsie Anker, Kevin Shelburne, and John Ivester. Special thanks to Renee Carvalho from the Engineering Office for her support with paper work. Thanks to Adam Cyr and Dr. Lorin Maletsky at the University of Kansas for providing the experimental data for the kneeling study. I most want to thank my wife Amal al Sherwi and my kids Raeef and Rawas for their love, enormous support and countless sacrifices to help me get to this point. This dissertation is dedicated to my parents; Ramadan and Anisa Abo-Alhol for their love, endless support and encouragement.

Table of Contents

List of Figures

List of Tables

Chapter 1. Introduction

1.1. Background

The patellofemoral joint is a crucial and very vulnerable joint in the human knee but it is insufficiently studied. It is known that patellofemoral joint is mechanically essential to achieve full functionality of the knee joint and little is known about the causes of anterior pain and patellar fracture. There have been several total knee replacement (TKR) studies that reported that the average occurrence of anterior knee pain was 12% (Helmy et al., 2008). Although more successful TKR surgical procedures have increased especially in the young and active, returning to normal activity has created a series of challenging decisions for orthopedic surgeons in the operating room. Advanced activities such as kneeling post TKR is an important goal of most patients in Japan, Asia, and the Middle East because of floor-sitting lifestyles (Hefzy et al., 1997, Park et al., 2007). In addition, kneeling has a significant positive association with achievement of patient expectations, restoration of a "normal" knee, and functional improvement after TKA (Devers et al., 2011). As a result of knee stance during kneeling, at least half of the body weight is concentrated on a small area, which increases contact pressures in patellofemoral joint.

There is limited information on patellofemoral (PF) kinematics after TKR for the upright kneeling position where PF contact pressures can be elevated relative other kneeling positions. Most TKR devices have been designed to better accommodate high knee flexion after surgery by introducing new tibiofemoral components. However, there is little known about the influence of the patellar component in knees involved in mechanically demanding activities such as kneeling. A number of studies have been devoted to determining how to improve high knee flexion and suggested a variety of new designs. However, there is concern about the trade-off between high flexion and post-TKR pain. New findings show potential sources of knee pain during kneeling include scar position (Nijs et al., 2006). The patellar bone contains numerous pain-sensing mechanoreceptors, and is a likely contributor to anterior knee pain. During kneeling, the ground reaction force on the tibial tuberosity and/or patellar bone causes a posterior shear force on the tibia and anterior compressive force on the patella (Goldstein et al., 2007; Incavo et al., 2004).

A few studies evaluated the outcome of patella resurfacing and suggested that patellofemoral design influences function following TKR (Andriacchi et al., 1997). Other studies showed that a high level of conformity of patellar with femoral components affects the patellofemoral joint's ability to allow natural movement (Rhoads et al., 1990; Stiehl et al., 2001). Shear stress at fixation sites increases because of the component's limited ability to reposition itself and this can lead to component failure or patellar fracture (Goldstein et al., 2007; Wulff et al., 2000). Prior TKR studies have reported bone

strains in resected patellae which are substantially higher than the natural knee (Fitzpatrick et al., 2011a; Lie et al., 2005; McLain et al., 1985; Reuben et al., 1991; Wulff & Incavo, 2000), with resected patellae being more vulnerable to fracture due to sagittal plane bending in deep flexion particularly in thinner patellae (Reuben et al., 1991).

In most bone strain experimental studies, a strain gage is limited to measuring bone strain in a localized area and does not fully capture the strain distribution in the entire bone. Computational models represent an efficient method for investigating these types of components in the TKR knee under the same conditions, but must be verified against experimental measurements to evaluate accuracy of model predictions. Subject-specific finite element models of the knee joint, including mapped material properties of the patellar bone, were developed for a series of specimens.

The main purpose of the current research was to perform a comparative evaluation of patellofemoral joint mechanics and patellar bone strain in multiple TKR designs and intact knee during kneeling. Many previous efforts to investigate factors affecting the pain and patellar fracture are limited by ignoring the effect of high compressive stresses during kneeling on the resected patellar bone after TKR. The current study is unique because it described a method that compares the effect of identical kneel loading conditions and material properties on the knee joint in three different TKR components and the intact knee.

1.2. Motivation

Kneeling is a knee function required for many patients' during their daily life, making its restoration following knee replacement essential. Increased attention has been given to the biomechanics of the knee joint during kneeling. However, almost none of the studies have looked at the effect of high compressive loads experienced during kneeling on the resurfaced patellar bone. Many TKR components have improved a patient's ability to perform activities of daily living. If the wrong components have been selected for patients who view kneeling as an important function, post-operative complications such as anterior patellar pain or fracture can arise due to prolonged and/or repetitive kneeling.

Two research objectives were determined to achieve the above purpose: (1) evaluate the patellofemoral mechanics of the natural and implanted knee during kneeling activity, and (2) develop a statistical shape and alignment model approach to describe the inter-subject variability in bone morphology and alignment for the structures of the knee, to demonstrate the statistical model's ability to describe variability in a training set and to generate realistic instances for use in FE evaluation of joint mechanics.

1.3. Organization

The following four chapters report the steps to address each of these objectives. Chapter two provides an overview of the current literature on knee anatomy, kneeling,

and FE computational and experimental models. Chapter three presents computational method and materials. Chapter four will cover the first study of patellar bone strain in the natural and implanted knee during kneeling. Chapter five describes, in detail, an experimentally verified kneeling model developed to examine the effect of component design on patellar mechanics during kneeling. Chapter six presents the statistical shape and alignment model to characterize the inter-subject variability in bone morphology and alignment for the structures of the knee. The final chapter contains a summary of the work and a number of recommendations for future research.

Chapter 2. Literature Review

The aim of this chapter is to present an overview on the important aspects of knee patellofemoral joint mechanics, total knee replacement, computational modeling with a focus on finite element analysis and previously published experimental models of the knee during high flexion activity such as kneeling.

2.1. Review of Human Knee

The number of TKR surgeries has increased rapidly in recent years. The estimated demand for primary total knee replacement is expected to grow by 673% to 3.48 million procedures in the United States by the year 2030 (Kurtz et al., 2007; Palastanga et al., 2006). In order to understand the knee and TKR it is essential to review the anatomy and kinematics of the knee joint.

2.1.1. Bones

There are three bones in the knee; femur, tibia and patella. Mechanically, the knee consists of three separate joints: two between the femur and tibia (medial condyle and

lateral condyle) and one between the femur and the patella. There are two separate articulations: the tibiofemoral (TF) joint and the patellofemoral (PF) joint (Figure 2.1). The TF is the main load bearing joint that allows flexion and extension. The PF joint is where the patella and femur meet. The joint acts as a lever that transmits the force of the quadriceps muscle to the lower leg.

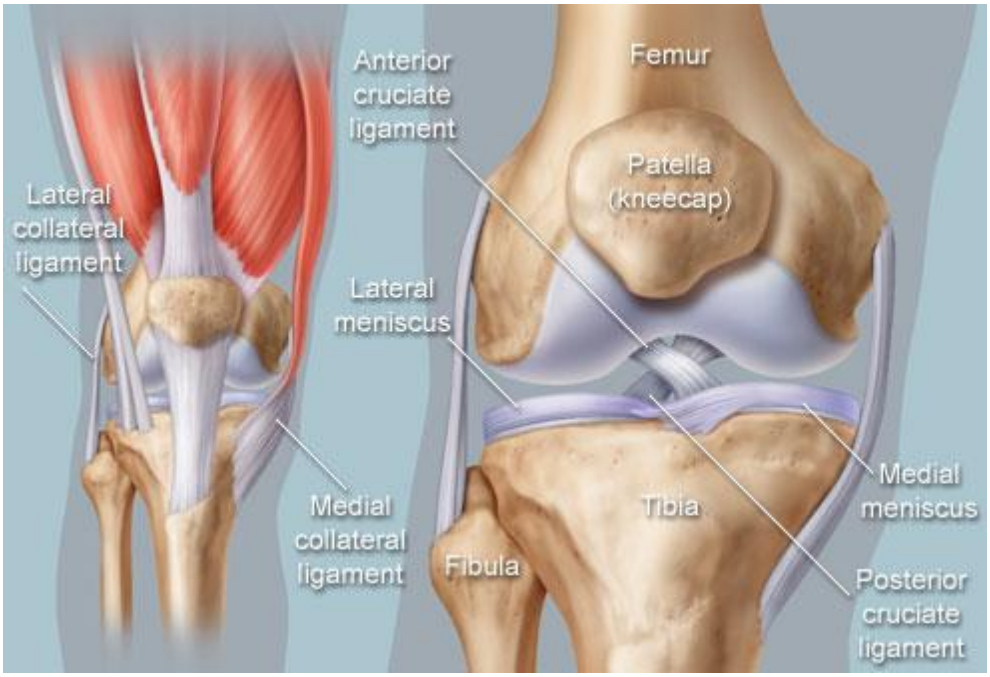

Figure 2.1 Front view of knee anatomy (webmd.com, with permission 2013)

2.1.2. Articular Cartilages

The articular surfaces of the bones are covered by articular cartilages, which protect the ends of the bone and help to distribute the large vertical forces. Their organized structure provides the biomechanical properties required for the tissue to bear

multiple forces due to movement (Palastanga et al., 2006). In the human knee, the articular surfaces are femoral medial and lateral condyles conforming to the articular surface of proximal tibia that also form two condyles, medial and lateral (Figure 2.2). Between the femoral condyles is the sulcus groove, which contacts the patellar cartilage during motion. The patella has a large lateral facet and a smaller medial facet separated by a vertical ridge. Articular cartilages, with their congruency between bones, help better distribute the weight across the joint, reduce friction and achieve a locking mechanism between bones.

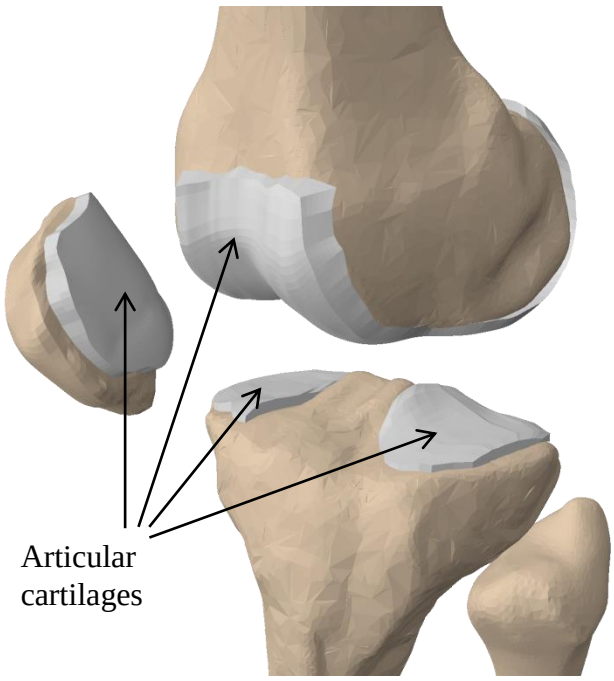

Figure 2.2 Articulating surfaces

2.1.3. Ligaments and Tendons

Ligaments are short fibrous bands of tough, flexible connective tissues that connect bone and or cartilage to hold a joint together. Four important ligaments are shown in Figure 2.3. The medial collateral ligament (MCL) and lateral collateral ligament (LCL) provide restraint to valgus and varus angulations of the knee, respectively. The anterior cruciate ligament (ACL) and posterior cruciate ligament (PCL) prevent hyperextension and hyperflexion of the knee, respectively. These and other ligaments keep the femur and tibia in alignment and in contact. The patellar tendon connects the patella to the quadriceps muscles and tibia. Quadriceps tendons and hamstring tendons are the main tendon groups anterior and posterior, respectively, of the femur. The knee joint extends (straightens) when the quadriceps muscles contract and flexes (bends) when the hamstring muscles contract. Different movements of the knee are visually represented in Figure 2.5.

The quadriceps muscles are very important to the patellofemoral joint. This group of muscles has four main tendons; rectus femoris, vastus medialis, vastus intermedius and vastus lateralis. Figure 2.3 shows how the tendons and ligaments play central role in providing joint stability and kinematics and load transmission. Patellofemoral Joint In normal and pain-free knee, the patella acts as a fulcrum to increase the mechanical efficiency of the knee extensor mechanism by increases the moment arm of the

quadriceps muscle. It also unifies the different forces of the quadriceps muscle and transmits the tension around the femur to the patellar ligaments.

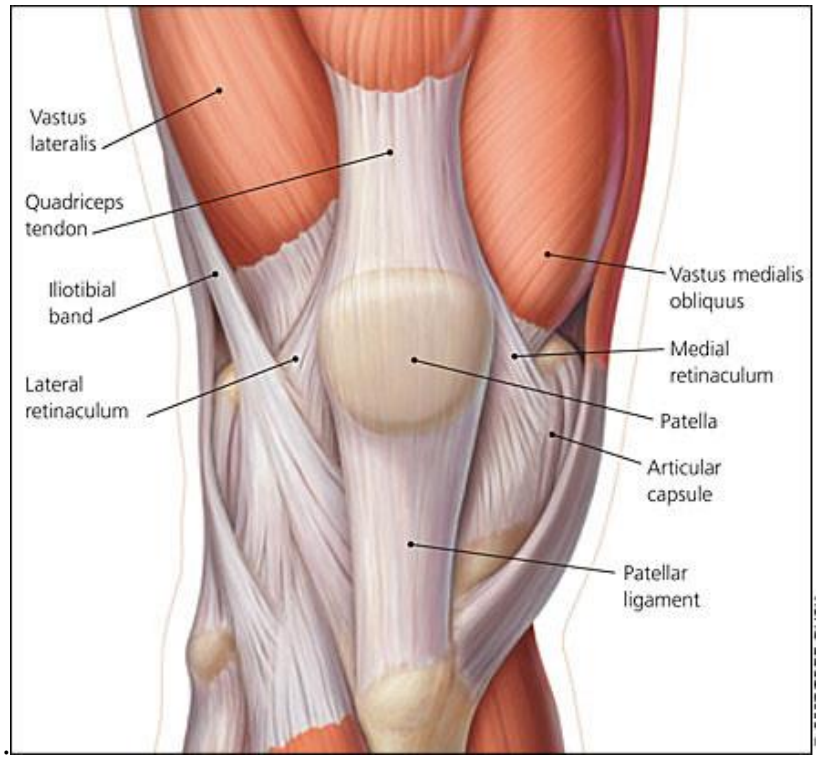

Figure 2.3 Diagram of the patellofemoral joint representing ligaments and tendons of human knee (www.aafp.org)

2.1.4. Contact Mechanics

The posterior surface of the patella is covered by articular cartilage that has medial and lateral facets divided by a vertical ridge. In full extension, the patellar cartilage sits on the femoral sulcus of the anterior region of the distal femur and only the distal part of the patella is in contact with the femur. As tibiofemoral flexion progresses, PF contact shifts superiorly to the posterior facet of the patella, and then moves outward

(away from the vertical ridge) toward the edge of the medial and lateral facets in higher flexion angles (Figure 2.4).

2.2. Total Knee Replacement

The goal of all total knee replacements is to restore, as much as possible, normal musculoskeletal function of the knee. Total knee replacement is a common surgical procedure to eliminate joint pain by replacing damaged cartilage and bony surfaces with prosthetic components. Damage could be due to osteoarthritis or rheumatoid arthritis or injury that prevents the patient from performing simple activities, such as walking or climbing stairs. The procedure consists of opening the joint through an incision on the medial side of the knee and performing bone cuts on the distal femoral, proximal tibial and posterior patellar bony surfaces (Figure 2.6).

Figure 2.4 Diagram showing a healthy (right), diseased (center) and implanted (left) knees (depuy.com)

2.2.1. Total Knee Replacement Designs

Although designs of TKR implants vary, the total knee replacement includes three components. The large majority of TKRs used today consist of the following components: femoral, tibial and patellar. The femoral component is made of cobalt-chrome alloy with an anatomical curve placed on the distal of the femur. The tibial component is a flat cobalt-chrome alloy or titanium alloy platform with a polyethylene insert. Finally, the patellar component is a very small piece of polyethylene fixed on the posterior aspect of resected patellar bone.

Different types of TKA designs may be used depending on surgeon judgment or patient requirements. In most cases, however, there are two main groups; designs that retain the posterior cruciate ligament (PCL) and those in which the ligament is routinely sacrificed (posterior stabilized). Walker et al. (2005) described many design factors which must be considered to achieve goals of the knee replacement; relieve pain, restore function, be able bear contact stresses and wear, tolerate variable loading conditions, and insensitive to misalignment.

2.2.2. Patellar Implant Design

Based on the patient's PF joint condition, surgeons may choose to resurface posterior part of the patellar bone including the articular cartilage and replace it with the

patellar component. Patellar component designs vary and play an essential role in TKR outcomes. In previous work Innocenti et al. (2009) and Stiehl et al. (2001) reported that patellar tracking, contact area, and pressure distribution are significantly different between native and prosthetic knees and also vary across subjects (Fitzpatrick et al., 2011a). Range of motion (ROM), fixation, stability, dimensions, are contact mechanics are the main mechanical factors considered in deciding what PF joint design should be used (Brick et al., 1988; Stiehl et al., 2001). Three patellar implant designs are commonly used; a central dome, offset (medialized) dome, or anatomically-shaped patellar components. In a study of 12,464 TKRs by Ortiguera et al. (2002), it was reported that in 85 patellar fractures, the prevalence is greater in resurfaced than in unresurfaced patellae. The study found that predominate causes for patellar fracture include; trauma, implant malalignment, excessive patellar bone resection, high activity level, large ROM of motion, patellar design.

2.2.3. Patellar Bone Strain

Previous studies have measured bone strain in the patella to predict the likelihood of patellar fracture. In these experimental cadaveric studies, anterior surface strain was measured using a uniaxial strain gage (Hofmann et al., 1997; Lie et al., 2005; Rand et al., 1996; Reuben et al., 1991; Wulff & Incavo, 2000). A strain gage measurement is limited to one direction and measures a localized bone strain and does not describe the strain distribution throughout the bone volume. Finite element models have been used to

compare patellar mechanics in natural, implanted and natural conditions (Fitzpatrick et al., 2011a). The study evaluated highly strained volume (HSV) for the whole patellar bone. The study predicted that a significant increase in HSV was noted in the implanted case compared to the natural, with differences in the location of the most highly strained bone and peak strain in different flexion angles.

One of important aspects of TKR procedures is to reproduce a physiologic patella thickness. Thicknesses that exceed preoperative values could lead to an overstuffed PF joint and complications such as increased shear stresses or anterior patellar strain (Ghosh et al., 2009; Star et al., 1996). On the other hand, excessive resection of the patella leads to weakening of the patella, making it more likely to fracture (Reuben et al., 1991). A recent finite element study used three cadaveric male knees with patellar bone resected to thicknesses which varied from 9 to 14mm, in different flexion angles (10 -100^{o}), during a dynamic squat cycle (Fitzpatrick et al., 2013). The analysis predicted that highest peak bone strain noted in the thinnest patellae which indicated of greatest risk of patellar fracture.

2.2.4. Patellofemoral Kinematics

The knee has a 12 degree of freedom system, with 3 translations and 3 rotations for both the TF joint and PF joint, Figure 2.5. As the TF joint flexes, the patella also rotates, and this rotation is called PFJ flexion or FE rotation.

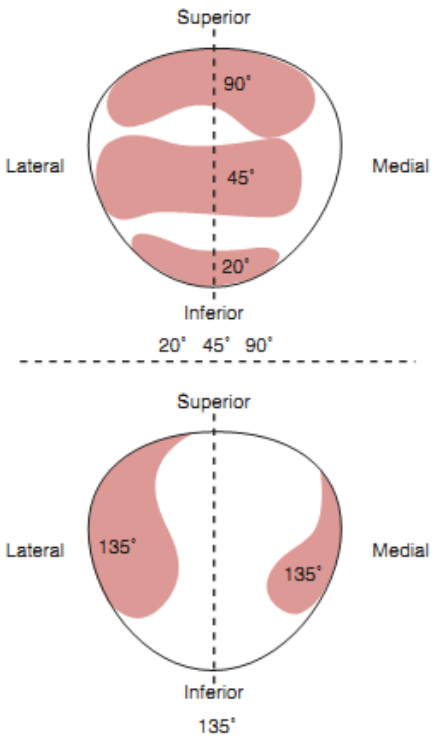

Figure 2.5 Patellofemoral contact mechanics change during knee flexion (Snyder-Macker L. et al., 2005, with permission 2013).

Rotation about the longitudinal axis is patellar tilt or IE rotation, and patellar rotation about an anteroposterior axis with respect to femur is termed patellar spin or VV. The patella glides superiorly and inferiorly with knee extension and flexion, respectively. During knee flexion-extension, medial-lateral translation of the patella also occurs and is known as patellar shift. Restriction of the patella to motion or excessive motion may lead to PF joint instability and pain.

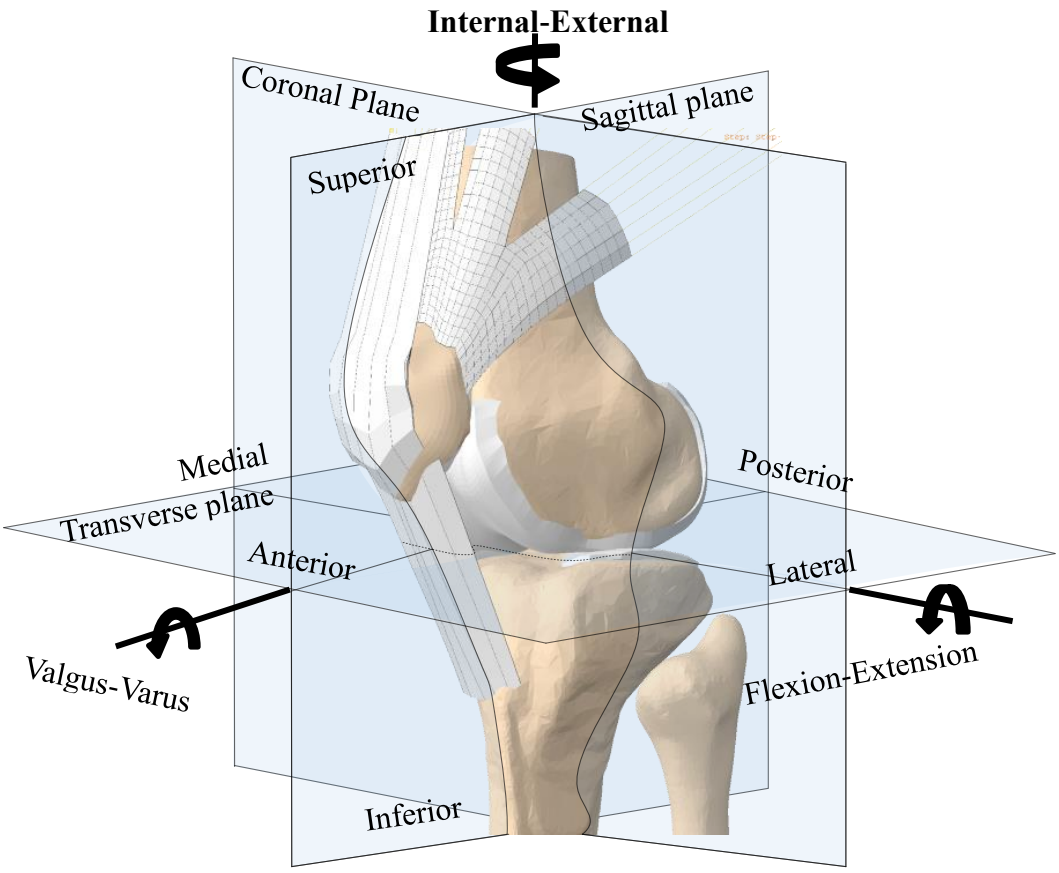

Figure 2.6 Six Degrees of Motion Present in Human Knee

2.3. High Flexion Activities

Although there have been technological advancements in total knee replacement surgery, patients still report experiencing limitations with TKA during highly demanding activities that require higher degrees of knee flexion such as squatting and kneeling (Weiss et al., 2002). Knee joint loading conditions increase with increased flexion angles (Barink et al., 2008; Conditt et al., 2004; Morra et al., 2005; Nagura et al., 2005). Conditt et al., 2004 found worse functional scores on squatting, kneeling, and gardening in patients with TKA (PS) knees. Another study by Noble et al. (2005) compared 243 TKR patient's ability to do many routine activities with 257 healthy individuals with no previous history of knee disorders (age- and gender-matched) found a substantial deficit remains in meeting the challenges of many functional tasks that are important to the patient, especially tasks involving kneeling or squatting.

2.3.1. Kneeling

Although patients undergoing total knee replacements generally have significant relief and improvement in function and quality of life, however, there is up to 20% complain of persisting pain (Al-Hadithy et al., 2012). Park et al. (2007) found that Korean patients who received TKR rated kneeling activities as the most difficult but older patients consider this activity less important than mobility and other basic

functions. For many patients, kneeling ability has a great effect on their satisfaction (Baker et al., 2007; Sharkey et al., 2011; Wilkens et al., 2007).

In another study on 367 patients after one year of TKR surgery, they were asked what activities were important to them; they reported that 58% of patients think that kneeling is an important activity after TKR (Weiss et al., 2002). According to the same study, follow-up of 176 TKR patients, 40% men and 60% women show that the activities most important to the patients were stretching exercises (56%), kneeling (52%), and gardening (50%). Unfortunately, patients with TKR still find squatting (75%), kneeling (72%), and gardening (54%) as the most difficult activities. In a study comparing TKR patients with age-matched and sex-matched subjects without knee disorders, Noble et al. (2005) found that control subjects had significantly higher knee function scores in a variety of activities including kneeling. They found that control subjects were approximately one third more likely to kneel and/or squat and were 4 times more likely to be symptom-free while doing so compared to TKR patients.

2.3.2. Patient Perception

In many cases, patients avoid kneeling for the fear of harming the prosthesis, scar position and skin hypoaesthesia or uncertainties about recommendations on kneeling are the main reasons that prohibit ability to kneel (Hamai et al., 2008; Hassaballa et al., 2004; Hassaballa et al., 2003; Incavo et al., 2004; Schai et al., 1999). A clinical study by Schai

et al. (1999) showed that 70 patients with 100 TKR, 44 % were able kneel easily, and 14% were unable to kneel. Scar pain and back related problems seemed to be major factors in limiting the kneeling ability. In a study of the change in skin sensation following TKR using three different incision types 72 patients, Hassaballa et al. (2012) suggested that the inability to kneel following knee arthroplasty is associated with increased area of hypersensitivity of the anterior knee. Hassaballa et al. (2004) reported that there is a clear difference between patients' perceived and actual ability to kneel. Only 37% of their 122 patients could kneel, whereas 81% were actually able to kneel. A study carried out by Palmer et al. (2002) investigated the ability to kneel after TKR. They found out that differences between the perceived and actual ability to kneel were noted. In 54 out of 100 knees patients avoided kneeling because of uncertainties or recommendations from third parties (doctors, nursing staff, friends, etc). However, a total of 64 patients were actually able to kneel and 12 of the remainder were unable to kneel because of problems which were not related to the knee. 24 patients were unable to kneel because of discomfort in the knee. It does not appear to be related to the presence of patellar resurfacing, the range of movement or the functional knee score.

2.3.3. TKR with Cruciate-Retaining and Posterior-Substituting Designs

A study by Kanekasu et al. (2004) used fluoroscopic analysis to study knee kinematics in a posterior-stabilized (PS) fixed-bearing TKA during deep flexion kneeling with the foot free to rotate. Kanekasu et al. reported a 2-phase femoral condylar

translation—posterior translation to 120° flexion and then anterior translation beyond 120° flexion with and average tibial internal rotation of 9°. Similar tibial rotation in fixed and rotating bearing TKA designs are reported by Dennis et al. (2005).

Contact mechanics are another important area in which a number of studies have reported variances between the two tibiofemoral designs during kneeling activity. Incavo et al. (2004) studied the tibiofemoral contact position of TKR components during kneeling *in-vivo*. Ten posterior-stabilized and ten cruciate-retaining (CR) designs were examined using radiography. During kneeling, both CR and PS TKR designs demonstrated function within intended design parameters with femoral posterior translation (rollback) occurring from 90° of knee flexion to deep flexion. The study suggested that neither subluxation of the CR design nor dislocation of the standard PS design appeared likely to occur. Another radiographic study of kneeling from 90 to 120^{o} of knee flexion after TKR using PS and CR designs, Hamai et al. (2008) found that the PS design has contact regions located far posterior on the tibial insert in comparison to the CR TKR and suggested that PS TKR may be preferable to CR TKR to reduce forces across the patellofemoral articulation.

An *in-vitro* study of on kneeling by Wilkens et al. (2007) showed that at a higher flexion angle (135^{o}) after TKR has a smaller effect on patellofemoral contact area and pressure than kneeling at lower flexion angles. Hanson et al. (2007) studied kneeling on 16 South Korean female patients and were imaged using a dual fluoroscopy while they

kneeled from initial to maximum flexion after (PS) TKR they found out that kneeling may be performed by patients after clinically successful (PS) TKR who feel comfortable with the activity and are free of pain. Contact area and contact pressure during kneeling was studied by Hofer et al. (2011) on two implant groups (CR) and (PS) that used five cadaveric knees and showed increased pressures when moving from double- to single-stance kneeling in the cruciate-retaining group but decreased pressures in the posterior-stabilized group. Kneeling activity, nonetheless, showed an increased contact areas and pressures in both designs.

In PS designs incorporated with cam-spine mechanisms, the cam-spine prevents the anterior translation and is thereby susceptible to breakage and damage due to the anterior forces it must withstand during 90° kneeling (Huang et al., 2006; Nagura et al., 2005). A study by Hassaballa et al. (2002) examined the physical characteristics and symptoms related to kneeling in a normal population. They found that the average percentage of body weight transmitted to the anterior aspect of the knee was (97%) at 90^{o} of flexion and 51% at full flexion. They suggested that improvements in the range of motion after arthroplasty may reduce the forces through the knee while kneeling. Unlike other deep flexion activities, the ground reaction force on the tibial tuberosity during kneeling causes a posterior shear force on the tibia and anterior compressive force on the patella (Hamai et al., 2008; Incavo et al., 2004).

2.3.4. Patellar Fracture

Patellofemoral complications remain to form a large percentage (up to 50%) of total knee replacement complications (Brick & Scott, 1988). Although patellar fracture is uncommon, however, previous observations showed that rate of occurrence increases after TKR from 0.05% in unresurfaced patella to 0.5% -5.2% following patellar resurfacing (Brick & Scott, 1988; Goldberg et al., 1988; Grace et al., 1988; Le et al., 1999; Ortiguera & Berry, 2002; Ritter et al., 1999; Tria Jr. et al., 1994).

Younger people tend to be more active but a recent analysis of 21,723 cases of patellar fracture by Singh et al. (2013) show that younger patients (less than 60 years) were associated with a higher risk of postoperative periprosthetic fractures following primary TKR. On the other hand, patients who were 61 years and older old had a 50% lower risk of periprosthetic fracture. Another study by Meding et al. (2008) investigated on patient and surgeon factors in 5640 patients (8530 total knee replacements) between 1983 and 2003, who received the same posterior cruciate ligament retaining knee prosthesis with all-polyethylene patellar implant. Failure occurred in 4.8% (409 knees) of total knee replacements because of loosening, 5.2% (444 knees) because of patellar fracture and 0.3% (25 knees) because of revision. Surgical technique is another primary factor affecting postoperative patellar alignment and tracking. Among the operation factors was the patellar resection angle (Fukagawa et al., 2011).

2.4. Finite Element Analysis

Two major methods have been used to evaluate the kinematics of both the intact and implanted knee in high flexion activates such as kneeling; *In-vivo* analyses (Coughlin et al., 2007; Hamai et al., 2008; Hanson et al., 2007; Incavo et al., 2004; Kanekasu et al., 2004; Nakamura et al., 2009) and *In-vitro* cadaveric biomechanical evaluation (Hofer et al., 2011; Ismaily et al., 2006; G. Li et al., 2004; Thambyah et al., 2005; Wilkens et al., 2007). Although in-vitro analysis can reproduce loading and boundary conditions with a certain degree of accuracy that cannot be done in-vivo, it might not be sufficient to answer many specific questions.

Finite element analysis has been used extensively in evaluating and predicting the mechanical behavior of the bone and implants. Many studies have used FE analysis as a comparative tool, examining the relative changes in mechanical parameters between implant designs and/or implanted and intact subjects. Explicit dynamic finite element analyses have been used to create dynamic models to efficiently determine tibiofemoral joint contact mechanics directly during dynamic loading conditions (Godest et al., 2002; Halloran et al., 2005b; Halloran et al., 2005a). Also, tibiofemoral joint kinematics of these models during gait simulations were verified with direct comparison with experimental data from knee simulators.

Specimen -specific and experimentally validated explicit FE analyses have been used to determine bone strain distributions in the hip, femur (Laz et al., 2007; Schileo et al., 2008; Taddei et al., 2006), tibia (Perillo-Marcone et al., 2007), and patella (Fitzpatrick et al., 2011a; Fitzpatrick et al., 2013) and have been used to assess fracture risk, and predict bone stress and strain at fixation sites as a function of material properties.

Chapter 3. Computational Modeling of Human Knee during Kneeling

3.1. Introduction

Many patients have difficulties performing advanced activates of daily living, such as kneeling on the floor. In order to protect the knees in such posture, there should be enough understanding of what the internal knee structures experience during kneeling. A FE model was developed to quantify the mechanical response (stresses and strains) and the knee structure motions (kinematic) in a dynamic kneeling simulation. The robustness of any finite element analysis is considerably dependent on input parameters such as material properties, loading and constraints applied to the problem. Therefore, a three dimensional explicit finite element model was created and validated through specimen-specific comparison with experimental PF kinematic data and used to study the effects of kneeling activity on knee joint mechanics and patellar bone strain distributions in intact and implanted across multiple specimens.

3.2. Modeling Subject-Specific Finite Element Model for The Knee Joint

Subject-specific FE models produced from imaging data can provide practical representation of anatomical structures and have been used to evaluate healthy and pathologic knee mechanics (Baldwin et al., 2010; Pena et al., 2006). The human knee joint is made up of many components (bones, cartilages, ligaments, and tendons) and are able to tolerate and transfer multiple loading conditions in many daily life activities.

3.2.1. Geometry Segmentation

A complete representation of the knee structure, including femur, patellar, tibia, cartilage and ligaments were extracted from magnetic resonance (MR) images by manually segmenting (ScanIP, Simpleware, Exeter, UK) and meshing the structures of interest for each specimen, Figure 3.1. Femur, patella, tibia and fibula surfaces were meshed with triangular elements using Hypermesh 11.0 (Altair Inc., Troy, MI). Except for the patella, all bones were modeled using shell elements and defined as a rigid body.

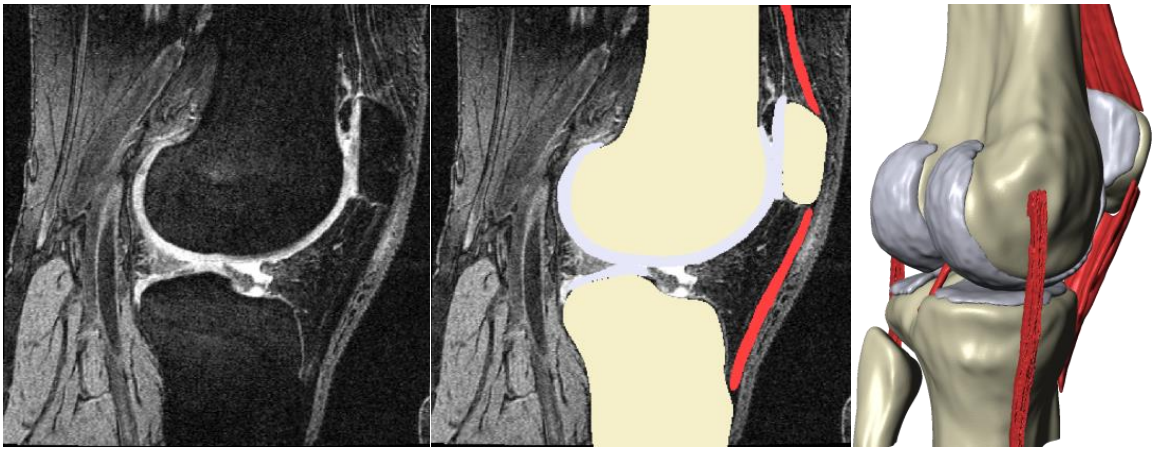

Figure 3.1Geometry segmentation process; (a) sagittal MRI scan of human knee, (b) bone, cartilage, and soft tissue manually segmented, (c) knee joint extracted in 3-D representation

For the bone strain study, the patellar bone geometry was extracted from computed tomography (CT) data to quantify differences in bone strain distributions in the natural and implanted knees. This will be discussed in Chapter 4.

3.2.2. Articular Cartilages and Mesh Morphing

All articular surfaces were initially extracted by manual segmentation and reconstructed into 3D stereolithography (STL) models. The study utilized integrated extraction and mesh morphing technique that previously developed and described by Baldwin et al. (2010).

Tool Command Language (tcl) custom-scripted code was used to define each cartilage surface as a series of corresponding points or handles, including 1200 femoral,

504 tibial and 390 patellar points. These surface handles were used to automatically morph standard template meshes for each cartilage volume to specimen-specific meshes, Figure 3.2. Fully deformable eight-noded (hexahedral) linear isoparametric solid meshes with average element edge length of 1.0 mm were created similar to a model developed by Fitzpatrick et al. (2011b). Minimizing difference in element size will improves model accuracy (Keyak et al., 1992).

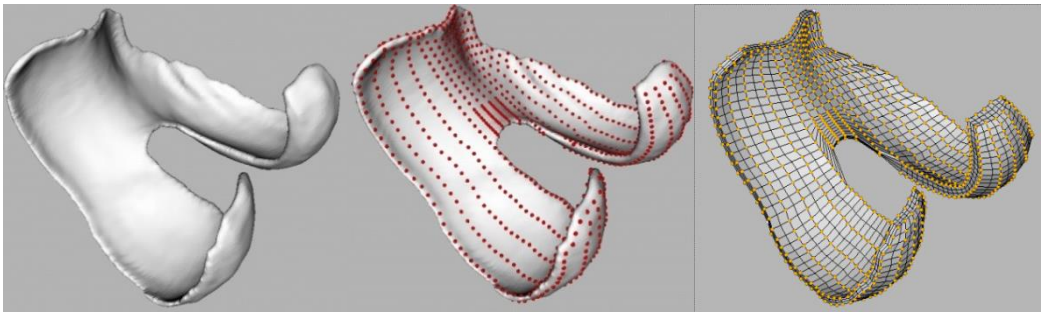

(a) (b) (c)

(d)

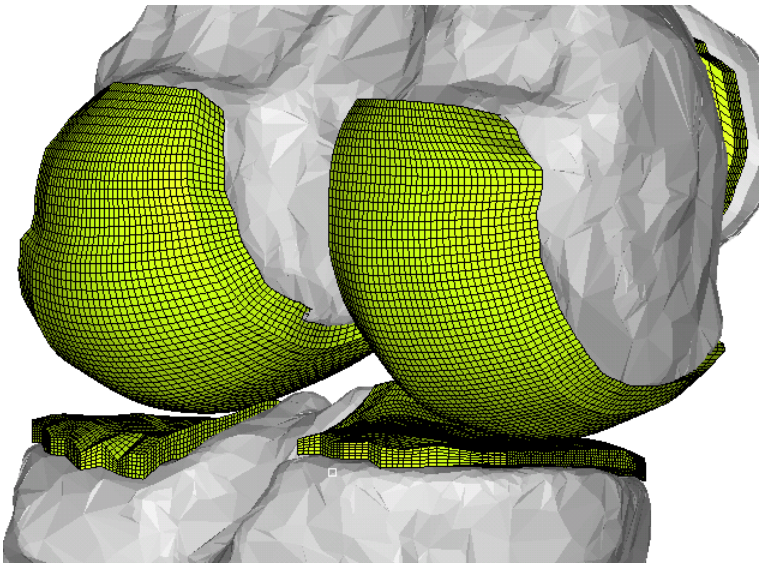

Figure 3.2 Specimen-specific segmented surfaces (a), corresponding points on cartilage surfaces (b) hexahedral mesh of femoral cartilage(c), articular surfaces developed (d).

To avoid unnecessary computational time, the material property of cartilage element was simplified for modeling from matrix and transversely isotropic fibers for three zones of cartilage (superficial, transitional and deep) to linear isotropic material with elastic modulus and Poisson's ratio of the cartilage were 12.0 MPa (MegaPascal, $N.mm^{-2}$) and 0.42, respectively (Hayes et al., 1978; W. Li et al., 2008). This assumption saved computation time 3 fold compared to modeling with anisotropic material properties and did not affect articular surface contact area or pressure measurements for multiple loading conditions ($P>.05$). Frictionless contact between articular geometries was defined by a literature-based pressure-overclosure relationship (Blankevoort et al., 1996).

3.2.3. Ligament and Soft Tissue Representations

The motion of the knee joint depends on the ligaments and other supportive soft tissue mechanical properties and anatomical constraints of the articular surfaces. In this study, the focus was on the patellofemoral joint mechanics and patellar bone strain during kneeling. It was important to locate ligament attachments sites, determine their dimensions, and to accurately reproduce mechanical responses for the primary load bearing structures crossing the joint as well as verifying the selected ligament. This study adopted similar soft tissues representations of two-dimensional (2-D) specimen-specific ligamentous constraint model developed by Baldwin, et al. (2009) and validated by comparing the kinematics from the FE model to the experimental six degree of freedom kinematic data from knee cadaver specimens tested using a knee simulator.

The fiber-reinforced (membrane with spring reinforcement) composite material model consisted of non-linear, tension only springs embedded in a low-modulus, hyper-elastic deformable 2D quadrilateral mesh (Figure 3.3). It was used to represent soft tissue structures of the extensor mechanism including rectus femoris (RF) and vasti tendons and patellar ligaments, with uniaxial tension characteristics matching literature values (Andriacchi et al., 1997; Stäubli et al., 1999).

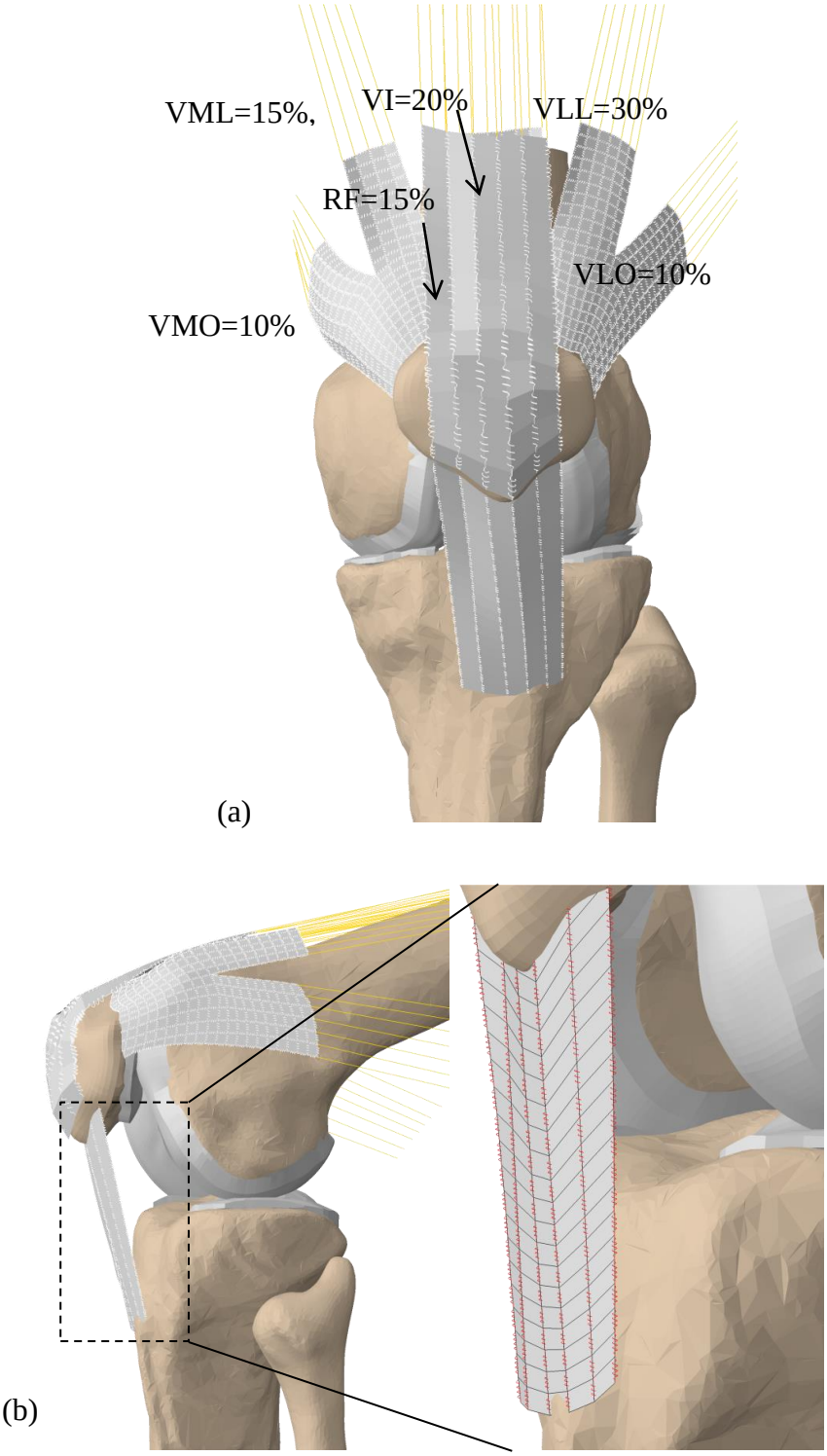

Figure 3.3 (a) Patellar ligament, rectus femoris, and vasti tendons of the extensor mechanism with quadriceps load distribution percentages (Atkinson et al., 1997; Baldwin et al., 2010; Stäubli et al., 1999) (b) 2-D fiber-reinforced patella ligament

Table 3.1 Spring elements representing ligaments and tendons

Spring element	Number of elements	Number of springs
Patellar ligament	100	120
Rectus femoris	120	144
Vasti	600	600 axial, 600 transverse

The distal and proximal ends of the patellar ligament mesh were rigidly constrained at the tibial tubercle and anteroinferior patellar edge, respectively. Rectus femoris tendon and the vasti tendon meshes were rigidly attached to the medial, lateral, and superior edges of the patellar bone. The proximal ends of the vasti split into five sections: the lateralis longus (VLL), lateralis obliquus (VLO), intermedius (VI), medialis longus (VML), and medialis obliquus (VMO) (Figure 3.3). The quadriceps load distribution was based on physiological cross-sectional area and orientations described in the literature (Farahmand et al., 1998).

3.3. Implant Representation

Different types of femoral, patellar, tibial high-flexion knee prostheses have been used in this study. However, the study focused on two designs of posterior stabilizer with fixed bearing implants. Three styles of patellar component: a dome-shaped patellar button with contemporary designs (Figure 3.4). The polyethylene patellar button and tibial insert were represented by linear isotropic hexahedral elements with an average edge length of 1.0 mm, and 1.5 mm, respectively. The femoral component was represented by linear 4-noded tetrahedral elements. Because of the greater stiffness of bone and CoCr relative to

polyethylene, the bone and the femoral components were modeled as rigid, and the patellar components were modeled as fully deformable. The patellar and tibial components were assumed linear elastic material with Young's Modulus and Poisson ratio as described in Table 3.2.

The contact mechanics between implanted component was based on previously defined and verified as rigid-deformable with pressure-overclosure relationship (Halloran et al., 2005b). A coefficient of friction of 0.04 was applied at the articular surface interfaces (Godest et al., 2002; Halloran et al., 2005b).

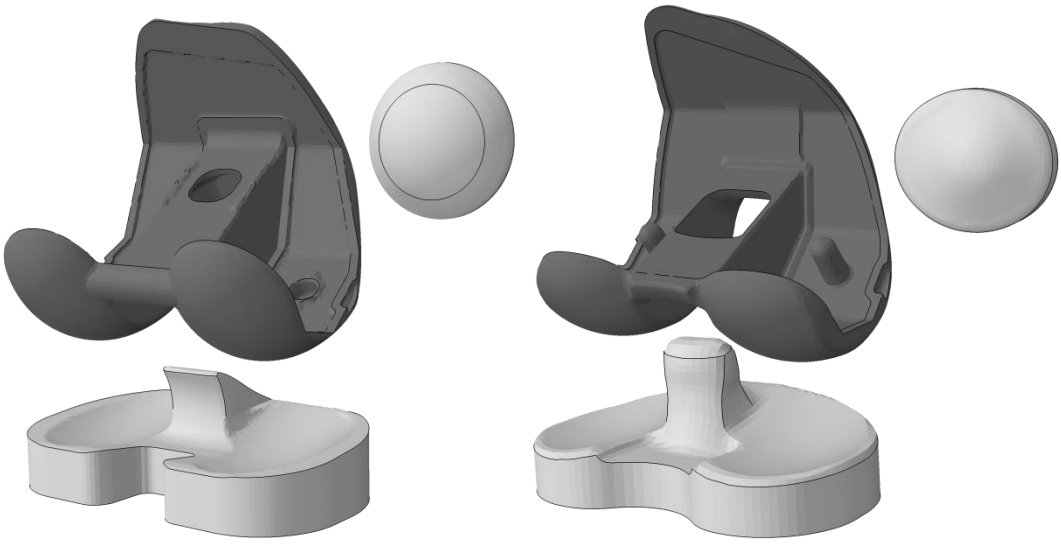

Figure 3.4 Designs of posterior-stabilized fixed-bearing implants with different patellar components; design A with dome shaped patellar component (left) and design B with medialized-dome patellar component (right).

Table 3.2 Material properties of TKR components

TKA	Young's Modulus (MPa)	Poisson ratio
Patellar button	572	0.45
Tibial insert	572	0.45
Cement	3,400	0.30
Femoral component	Rigid	

Chapter 4. Natural and Implanted Conditions during Kneeling

4.1. Introduction

Kneeling is considered an important activity by more than 50% of patients with total knee replacement (Weiss et al., 2002), but patients often experience anterior knee pain and reduced functionality during kneeling-type activities (Conditt et al., 2004; Conditt et al., 2007). In addition, implanted patellae have a greater risk of patellar fracture (Chalidis et al., 2007). A cadaveric study was performed by Conditt et al. (2005) to assess patellar contact and tibiofemoral kinematics during kneeling. Many factors influence the ability to kneel, including articular geometry, soft tissue impingement and implant design. A painful TKR causes a lot of social and medical problems.

Patients who have had knee replacement operations, normally they increase their activities. Many reports have indicated an increase of anterior knee pain during high flexion activities such as kneeling (Kim et al., 2010; Park et al., 2007; Schai et al., 1999). Joint kinematics and performance after TKR are significantly different from the natural knee (Kanekasu et al., 2004; Komistek et al., 2003; Stiehl et al., 1995). Also, patellar fracture remains one of the common complications following total knee replacement. TKR studies reported in the literature have shown that patellar fracture cases due to high

flexion activities (Lee et al., 1999; Shafi et al., 2005) and recent studies reported the frequency range of this complication is 1.51% to 5.2% (Jujo et al., 2012; Meding et al., 2008).The objective of the this study was to perform a comparative evaluation of patellofemoral joint mechanics and patellar bone strain distributions in the natural and implanted knee during simulated kneeling in multiple specimens.

4.2. Materials and Methods

Specimen-specific finite element models for eight male specimens were developed from computed tomography (CT) and magnetic resonance (MR) scans of cadaveric knees. The patellar bone geometry was extracted from CT data to develop heterogeneous material properties using BoneMat (Taddei et al., 2007) and an empirical density-modulus relationship (Keller, 1994). MR data was used to reconstruct the femoral and tibial bone, cartilage, and ligament attachment sites. Knee joint bones and cartilage were segmented from MR images, while the patellar bone geometry was extracted from CT data. The articular cartilages were semi-automatically generated from the segmented geometries using custom-scripted coordinate data extraction and mesh morphing techniques (Baldwin et al., 2010). Tetrahedral meshes with average element edge length of 1.0 mm, previously used by Fitzpatrick et al. (2011a) and Perillo-Marcone et al. (2007), to properly capture material property heterogeneity described by the CT data and strain gradients within the bone. Two models were contracted to represent natural knee

with bone and cartilage, and an implanted knee with a size-matched domed patellar button, femoral component, and tibial insert.

For a comprehensive side by side comparison between natural and implanted cases, patellar bones for all specimens were meshed using four-noded tetrahedral elements so that in the two cases the patellae shared same element sets (Figure 4.1). In TKR model, cement-bone interface shared same nodes (equivalenced) and same boding was assumed between the button and cement. Two model representations were developed for each specimen analyzed using in Abaqus/Explicit (Simulia, Providence, RI). For more computationally efficient models, femoral and tibial bone, the tibial insert and the femoral component were modeled as rigid. However patellar components were modeled as deformable bodies.

Bone strains depend on functional activity; complex loading condition, contact mechanics, local muscle forces, and most importantly on material properties of the bone. With the aim of accounting for specimen-specific bone material properties, mapped material properties of the patellar bone were extracted from the CT data using BoneMat (Taddei et al., 2007). Tuning of the CT data to correlate Hounsfield Units (HU) to apparent density (ρ) was performed using a linear relationship previously used by Fitzpatrick et al. (2011a) and taken from the literature (Peng et al., 2006).

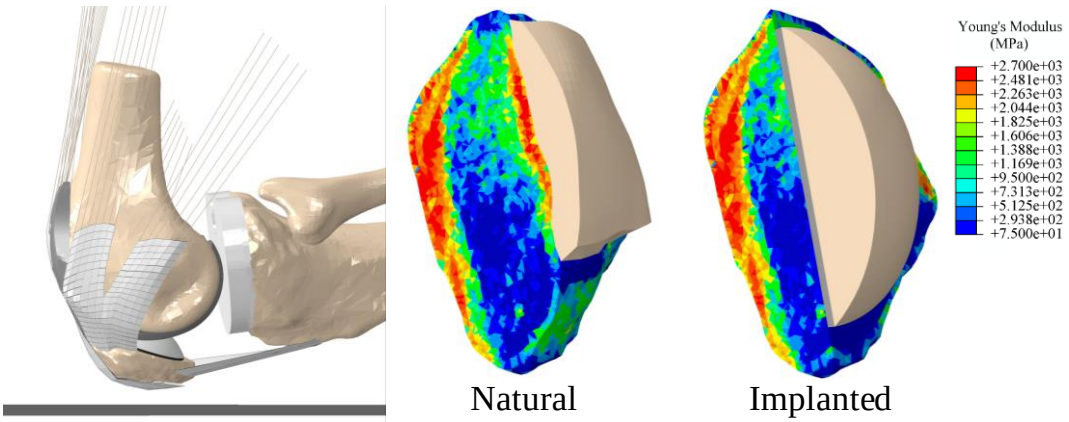

Figure 4.1 Implanted kneeling model (left) and distribution of material properties (right) of the patellar bone in natural and implanted condition.

Each natural and implanted model was incorporated into a finite element model to focus on patellofemoral joint. Patellofemoral soft tissue was represented with 2-D fiber-reinforced membrane representations of the extensor mechanism (patellar ligament, vasti and rectus femoris) (Bayraktar et al., 2004). The attachment sites of ligaments and tendons were defined on the surface of the patellar bone. To insure that muscle load transfer evenly to patellar bone, closet nodes on soft tissue were individually beamed to patellar bone using a multi-point constraint method. The eight specimens were male and of similar weight and height, therefore a similar loading condition was used across specimens for an intra-specimen comparative analysis (Amis et al., 2006). Corresponding to a foot propped kneeling condition, the knee was flexed to 110° using tibiofemoral positions prescribed from fluoroscopy data and a 1000 N distributed quadriceps load among the heads of the quadriceps muscle (Fitzpatrick et al., 2012b) in proportion to their physiological cross-sectional areas (Farahmand et al., 1998).

To appropriately align the patellofemoral joint before flexion (from 0^o to 110^o) and to bring the PF articular joints into contact, a 300 N of quadriceps load was applied and held constant. Then, the load linearly ramped to 1,000N at full flexion (110^o) before kneeling simulation. From this flexed position, the model simulated foot-propped kneeling condition (Noble et al., 2006). The knee contacted the floor with a load of 660N, single-stance kneeling (Wilkens et al., 2007), while the relative position of the femur and tibia were constrained. However, patellofemoral joint was unconstrained in six degree of freedom. The boundary and load conditions used to simulate kneeling are similar previous analyses prescribed by Hamai et al. (2008) and Hofer et al. (2011) Table 4.1.

Contact pressure and area, and minimum and maximum principal strains were computed in the natural and implanted conditions. For bone strain analysis, a previously modeled approach developed by Fitzpatrick et al. (2011a) was used in this study to quantify the amount of strained bone as indicator of risk for patellar fracture or anterior knee pain. Highly strained volume (HSV) defined as strains above a threshold of 0.5% (just below reported bone yield strain by Bayraktar et al. (2004) and Kopperdahl et al. (1998) was selected for comparison between the natural and implanted cases. However, this measure is used to show the likelihood of increasing bone strains and where might be occurring and it is not to study bone fracture in whatsoever. Additionally, patellar bone volume was divided into four discrete regions: superior, medial, lateral and inferior, centered at the mid-point of the patellar component. Maximum and minimum principal strains in the patella were quantified before and after kneeling. Strain distributions throughout the bone volume were compared between natural and implanted conditions

Table 4.1 Physiological boundary and load conditions used to simulate kneeling

Natural Case				
Step 1	Femur	Tibia	Patella	Others
AP	Ramped from 0 to 8.6 mm (anterior)	Fixed	Unconstrained	
ML	Fixed	Fixed		
SI	Vertical load of 360 N	Fixed		1000 N Quad load
FE	Ramped from 0^o to 110^o	Fixed		
IE	Fixed	Ramped from 0 to 8.1^o (internal rotation)		
VV	Unconstrained	Fixed		
Step 2	Femur	Tibia	Patella	Others
AP	Fixed at 8.6 mm (anterior)	Fixed	Unconstrained	660 N Kneeling load
ML	Fixed	Fixed		
SI	Fixed	Fixed		1000 N Quad load
FE	Flexed at 110^o	Fixed		
IE	Fixed	Fixed at 8.1^o (internal)		
VV	Fixed	Fixed		
Implanted Case				
Step 1	Femur	Tibia	Patella	Others
AP	Unconstrained, post-cam contact prevents AP translation	Fixed	Unconstrained	
ML	Fixed	Fixed		
SI	Vertical load of 360 N	Fixed		1000 N Quad load
FE	Ramped from 0^o to 110^o	Fixed		
IE	Fixed	Ramped from 0 to 6.4^o (internal rotation)		
VV	Unconstrained	Fixed		
Step 2	Femur	Tibia	Patella	Others
AP	Fixed	Fixed	Unconstrained	660 N kneeling load
ML	Fixed	Fixed		
SI	Fixed	Fixed		1000 N Quad load
FE	Flexed at 110^o	Fixed		
IE	Fixed	Fixed at 6.4^o (internal)		
VV	Fixed	Fixed		

As peak maximum or minimum strain may occur in a very small localized region and may not provide an appropriate comparison (Fitzpatrick et al., 2011a), evaluations of a HSV were performed representing the bone volume experiencing strain above a specific threshold level. To identify what region of the patellar bone has a greater likelihood of HSV that may lead to fracture due to kneeling activity.

4.3. Results

Natural and implanted conditions showed an increase in bone strain during kneeling. Due to the compression-dominated loading, min principal bone strains and highly strained volumes were (2.1X) larger in magnitude than the max principal strains. Distributions of bone strain were obtained throughout the volume of the patellar bone for both the natural and implanted cases. The regions of bone experiencing high strains were evaluated in terms of a highly strained volume (experiencing strains above 0.5%) and the location of this volume was compared between the natural and implanted conditions. Bone strains were (1.34X) greater in the implanted case both before and after kneeling, as the cortical bone has been resected. The bone strain distribution after kneeling reflected the differences in patellar contact and resulted in larger compressive strains centrally in the natural and inferiorly in the implanted case (Figures 4.2 and 4.4). Also, peak compressive strains were centrally in the softer cancellous bone in the natural, and around pegs and inferiorly in the implanted case.

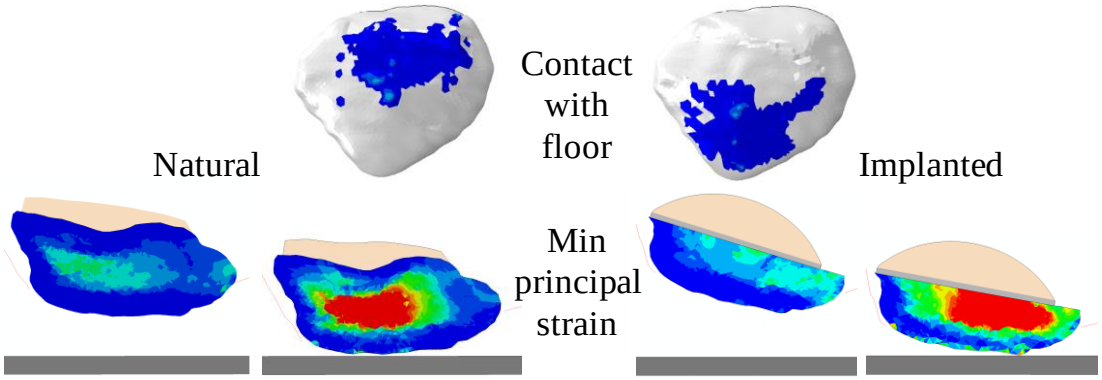

Figure 4.2 Representative contact region of anterior patella against floor and minimum principal strains at 110° flexion before and after kneeling.

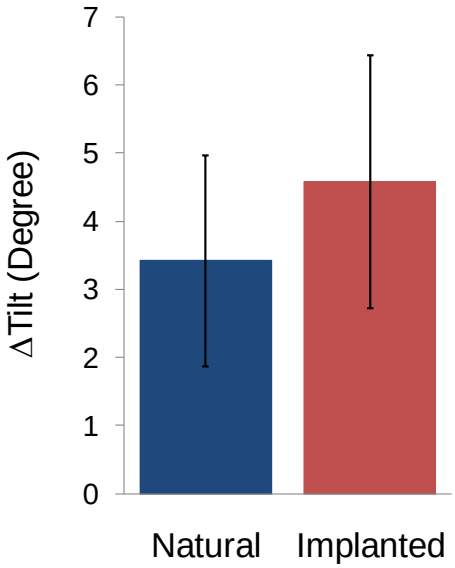

Figure 4.3 Change in patellar tilt with kneeling in sagittal plane. Error bars = 1 standard deviation

Visual examination of strain throughout the bone volume before and after kneeling indicated that strain location, as well as magnitude, changed between the natural and implanted conditions. Before kneeling in the natural specimens, HSV of the patellae were seen in superior region. Due to the anterior load on the patellar bone after kneeling, the HSV was focused centrally in the natural patellae. In the implanted patellae, however,

dome-shaped patellar component allowed a more even HSV distribution between inferior and superior regions before the kneeling load was applied. After kneeling, HSV was increased significantly in the inferior region and around the pegs. The medial and lateral quadrants experienced a modest (16-42%) increase in HSV in the implanted cases (Figure 4.5). However, statistically significant differences (p=0.05) were only noted in the inferior (2X increase) and superior (2/3X decrease) regions of the implanted patellae compared to the natural.

Kinematics and bone strain distributions were predicted for the eight specimens. Prior to kneeling, patellar tilt relative to the long axis of the tibia was greater in the implanted case than the natural case, resulting in a more inferior contact patch on the anterior surface of the patella against the floor (Figures 4.2 and 4.3). As a result, implanted patellae tilted significantly to accommodate the anterior load (floor) that was transferred through the distal region of the bone and caused an increase in HSV inferiorly.

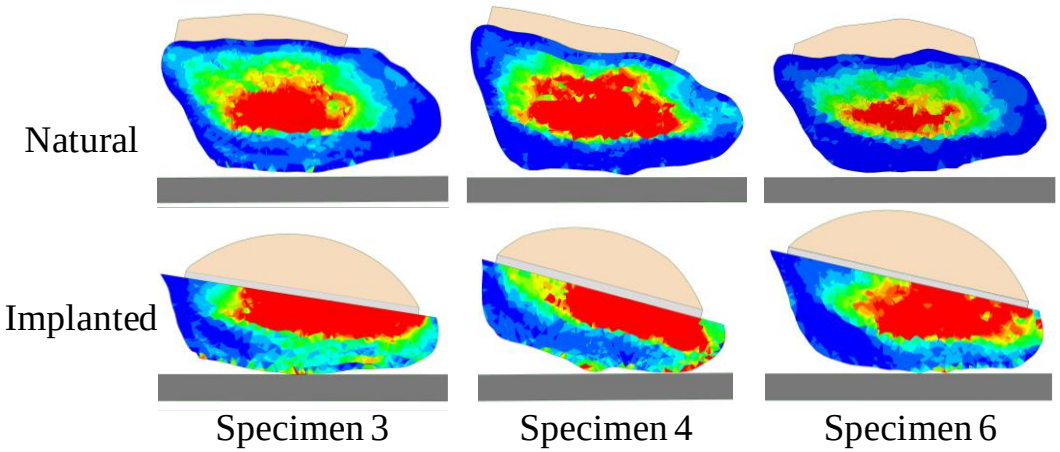

Figure 4.4 Minimum principal strains after kneeling in the natural and implanted patella for 3 of 8 specimens.

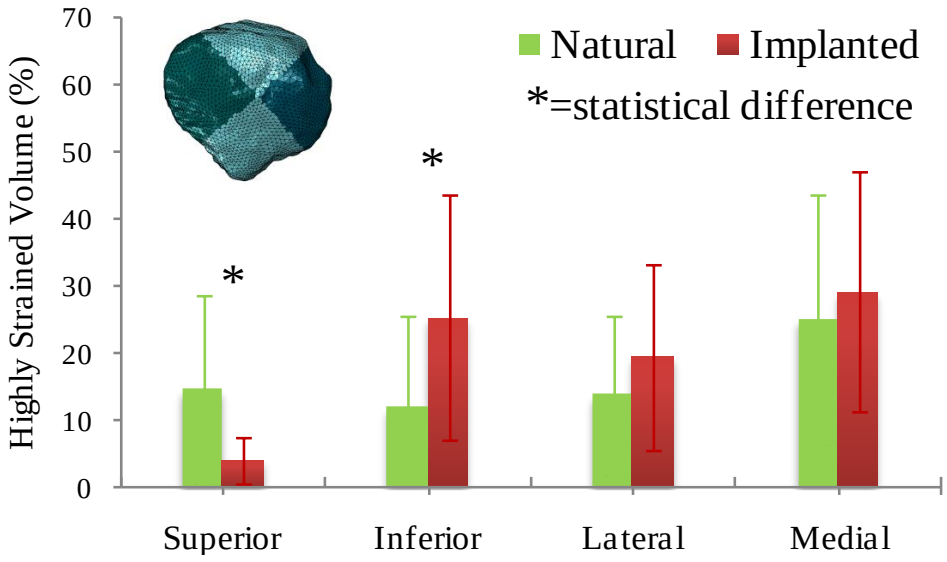

Figure 4.5 Highly strained volume by quadrant comparing natural and implanted conditions after kneeling. Error bars = 1 standard deviation.

4.4. Discussion

Computational models of eight cadaveric specimens were used to assess the kinematics, contact mechanics and patellar strain distribution during a kneeling activity. In the natural patella, the cartilage and patellar cortical bone distributed the kneeling loads around the periphery of the patella with minimum principal strains centrally in the softer cancellous bone. In the implanted patella, the increased tilt in TKA specimens caused the strain distribution to shift inferiorly in both the flexed and kneeling conditions, resulting in statistically significant differences in inferior and superior highly strained bone volumes. Model predicted a strong negative linear relationship between HSV and the resurfaced patellar volume (r = -0.79). Unresurfaced patella approach may reduce the likelihood of patellar fracture for smaller patellae. Previous studies report that patellar

resection thickness is an important contributing factor to patellar fracture (Dalury et al., 2003). The current study did not consider bone remodeling. Accordingly, strain distributions are representative of conditions immediately post-operative. The results of the current study can ultimately provide guidance related to the amount of bone resection and component placement to reduce the likelihood of patellar fracture.

Chapter 5. Patellar Bone Strain and Patellofemoral Joint Mechanics during Kneeling; Natural vs. Implanted with Various Designs

5.1. Introduction

Kneeling after total knee replacement has frequently been cited as a limiting activity for patients (Noble et al., 2005; Weiss et al., 2002). Many patients have reported that they cannot kneel due to pain, or avoid kneeling due to discomfort (Hassaballa et al., 2002; Nijs et al., 2006; Palmer et al., 2002; Shafi et al., 2005). For many TKR patients, kneeling is of particular cultural relevance, or is a requirement of their daily activities (praying, gardening) (Weiss et al., 2002). As a result, the ability, or otherwise, to kneel without discomfort, critically impacts their quality of life and perceived success of the TKR procedure.

While there are a variety of potential sources of knee pain during kneeling, including scar position (Nijs et al., 2006; Schai et al., 1999), the patellar bone contains numerous pain-sensing mechanoreceptors, and is a likely contributor to anterior knee pain. During kneeling, the ground reaction force on the tibial tuberosity and/or patellar bone causes a posterior shear force on the tibia and anterior compressive force on the patella (Goldstein et al., 2007; Incavo et al., 2004).

After TKR, patellofemoral conformity, patellar tracking and mechanics are significantly altered from the native joint. Prior TKR studies have reported bone strains in resected patellae which are substantially higher than the natural knee (Fitzpatrick et al., 2011a; Lie et al., 2005; McLain & Bargar, 1985; Reuben et al., 1991; Wulff & Incavo, 2000), with resected patellae being more vulnerable to fracture due to sagittal plane bending in deep flexion, particularly in thinner patellae (Reuben et al., 1991). A high flexion, high patellofemoral (PF) contact force activity, such as kneeling, suggests that patients kneeling after TKR may be particularly susceptible to anterior knee pain and patellar fracture (Windsor et al., 1989).

A number of clinical studies have attributed patellofemoral complications, including patellar fracture and patellar bone strain, to prosthesis design (Brick & Scott, 1988; Healy et al., 1995; McLain & Bargar, 1985; Meding et al., 2008; Theiss et al., 1996). Studies which have investigated the biomechanics of kneeling in the TKR knee have predominantly focused on tibiofemoral kinematics, evaluating *in vivo* six-degree-of-freedom (6-DOF) kinematics through radiographic techniques (Coughlin et al., 2007; Hamai et al., 2008; Hanson et al., 2007; Incavo et al., 2004; Kanekasu et al., 2004). A number of cadaveric studies have utilized pressure-sensitive film to measure PF or TF contact area and pressure in response to kneeling, employing an anterior force, in addition to a quadriceps load, in order to simulate the loads encountered during kneeling (Hofer et al., 2011; Wilkens et al., 2007).

Other *in-vitro* studies have measured patellar bone strain using strain gauges attached to the anterior surface of the patella, but have not performed these analyses during a kneeling activity (Lie et al., 2005; McLain & Bargar, 1985; Reuben et al., 1991; Wulff & Incavo, 2000). Computational methods have been used to develop high flexion models which have been applied to predict ligament and joint forces but have not been utilized to evaluate knee mechanics under loading conditions which simulate kneeling (Yang et al., 2010; Zelle et al., 2011), or to compare component designs under the high flexion, such as performing a deep squat activity (Fitzpatrick et al., 2012a).

The objective of the current study was to evaluate the effect of component design on patellar mechanics during a kneeling activity. A computational model of the knee joint was developed and validated against experimental cadaveric studies. A series of computational models, which included representations of both the native joint and TKR knee implanted with a variety of component designs, were compared during a dynamic kneeling activity. PF joint mechanics and patellar bone strains were compared across multiple FE specimen-specific models. An understanding of the effect of implant design on patellar mechanics during kneeling may ultimately provide guidance to component design that may reduce the likelihood of knee pain and patellar fracture during kneeling.

5.2. Material and Methods

5.2.1. *In-Vitro* Testing

A series of in vitro tests, designed to simulate a kneeling activity, were performed on four cadaveric knee specimens (male; age: 61.8 ± 13.8 years; height: 1.76 ± 0.08 m; weight: 76.6 7 ± kg). Each test was initially conducted on the natural knee, with the skin, joint capsule, knee ligaments and musculature intact. Subsequently, testing was performed on two posterior-stabilized (PS) TKR knee systems, implanted by an orthopaedic surgeon, with distinct styles of patellar component: medialized dome and anatomic with contemporary TKR designs.

The femoral and tibial bone of each specimen was transected approximately 20 cm from the joint line, cemented into aluminum fixtures and mounted in a quasi-static knee rig (QKR) which permitted loading of the quadriceps and application of anterior force to simulate kneeling. An aluminum clamp was used to rigidly attach the proximal portions of the rectus femoris (RF) and vastus intermedius (VI) tendons such that they were actuated along the line-of-action of the femoral shaft. The tibia was positioned such that superior-inferior (S-I) and anterior-posterior (A-P) translation of the simulated ankle position was constrained Figure 5.1. The femur was positioned vertically with TF flexion unconstrained. Knee flexion was achieved through S-I and A-P motion of the simulated hip. The knee was flexed to 90º TF flexion, while maintaining a vertical femur, until the

patella made contact with the ‘floor’, which was represented by a metal plate attached to a scissor jack for adjustable floor height. A 90 N load was applied to the quadriceps through free weights attached to the quadriceps tendon, while a contact force of approximately 180 N between the patella and the floor was applied as a result of the weight of the femur and fixtures. The floor was gradually lowered with the knee maintaining contact as far as the knee or equipment would allow, simulating the tibia moving from a plantar to dorsal flexion position.

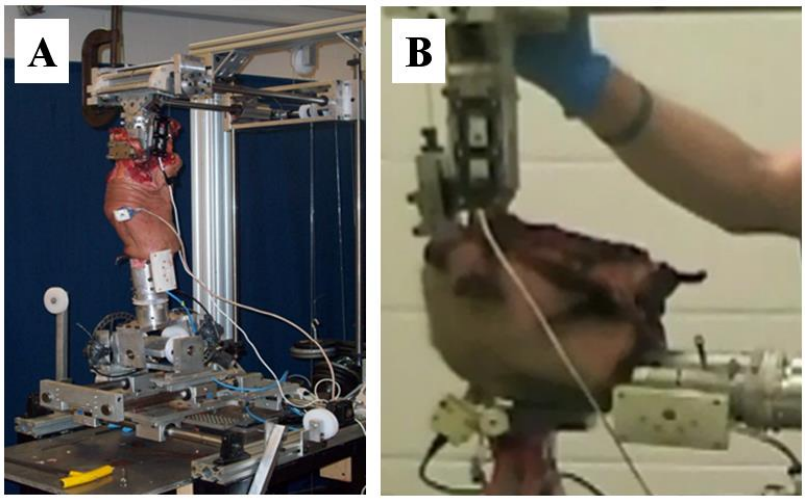

Figure 5.1(A): Knee specimen fixed in the quasi-static knee rig; (B): Experimental kneeling simulation in the quasi-static knee rig.

An Optotrak 3020 (Northern Digital, Waterloo, Ontario) motion analysis system was used to track 6-DOF kinematics of the femur, tibia and patella bones throughout the activity through light emitting diode markers which were rigidly fixed to each bone. A hand held digitizer was used to collect 3-D point data on each TKR component and bone surface relative to its respective local coordinate frame in order to determine component alignment relative to the bone. Magnetic resonance (MR) images (slice thickness of

1mm; in-plane resolution of 0.234 x 0.234) were obtained for each specimen prior to implantation.

5.2.2. Finite Element Development and Kinematic Validation

Specimen-specific FE models, which reproduced the in vitro experiment, were developed in Abaqus/Explicit (SIMULIA, Providence, RI). 3-D representations of femoral, tibial and patellar bone and cartilage geometry were extracted from the MR scans using ScanIP software (Simpleware, Exeter, UK). Size-matched TKR component geometry was generated from CAD surfaces obtained from the manufacturer. Bones were meshed with 2-D triangular shell elements; femoral components were meshed with 3-D tetrahedral elements; and tibial and patellar components and all articular cartilage surfaces were meshed with eight-noded hexahedral elements. Implanted models also included a layer of cement between the patellar component and bone which was meshed with hexahedral elements.

Due to greater stiffness of bone and CoCr relative to polyethylene, bone and the femoral component were modeled as rigid for computational efficiency, Figure 5.2. Tibial and patellar components (E = 572 MPa, v = 0.45), cement (E=3400 MPa, v = 0.3) and femoral, tibial and patellar articular cartilage (E=12 MPa, v = 0.45) were modeled as fully deformable. A coefficient of friction of 0.04 was applied to articulating surfaces (Godest et al., 2002; Halloran et al., 2005a). The patellar tendon, RF and vasti tendons were represented by deformable hyperelastic 2-D membrane elements with fiber-

reinforced springs, with uniaxial tension characteristics tuned to match literature values (Atkinson et al., 1997; Stäubli et al., 1999). The vasti tendon was separated into five bundles representing the VI, vastus lateralis longus (VLL), vastus lateralis obliquus (VLO), vastus medialis longus (VML) and vastus medialis obliquus (VMO) similar to quadriceps load distribution described by Fitzpatrick et al. (2011a). Contact was defined between all soft-tissue structures and relevant bone and articular surfaces to allow wrapping in deep flexion. In order to directly reproduce the experimental setup, loading was only applied to the VI bundle of the vasti tendon.

Bones and cartilage/components were aligned in the initial position of the kneeling activity based on the probed points obtained during cadaveric testing. During the kneeling simulation, TF kinematics were fully prescribed based on the experimentally measured kinematics. The patella was kinematically unconstrained, with a 90 N load applied to the RF and VI bundles of the quadriceps, and an anterior load matching the experimental loading condition (approximately 180 N) applied to the patella through contact with the floor. 6-DOF PF kinematics were measured in the same manner as the experiment throughout the activity, and compared to the in vitro data, Table 5.1.

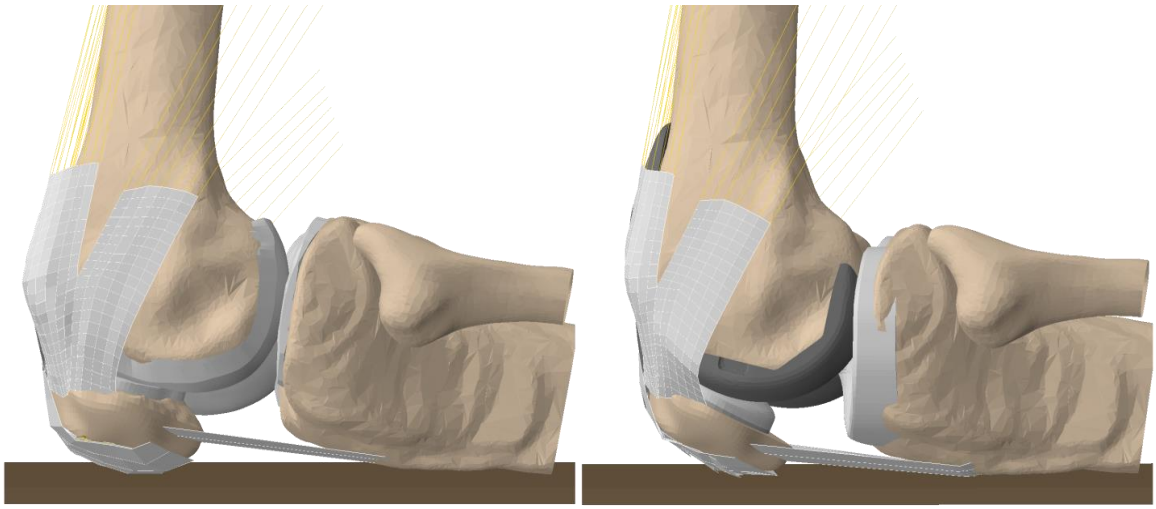

Figure 5.2 Finite element models of specimen 8; natural (left) and implanted knee (right) during floor-knee contact.

Table 5.1 Boundary and load conditions used to simulate kneeling

DOF	Femur	Tibia	Patella	Others
AP	Kinematically prescribed	Encastered	Unconstrained	180 N Kneeling load
ML	Kinematically prescribed			
SI	Kinematically prescribed			90 N Quad load
FE	Fixed at 90^{o}			
IE	Kinematically prescribed			
VV	Kinematically prescribed			

5.2.1. Convergence Study

A convergence study was performed to determine the optimal element size for the patellar bone mesh. Hexahedral (hex) elements are preferred by many researchers to the tetrahedral element. In comparing linear tetrahedral and hexahedral elements it has been evaluated that hexahedral elements were more stable and less influenced to the degree of refinement (Kallemeyn et al., 2012; Ramos et al., 2006). In the current study, FE models

were generated with 1.5, 1.25, 1.0, 0.8, and 0.5 mm as average element edge lengths for patellar bone Figure 5.3. Number of hex elements increased with mesh refinement from 4567 (for 1.5 mm) to 93203 (for 0.5 mm).

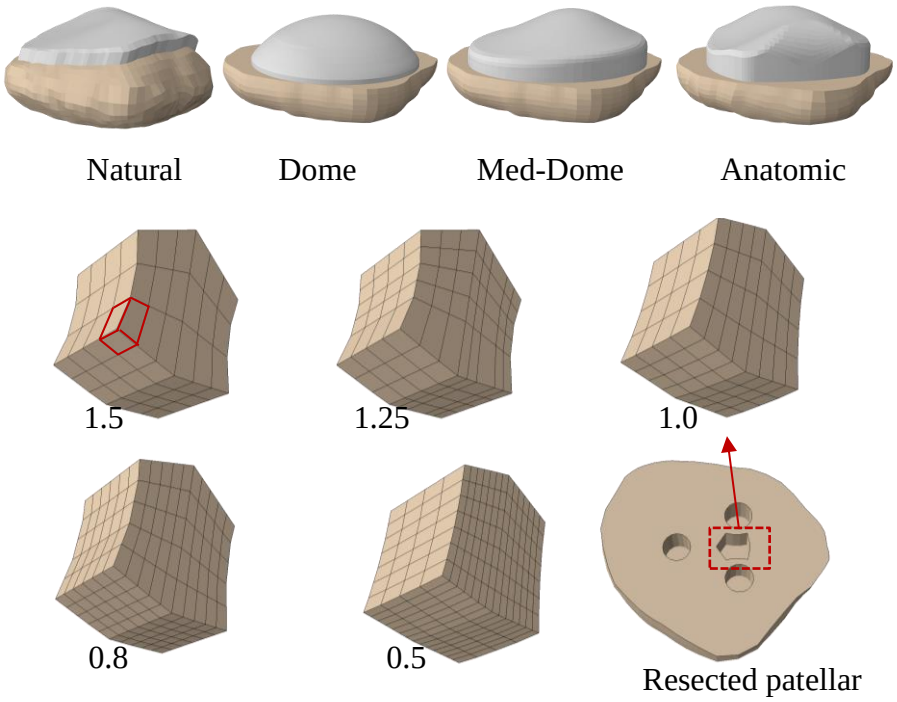

Figure 5.3 Diagram of five different densities of hexahedral meshes used for convergence study.

The model converged with patella bone element edge length of 1.0 mm, Figure 5.4. The patellar bones were meshed using eight-noded hexahedral elements, such that both the natural and implanted patellae shared an element subset.

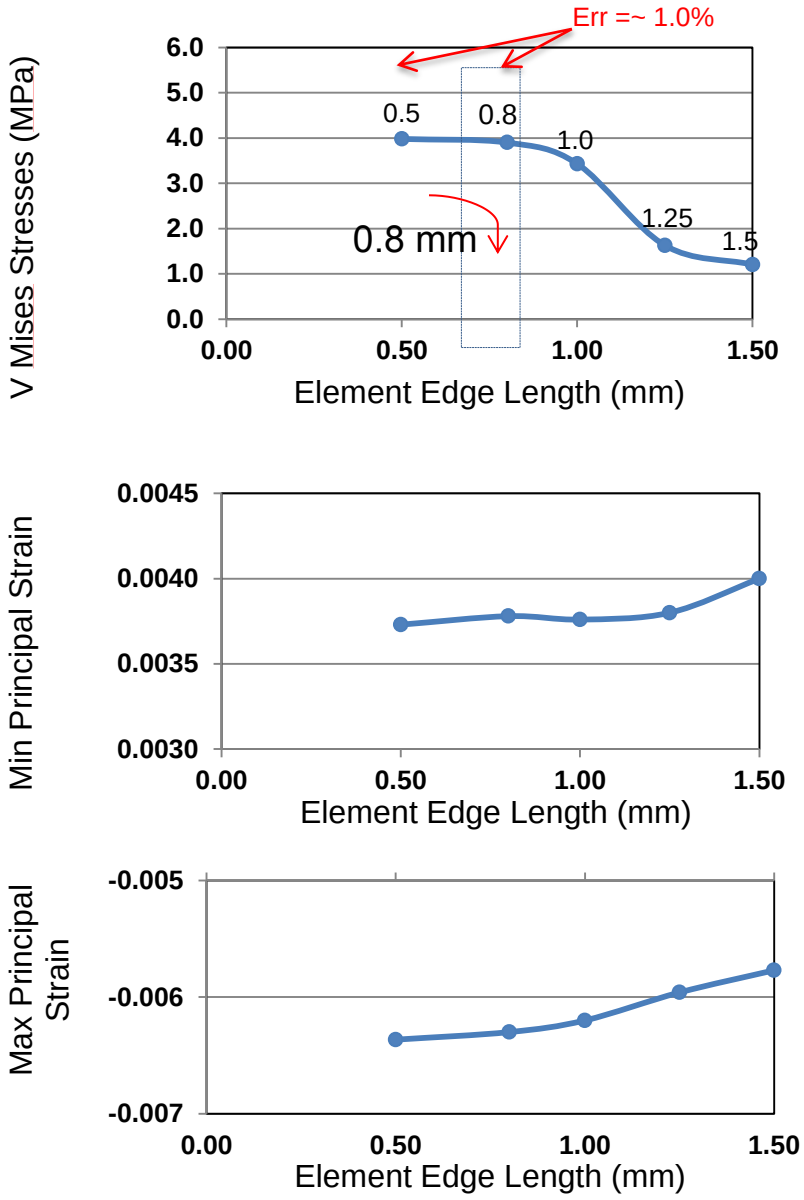

Figure 5.4 Three field variables; Von Mises stress, maximum and minimum principal strains, used to determine mesh convergence.

5.2.2. Finite Element Application

Utilizing the computational model described above, the boundary conditions were adapted to better represent the physiological loads applied during kneeling which were not feasible to implement experimentally (quadriceps load distributed throughout rectos femoris and all vasti bundles). Specimen-specific models were developed for an additional set of eight specimens (male; age: 67 ± 10 years; height: 1.78 ± 0.05 m; weight: 83 ± 14 kg). In addition to MR images, computed tomography (CT) images were obtained for each specimen. The CT scans were used to develop specimen-specific models of the patellar bone with mapped material properties in order to evaluate strain in the patellar bone similar to Laz et al. (2007). Patellar bone was meshed with hexahedral elements with mapped material properties developed from the CT data using BoneMat (Taddei et al., 2007). A linear relationship taken from the literature (Peng et al., 2006) was used to correlate Hounsfield units (HU) to apparent density (ρ) for femur bones. The empirical relationship, Young's Modulus (E) = 1990ρ, was applied to convert bone density to mechanical properties (Keller, 1994). A convergence study was performed on a single specimen to determine the optimal element size for the patellar bone mesh. Meshes were generated with average element edge lengths of 1.5, 1.25, 1.0, 0.8 and 0.5 mm. Bone strain prediction from the bone converged with a patellar bone element edge length of 1.0 mm, and this was subsequently applied to all models.

The knee was flexed to a 90º TF kneeling position, with other TF kinematics prescribed according to kinematic measures taken from the literature; the natural knee was positioned in with 1.5º internal tibial rotation and 1.8 mm of femoral posterior translation (Hofer et al., 2011), while implanted models were positioned with 5.6º internal tibial rotation, with A-P displacement guided by the geometry of the TKR components (Hamai et al., 2008; Hanson et al., 2007). The variations reported in the literature did not affect overall results. A muscle load of 550 N was distributed among the quadriceps bundles according to their physiological cross-sectional area (Farahmand et al., 1998), while an anterior load of 330 N (½ BW, representing double-stance kneeling) was applied through the floor (Hofer et al., 2011; Wilkens et al., 2007), Table 5.2. During the kneeling simulations, TF kinematics were held constant, while the patella was unconstrained in all DOFs (Hofer et al., 2008; Wilkens et al., 2005). In addition to the natural knee and two TKR knee systems evaluated previously, a third contemporary TKR design with a dome-compatible patellar component, which was not available during the experimental simulations, was also evaluated in the computational setup.

Patellar bone strain (as a surrogate measure for likelihood of anterior knee pain and fracture) was predicted from the FE models and compared between natural and implanted conditions, and also compared between regions (superior, inferior, medial and lateral quadrants) of the patellar bone. A highly strained bone volume was used to compare changes in bone strain between conditions (Fitzpatrick et al., 2011a).

Table 5.2 Physiological boundary and load conditions used to simulate kneeling

Natural Case				
Step 1	Femur	Tibia	Patella	Others
AP	Ramped from 0 to 1.8 mm (anterior)	Fixed	Unconstrained	
ML	Fixed	Fixed		
SI	Vertical load of 360 N	Fixed		550 N Quad load
FE	Ramped from 0^o to 90^o	Fixed		
IE	Fixed	Ramped from 0 to 1.5^o (internal rotation)		
VV	Unconstrained	Fixed		
Step 2	Femur	Tibia	Patella	Others
AP	Fixed at 1.8 mm (anterior)	Fixed	Unconstrained	330 N Kneeling load
ML	Fixed	Fixed		
SI	Fixed	Fixed		550 N Quad load
FE	Flexed at 90^o	Fixed		
IE	Fixed	Fixed at 1.5^o (internal)		
VV	Fixed	Fixed		
Implanted Case				
Step 1	Femur	Tibia	Patella	Others
AP	Unconstrained, post-cam contact prevents AP translation	Fixed	Unconstrained	
ML	Fixed	Fixed		
SI	Vertical load of 360 N	Fixed		550 N Quad load
FE	Ramped from 0^o to 90^o	Fixed		
IE	Fixed	Ramped from 0 to 5.6^o (internal rotation)		
VV	Unconstrained	Fixed		
Step 2	Femur	Tibia	Patella	Others
AP	Fixed	Fixed	Unconstrained	330 N kneeling load
ML	Fixed	Fixed		
SI	Fixed	Fixed		550 N Quad load
FE	Flexed at 90^o	Fixed		
IE	Fixed	Fixed at 5.6^o (internal)		
VV	Fixed	Fixed		

The highly strained bone volume, representing the bone volume experiencing strain above a specific threshold level, was believed to be a better predictor of bone failure than a peak strain value, which may occur in a small localized region and can be highly dependent on mesh construction. A threshold of 0.5% (just below reported bone yield strain) was applied in the current analysis. In addition to bone strain, PF contact pressure and area were compared between analyses.

5.3. Results

Experimentally-measured TF kinematics at 90º flexion were measured. The anterior load caused by knee contact with the floor with half body weight altered TF kinematics in all cases and caused an increase in flexion angle 6.8^{o}(2.8) and 7.2^{o}(0.3) in natural and medialized dome. However, this change was 3.7^{o} (3.1) flexion in anatomic patellar case. There is no significant change in IE rotation in all cases; 0.44^{o} (0.2), 0.29^{o} (0.1) and 0.46^{o} (0.2) in natural, anatomic and medialized dome respectively. Due to the post cam mechanism in PS design, the AP translation was greater in natural case 1.22(0.27) mm than anatomic and medialized dome cases; 0.27(.11) and 0.34(0.24) mm, respectively. This shows that PS design has greater influence in TF kinematics alteration, tibial anterior-posterior translation in particular, at 90^{o} during kneeing than patellar component design. These differences between natural and implanted cased were also noted in previous studies (Hofer et al., 2011; Lin et al., 2011).

TF kinematics obtained from in vitro testing in response to kneeling demonstrated subtle variation in kinematics based on implant design. The natural knee achieved greater A-P translation than the implanted conditions as post-cam contact impeded A-P motion in the PS TKR devices. Comparing PF kinematics between the experiment and the computational model, maximum differences in PF translations and rotations were 1.1 mm and 1°, respectively, across all four specimens in both the natural and implanted conditions (Figure 5.5).

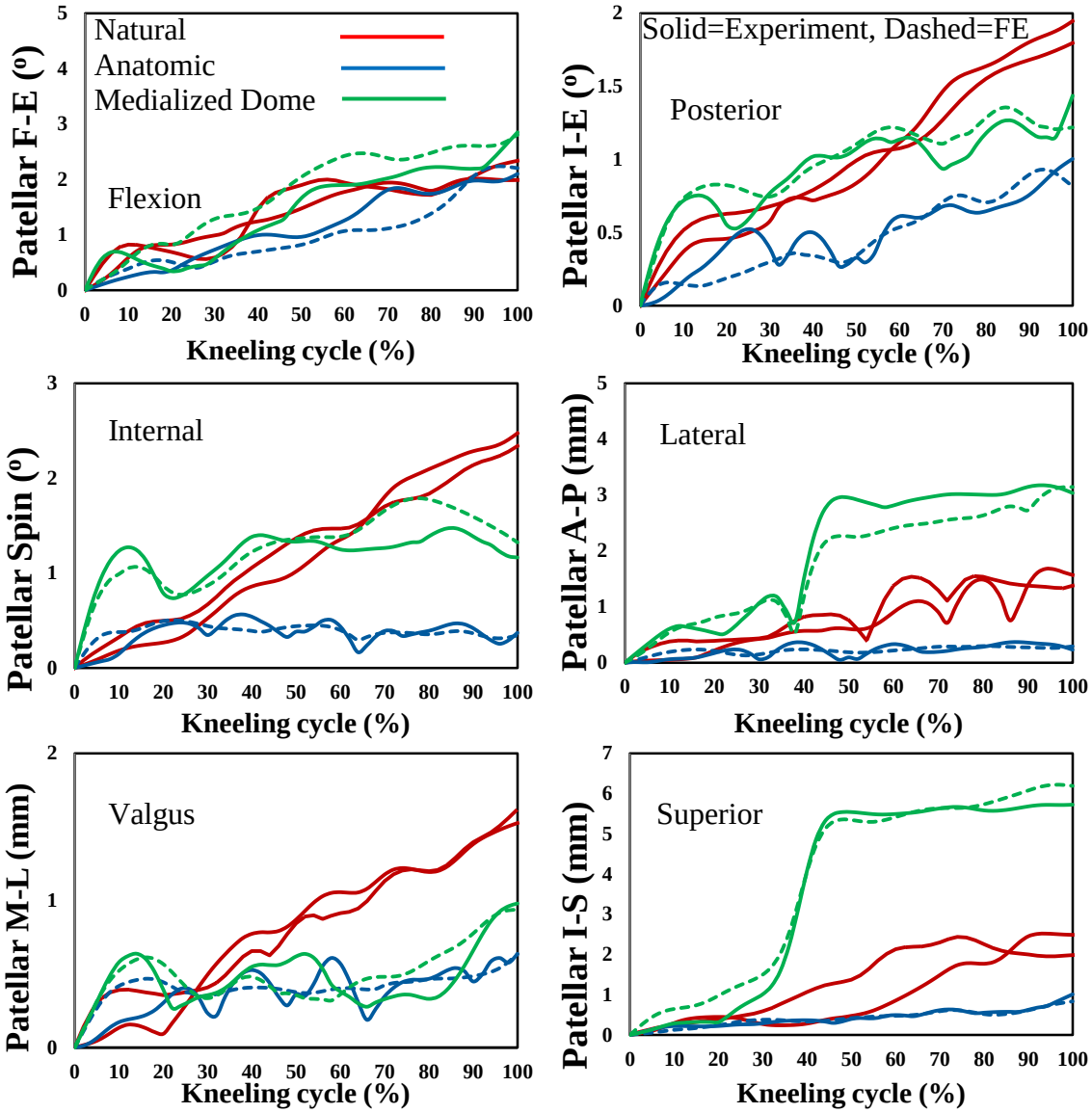

Figure 5.5 Comparison between experimentally-measured and FE model predicted PF kinematics during kneeling for the natural knee, modified dome and anatomic patellar components. Shown for the average of all four specimens.

Table 5.3 Average RMS differences (± Standard Deviation) between model and experimental of patellofemoral kinematics during kneeling for all four specimens.

Kinematic Output Average RMS Difference (Standard Deviation)						
	Natural		Anatomic		Medialized Dome	
	RMS	Std	RMS	Std	RMS	Std
Patellar Flexion (^{o})	0.25	0.07	0.29	0.12	0.42	0.13
Internal-External Rotation(^{o})	0.12	0.01	0.12	0.02	0.11	0.02
Patella Spin(^{o})	0.19	0.03	0.10	0.02	0.21	0.06
Anterior-Posterior Translation (mm)	0.27	0.08	0.08	0.01	0.35	0.14
Medial-Lateral Shift (mm)	0.14	0.02	0.12	0.02	0.15	0.03
Superior-Inferior Translation (mm)	0.65	0.47	0.05	0.01	0.33	0.12

Prior to kneeling, sagittal plane patellar tilt was significantly greater in all implanted conditions than the natural case (tilt of 10.2 ± 4.2°, 20.6 ± 5.2°, 24.4 ± 4.5° and 25.3 ± 3.9° for natural, anatomic, medialized-dome and dome conditions, respectively). After contact with the floor, sagittal plane patellar tilt was reduced to 7.9 ± 2.6°, 18.5 ± 5.2°, 19.5 ± 3.7°, 19.6 ± 3.6° for natural, anatomic, medialized-dome and dome conditions, respectively. Due to the less conforming nature of the designs, change in sagittal plane tilt as a result of kneeling was significantly larger for the medialized-dome and dome implants than the natural case or anatomic implant (Figures 5.6, 5.7).

This resulted in more inferior contact on the anterior surface of the patella against the floor for the natural and anatomic designs, compared to the medialized-dome and dome designs. As a result of the anterior load on the patella, there was a considerable increase in both PF contact pressure and area before and after kneeling (Figure 5.8).

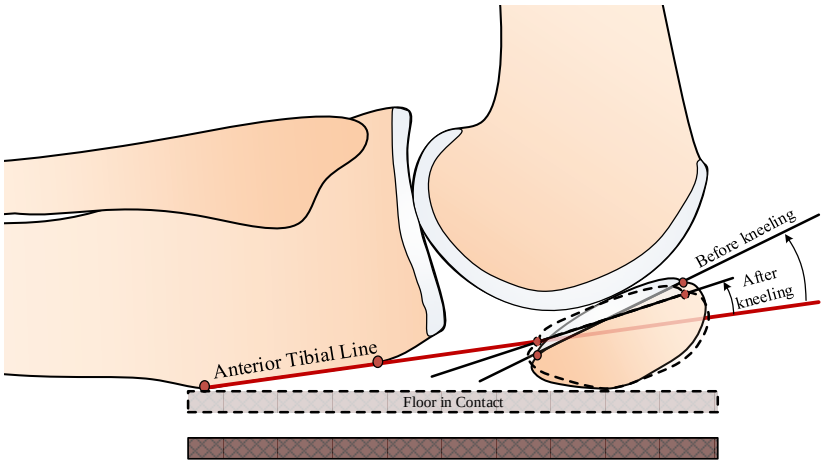

Figure 5.6 Measurement of sagittal plane patellar tilt, and representation of the typical change (reduction) in tilt as a result of kneeling.

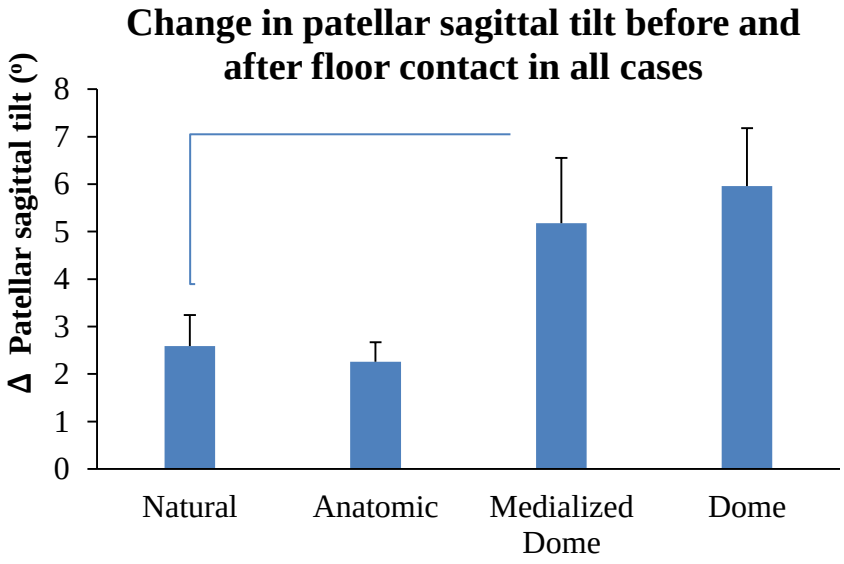

Figure 5.7 Average change (and standard deviation) in sagittal plane tilt for natural and TKR knees as a result of kneeling.

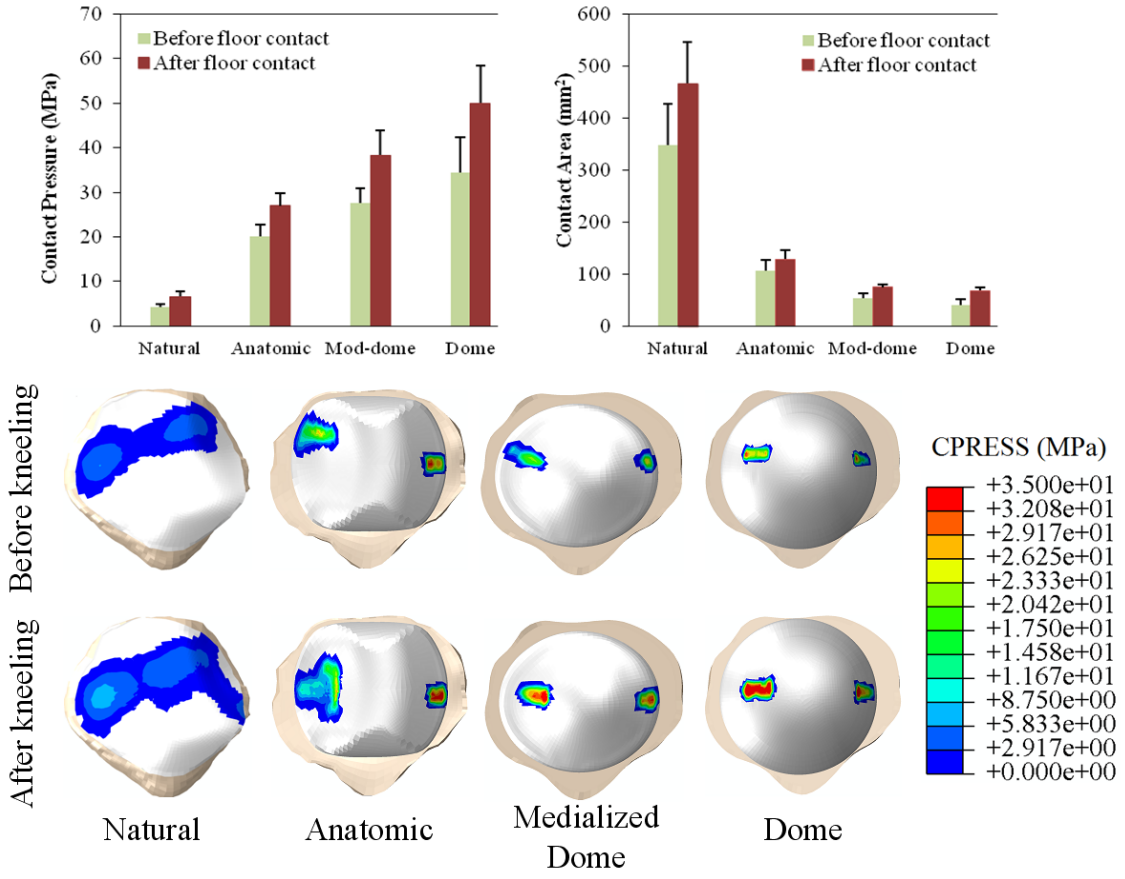

Figure 5.8 Mean and standard deviations in peak contact pressure and contact area before and after kneeling for natural with cartilages and TKR conditions with polyethylene patellar components (top); contact pressure for a representative specimen before and after kneeling (bottom).

Due to the compression-dominated loading condition, minimum principal strains were in the order of 3.2x, 3.0x, 3.3x, 2.1x (natural, anatomic, medialized-dome and dome conditions, respectively) larger than maximum principal strains, and so are of primary concern in the current study. Strain bone results, unless otherwise stated, refer to minimum principal strains. Kneeling resulted in an average of 8.3, 16.0, 12.5 and 13.2% increase in highly strained bone volume in natural, anatomic, medialized dome and dome conditions, respectively. Of the three TKR systems assessed, the medialized dome

demonstrated the lowest bone strain, both before and after kneeling. Highly strained bone volumes were on average 2.3, 1.8, and 2.1 times higher than the natural case for anatomic, medialized dome and dome designs, respectively (Figures 5.9 and 5.10).

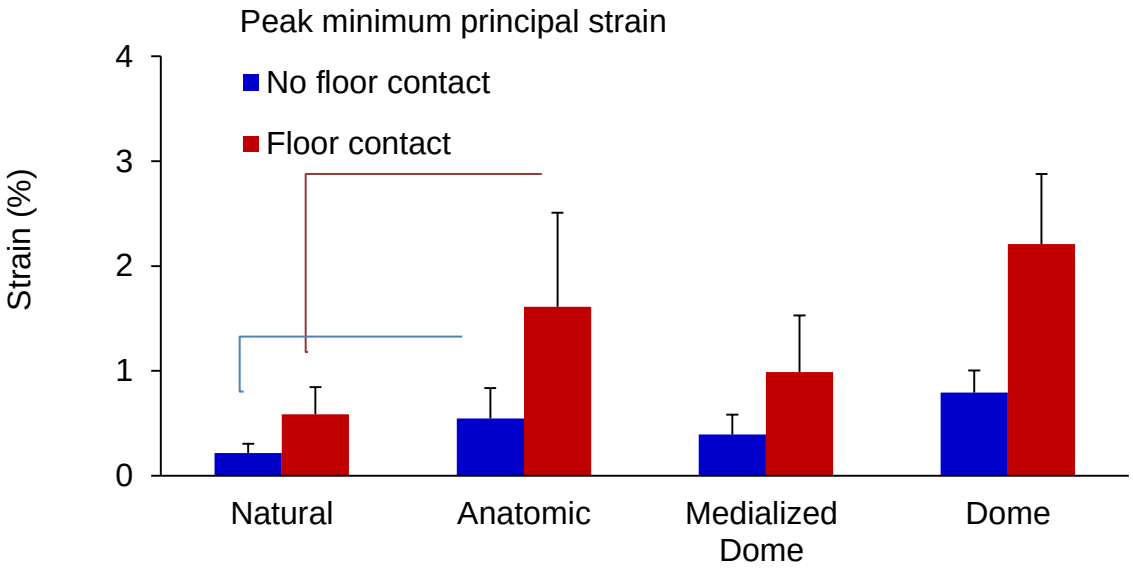

Figure 5.9 Peak compressive principal strains in implanted specimens were higher than natural specimens ($p<0.05$)

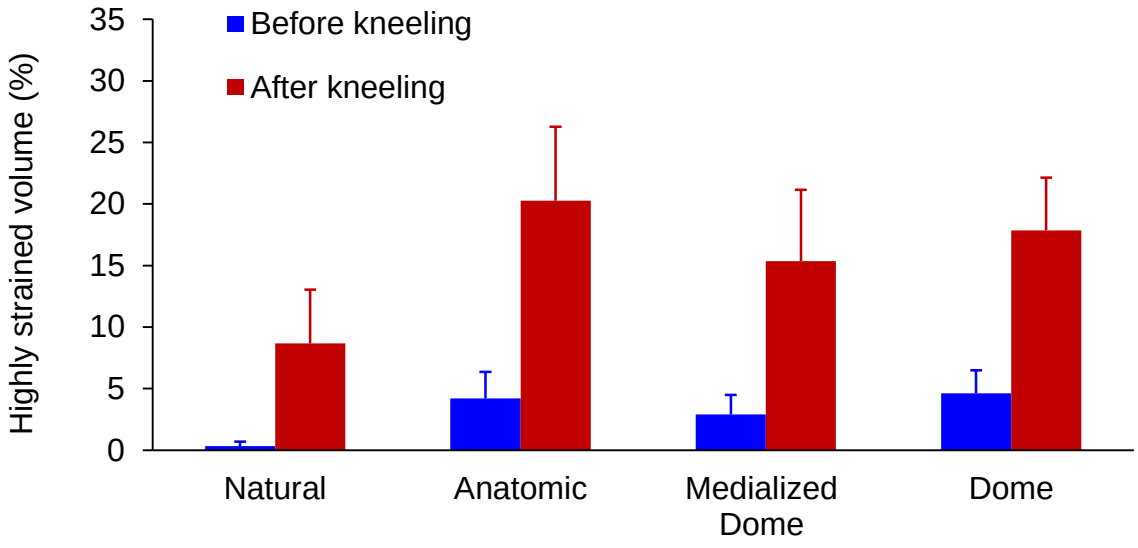

Figure 5.10 Mean and standard deviation in highly strained bone volume before and after kneeling for natural knee and TKR implants.

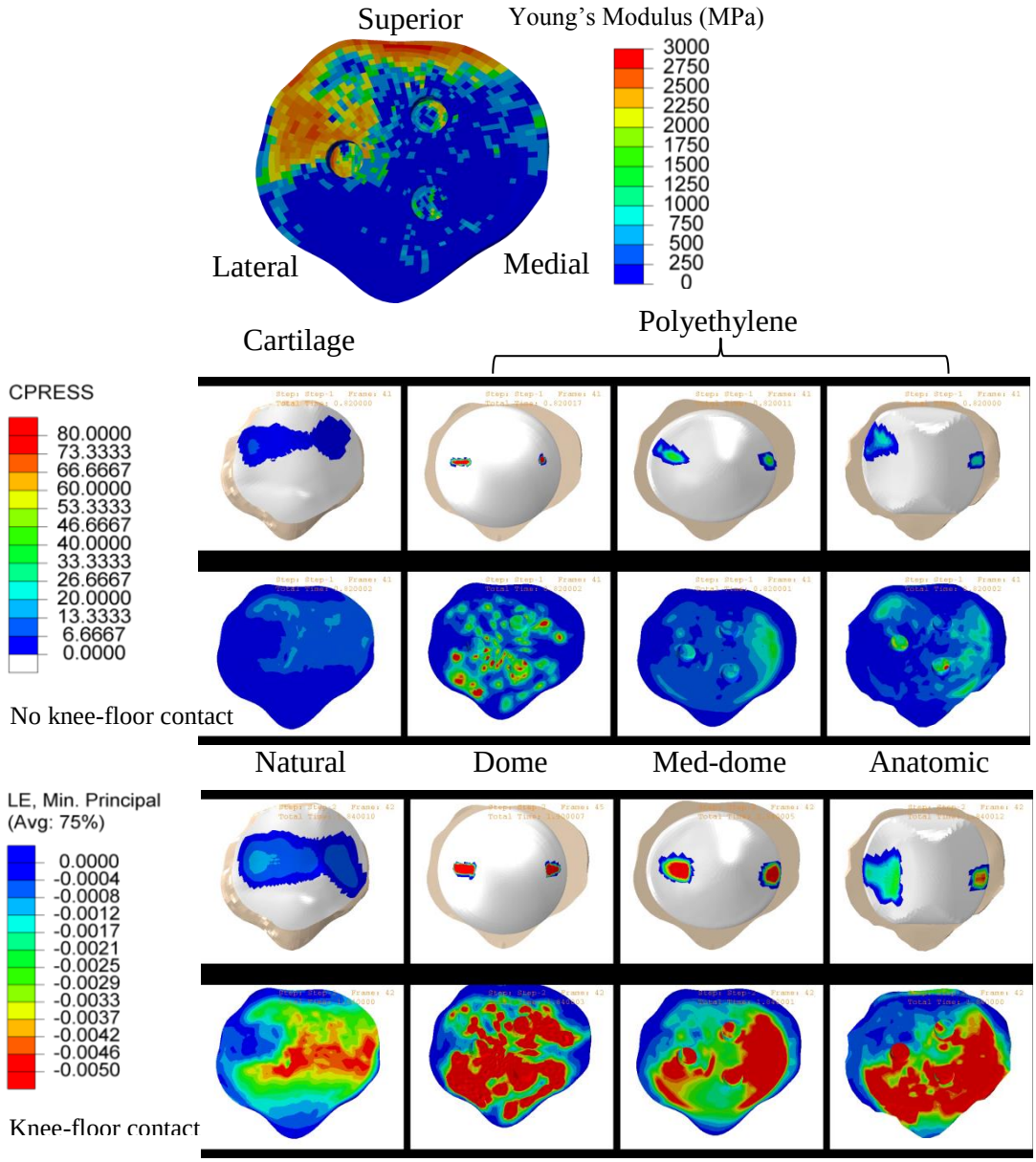

Figure 5.11 Diagram describes relationships between HSV and elastic modulus distributions and between HSV and contact mechanics; Young's Modulus distribution (top), changes in contact pressure and bone strain distributions for a representative specimen before (center) and after kneeling (bottom).

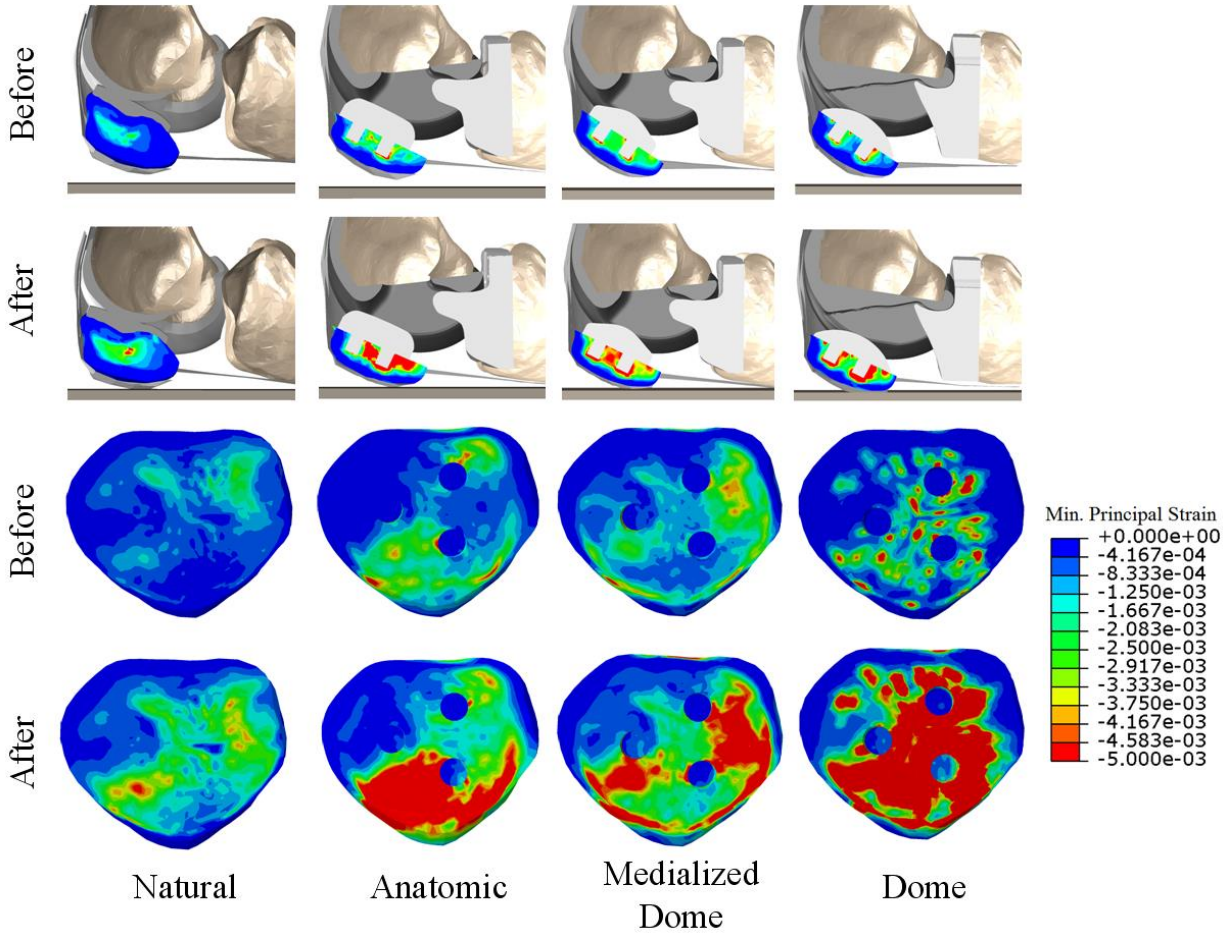

Figure 5.12 Compressive bone strain before and after kneeling for natural knee and TKR implants, shown for a representative specimen.

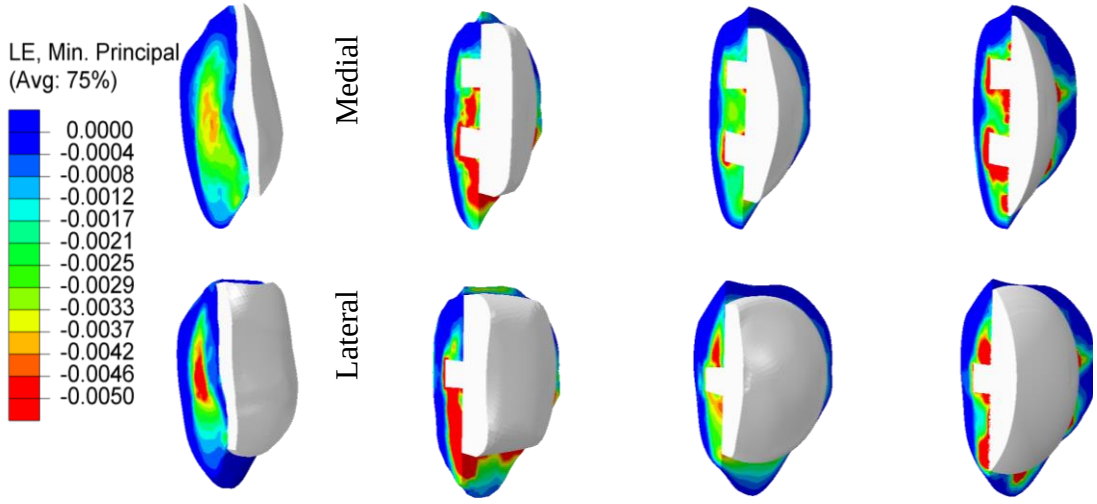

Figure 5.13 Diagram shows bone strain distributions in patellar bone (sagittal cut view)

Bone strain distribution after kneeling reflected the differences in patellar contact, and resulted in larger compressive strains centrally in the natural condition, and inferiorly, medially and laterally in the implanted cases, Figure 5.11. The medial and lateral quadrants experienced the largest highly strain bone volumes across all conditions; this increased significantly as a results of kneeling for all implanted conditions, but there was no significant change in the natural condition, Figures 5.12, 5.13. Anatomic and dome components also experienced significant increase in bone strain in the inferior portion of the patellar bone (Table 1). It should be noted that HSV measure is not used in this work to study pain or bone fracture, this measure is used to show the likelihood of increasing bone strains and where the peak strain might be localized.

Table 5.4 Highly strained bone volume before and after kneeling in the 4 regions (%).

	Inferior	Superior	Medial	Lateral
Natural	0.0 – 2.0	0.0 – 2.9	0.1 – 4.6	0.3 – 6.8
Anatomic	1.5 – 21.4	0.5 – 1.3	3.1 – 17.8	7.2 – 18.1
Medialized-dome	0.2 – 7.0	0.1 – 1.0	2.8 – 20.5	5.4 – 14.0
Dome	3.4 – 14.9	1.1 – 5.1	3.1 – 16.3	6.0 – 16.5

5.4. Discussion

Experimentally-measured TF kinematics during kneeling demonstrated good agreement with previous studies. When these TF kinematics were implemented in the computational model, medial and lateral contact location were also in agreement with prior work (Hamai et al., 2008; Hanson et al., 2007), Figure 5.14.

(a)

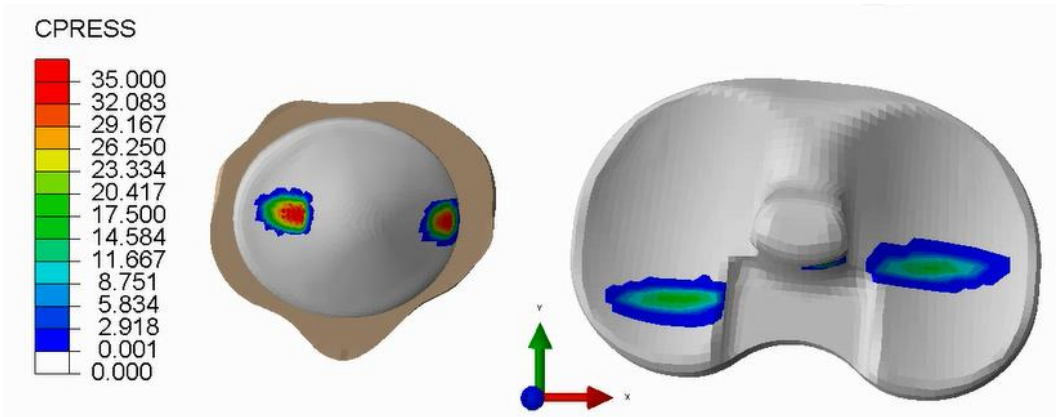

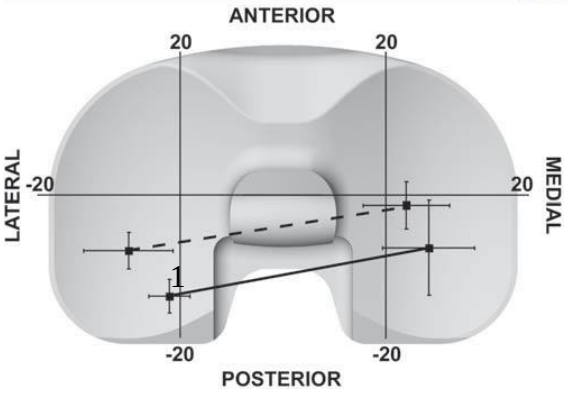

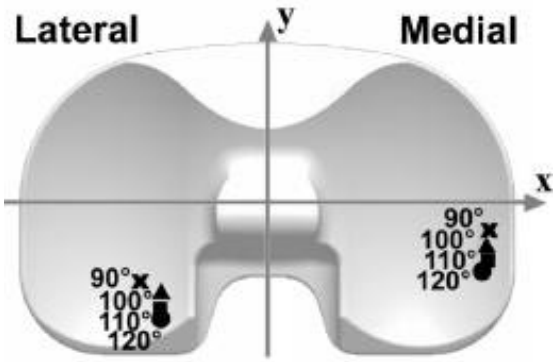

(b)

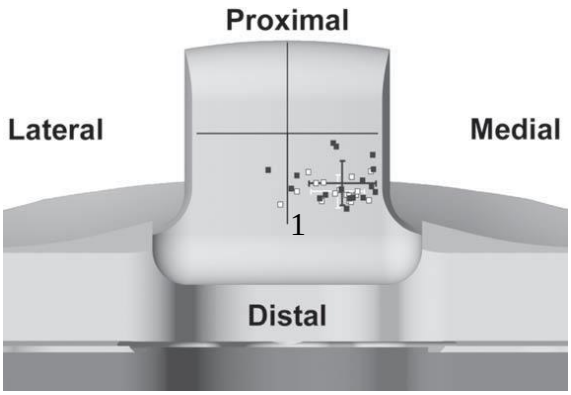

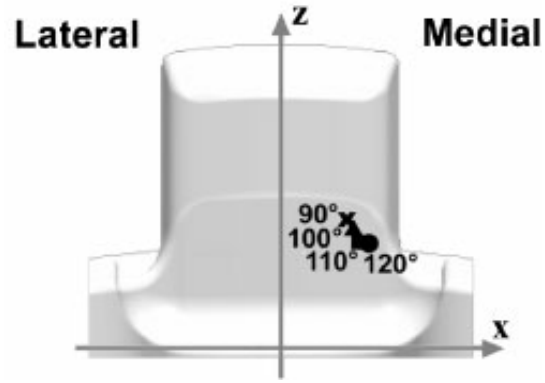

(Hanson et al., 2007) (Hamai et al., 2008)

Figure 5.14 (a) FE model prediction of Tibiofemoral and patellofemoral contact patch and locations at 90^{o} knee flexion after kneeling in the current study. (b) Articular contact location between the femoral cam and polyethylene tibial insert and post during kneeling reported in the literature

Good agreement in PF kinematics between experimental measurements and computational predictions, and appropriate differentiation between conditions, highlight the applicability of the computational model as a complementary tool to experimental testing.As in this study, a limited number of experimental tests may be performed to provide adequate kinematic validation for the computational model, and the model can subsequently be employed to perform additional simulations or slight modifications to the boundary conditions that would be unfeasible (for time, cost or logistically reasons) to perform in vitro.

Computational models also provide additional contact mechanics, stress and strain information that is typically not available from experimental simulations. Patellar contact area predictions from the current model were in excellent agreement with values reported in the literature (Hofer et al., 2011; Wilkens et al., 2007). While it is not possible to provide experimental data to verify the bone strain predictions from this study, good agreement in kinematics and contact mechanics provide confidence in the boundary conditions being applied in the model.

The largest difference between patellar designs was bone strain in the inferior portion of the patellar between anatomic components and medialized-dome and dome components. The anatomic patella, while having sagittal plane tilt closest to the natural condition prior to kneeling, has the greatest amount of congruency between femoral and patellar components. As a result of this geometric constraint, the anatomic component

experienced the smallest reduction in sagittal plane tilt and consequently the anterior surface of the patella experience more inferior contact with the floor, increasing the bending moment and bone strain in the distal pole of the patella. This result is supported by prior clinical studies which reported PF complications due to the inability of an anatomic PF joint to accommodate variations in motion. In a series of 87 TKR knees with anatomic patellar components. MacCollum et al. (1989) reported five cases of patellar fracture caused by increase forces in the patellar bone due the shape of the PF articulation. This was not seen in medialized-dome and dome designs as the change in sagittal plane tilt was significantly higher than the anatomic design, moving the contact between the anterior patella and the floor more superior, which facilitated loading sharing of the compressive load between medial, lateral and inferior regions.

While sagittal plane tilt for the dome was similar to the medialized dome design, the dome experienced higher bone strain as a result of higher contact pressure due to lack of congruency and smaller PF contact area. Predictions from the current study indicate the medialized dome design achieved the optimal balance between sufficient congruency between PF articular surfaces to obtain reasonable contact mechanics, while still facilitating sagittal plane tilt to reduce isolated loading of the distal nose of the patella during kneeling.

The study assessed a single style of kneeling – anterior force was predominately on the patella. Alternative kneeling conditions could result in shifting of floor contact

from the patella to the tibial tubercle. These conditions may warrant further investigation, and the kneeling model described in this study provides an appropriate platform for further comparative analyses. While there are a multitude of TKR designs available, we believe that the three designs evaluated in the current study were representative of the primary styles of patellar components (anatomic, medialized dome, dome) that are currently commercially available.

Chapter 6. Statistical Shape Model

6.1. Background and Motivation

In addition to the shape and type of implants, knee joint morphology also influences knee joint mechanics and patellar bone strain. Therefore, implant performance can vary dramatically between patients. The use of a statistical shape model (SSM) of the joint articular surfaces and the anatomical shape of the ligaments has the potential to more effectively capture the 3D geometry and common modes of shape variation of the joint. Previous studies of statistical shape models of the knee have focused primarily on bone morphology, and have not been linked with functional performance of the joint. There are several patellofemoral joint studies that have looked at the effects of kneeling on contact areas and pressures, knee joint reaction force, and patellar kinematics in eastern and western populations. However, the current research literature lacks a clear basis for understanding the effects of anatomical variations in articular cartilage surfaces and soft tissues.

The main objective was to develop a platform to enable population-based evaluations a statistical shape model with bone, cartilage and ligaments to study the effects of intersubject anatomic variability on natural joint mechanics and to create a

statistical shape model of the knee characterizing the modes of variation using PCA approach. Also to compare geometries and predicted kneeling kinematics using FE analyses.

6.2. Introduction

Subject-specific finite element models including anatomical articular cartilage surfaces and soft tissue geometric representations can provide a powerful framework for analyzing knee mechanics (Pena et al., 2006; Suggs et al., 2003). Predicting knee joint performance based on a single, representative model may not be appropriate; therefore the influence of patient variability must be accounted for (Taylor et al., 2013). A SSM model developed by Baldwin et al. (2010) was used for FE analysis of the articulating cartilages of the knee joint using a mesh-based registration method that represents all specimens with the same number of nodes and elements. Other statistical models have incorporated geometry and material property variations of the femur (Bryan et al., 2010; Querol et al., 2006) and bone-implant interface (Galloway et al., 2012) to develop FE models. Previous work also looked at the relationships between shape and function to study the influence of articular geometry on kinematics and contact mechanics (Fitzpatrick et al., 2011b).

The study was able to develop a novel statistical relation between the shape and mechanics of the patellofemoral joint. A 3D SSM of knee model was used to identify differences among Caucasian, African American, and East Asian populations (Mahfouz

et al., 2012). Additional studies are required to determine whether these differences are clinically important for TKR procedure. A recent study conducted by Rao et al.,(2013) used MR images and relative alignment of the structures at a certain, loaded position in an experimental knee simulator for a training set of 20 specimens. The study developed a procedure that characterized the intersubject variability in bone morphology and alignment for the knee and generated realistic instances for use in FE analysis.

6.2.1. Statistical Shape Modeling

Capturing the variation in our bones plays an important role in subject-specific pre- and intraoperative evaluation and is useful for computational modeling. Several steps are required to build a statistical shape model. Structures of the knee including the bone, cartilage and ligaments can be segmented into virtual 3D geometries for each specimen using their MR or CT images. In order to evaluate intersubject variability within a training set, all 3D geometries should have the same number of nodes and elements and must be aligned in the same space using the same coordinate axes. Through a registration process, each specimen represented by a column of data based, surfaces to point coordinates. This can be done by using an iterative closest point algorithm (ICP) to transform the nodes of a template mesh to match the shape and size of a particular specimen. In the ICP algorithm, the nearest neighbor search was accelerated using k-dimensional (k-d) trees similar to Bryan et al. (2010). Subsequently, each member of the training set was represented by an equal number of data points (nodes) for each bone (Figure 6.1).

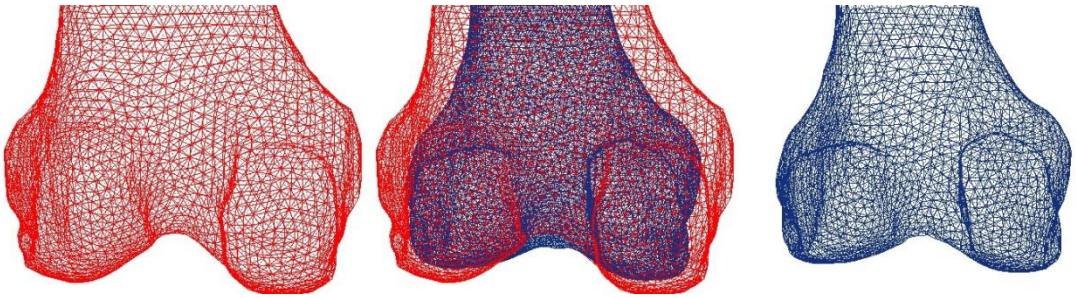

(a) (b) (c)

Figure 6.1 Diagram of 3D mesh of specimen distal femur. (a) Reference mesh, (b) superimposition of a specimen femur with refrenece mesh bofore applying ICP algorithm, (c) specimen femur genereted from reference mesh.

6.2.2. Principal Component Analysis

Jolliffe (2002) defines principal component analysis (PCA) as:

> A process aimed to reduce the dimensionality of a data set consisting of a large number of interrelated variables, while retaining as much as possible of the variation present in the data set. This is accomplished by transforming to a new set of variables, the principal components (PCs), which are uncorrelated, and which are ordered so that the first few retain most of the variation present in all of the original variables.

The PCA approach was used in this study to reduce the size of the training set data into its principal modes of variation and allow the generation of new specimen instances.

6.3. Materials and Methods

This study developed a FE platform to perform population-based evaluations of the healthy normal knee in activities of daily living such as kneeling while considering the impact of variability. The framework of method in illustrated in Figure 2.6.

6.3.1. Preparation of The Training Set

Forty natural knees were included in the training set. The specimens were on average 65 years with an average weight of 72 kg and average body mass index (BMI) of (25.1). Detailed statistics on the specimens based on gender have been shown in Table 6.1.

Table 6.1 Demographic details of specimens used in study (male-female)

	Age (years)	Height (m)	Weight (kg)	BMI (kg/m^3)
Mean	66-63.45	1.76-1.62	77.42-66.95	24.87-25.26
Standard deviation	9.90-8.42	0.06-0.06	12.26-13.37	3.57-3.92
Max	80-78	1.85-1.73	100-91.8	29.9-33.85
Min	52-52	1.66-1.49	60.78-42.60	19.79-18.97

6.3.1.1. Bones

Of the 40 specimens, 20 males (cadaveric) and 20 females from the Osteoarthritis Initiative (OAI) were scanned and segmented from MR images with an in-plane resolution of 0.35 mm and an axial slice thickness of 1 mm, using ScanIP (Simpleware, Exeter, UK). As a reference, the left knee joint was segmented for each specimen. Sixteen specimens were right knees that were later modeled as left knees by mirroring the model at the mid sagittal plane. The template mesh of the bony structures was developed for a median-sized specimen of the training set. The template mesh for the femur, tibia and patella consisted of 2384, 1101 and 472 nodes, respectively. All bones were represented by a triangular finite element surface mesh.

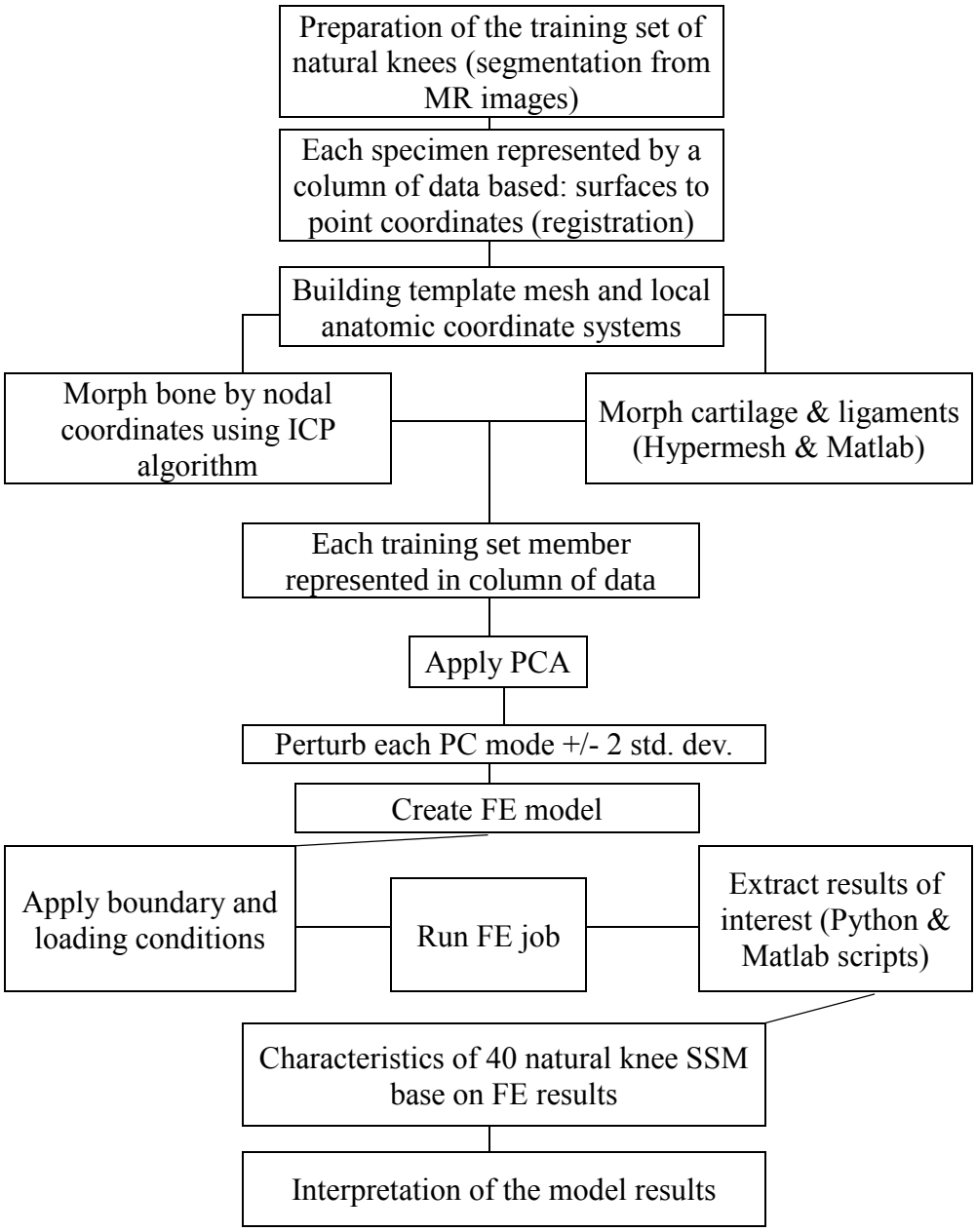

Figure 6.2 Workflow diagram of SSM and function model as used in this study

6.3.1.2. Articular Cartilages

The cartilage structures were also segmented manually and represented by 3D linear hexahedral elements because of their improved behavior in FE contact mechanics. The cartilage meshing process was based on previous work by Baldwin et al. (2010). An average structure or template of these hexahedral elements in the shape of the cartilage was developed. This template mesh was subdivided into sets of contiguous hexahedral elements to create groups (domains) bounded by control points (handles) on the group angles (Figure 6.3). Nodal handles were used to morph the hexahedral mesh template to the subject-specific geometry using a custom TCL/VTK script with Hypermorph (Altair, Troy, MI) developed by Fitzpatrick et al. (2012). The script creates 1200, 264, 240 and 390 handles for femoral-cartilage, tibial-medial-cartilage, tibial-lateral-cartilage, and patellar-cartilage geometries, respectively, and produced hexahedral elements (2748, 990, 825, and 504 elements for each cartilage, respectively) across the thickness of each cartilage.

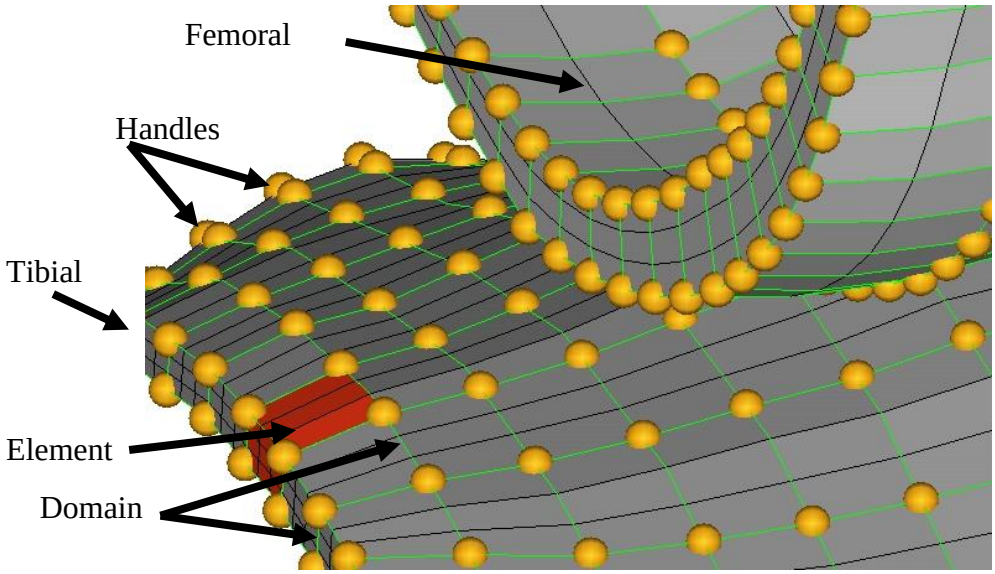

Figure 6.3 Diagram describing an element group, domains and control handles within a template mesh.

6.3.1.3. Ligaments and Tendons

Based on a similar concept described by Baldwin et al. (2010), differences between the soft tissue template (comprised of ligaments and tendons) and the subject-specific point coordinates of their landmarks were automatically exported and applied as morphing commands to the template mesh within Hypermesh. This was done during the segmentation process of reproducing bones and cartilages from MR images for each member in the training set.

There were seven attachment sites of ligamentous and tendinous tissues including: (1) the anterior cruciate ligament (ACL), (2) posterior cruciate ligament (PCL), (3) the medial collateral ligament (MCL), (4) the lateral collateral ligament (LCL), (5) patellar

ligament (PL), (6) rectus femoris (RF), (7) vasti tendon was separated into five bundles representing the vastus intermedius (VI), vastus lateralis longus (VLL), vastus medialis longus (VML), vasti lateralis obliquus (VLO), and vasti medialis obliquus (VMO) (Fitzpatrick et al., 2011b). 127 ligament attachment points are shown for mean specimen of training set in Figure 6.4.

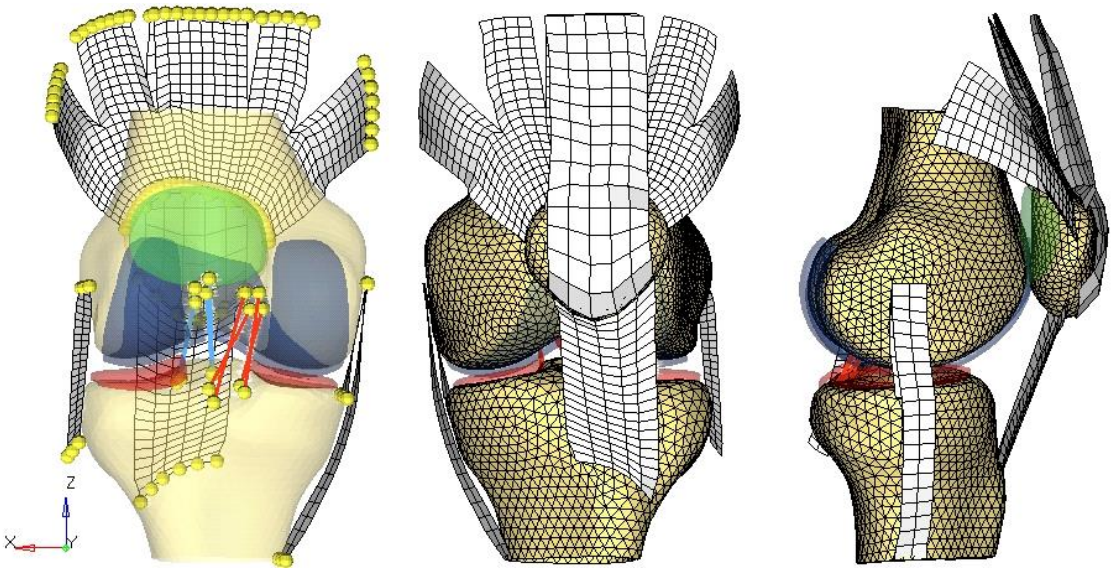

a b

Figure 6.4 Diagram illustrates soft tissue morphing process based on their attachment sites, (a) ligaments landmarks presents in numbers of points, (b) frontal and medial views after morphing.

Rectus femoris and vasti tendons' scale and proximal point locations were approximated based on colorations between the soft tissue attachments sites lengths on the anterosuperior patellar spur at the quadriceps tendon insertion site and proximal rectus femoris width measured from MR images. Morphing process included; registration of attachments sign by a number of points for each ligament, create a column of data for

their coordinate information, then using Matlab code to morph the points on the template to the new positions for each subjects.

6.3.2. Finite Element Model

Using the computational model described in Chapter 5, identical boundary conditions were used to represent the physiological loads applied to the knee joint during kneeling. The cartilages and soft tissue representation and properties were used for all subject models reported in the literature. The current analysis was based on physiological loading conditions and prior finite analyses; quadriceps load (Atkinson et al., 1997; Farahmand et al., 1998; Stäubli et al., 1999), anterior kneeling load (Hofer et al., 2011; Wilkens et al., 2007), articular surface representations and morphing process, (Baldwin et al., 2010) and contact interaction (Fitzpatrick et al., 2012a). Specimen-specific models were developed for the 40 specimens of the training set (Table 6.1).

Bones, cartilage and ligaments were aligned in the initial position of the kneeling activity based on scan space obtained MRI images. During the kneeling simulation, TF kinematics were fully prescribed based on experimentally measured kinematics. The kneeling position used in this study was ankle extended and in contact with the floor along with the knee. The knee was flexed to a 90º TF kneeling position, with other TF kinematics prescribed according to kinematic measures taken from the literature (Hamai et al., 2008; Hanson et al., 2007; Hofer et al., 2011). A muscle load of 550 N was distributed among the quadriceps bundles according to their physiological cross-sectional

area (Farahmand et al., 1998), and an anterior load of 330 N (½ BW, representing double-stance kneeling) was applied through the floor (Hofer et al., 2011; Wilkens et al., 2007). During the kneeling simulations, the patella was unconstrained in six degree of freedom. TF was constrained in 5-dof and IE rotation was prescribed as reported by Hofer et al. (2008) and Wilkens et al. (2005).

Knee bones were represented by 3-noded linear rigid triangular surface elements for each specimen. The number of elements for the femur, tibia and the patella were 4725, 2161 and 940, respectively. The cartilage structures were represented by three layers of eight-noded linear hexahedral meshes (Baldwin et al., 2010). MCL, LCL, PL, RF and Vasti were represented by deformable hyperelastic 2D membrane elements; with uniaxial tension characteristics tuned to match literature values (Atkinson et al., 1997; Stäubli et al., 1999) whereas ACL and PCL were each represented by four 1-D springs (Figure 6.4a). These springs were carefully orientated to represent attachment area centers of four subdivided areas on femoral and tibial bones. This method along with ACL and PCL ligament mechanical properties were similar to previous work by Baldwin et al. (2009b). The extensor mechanism representation was also similar to Baldwin et al. (2009) and Fitzpatrick et al. (2012a).

6.4. Results

The training set data used in this study has specimens' nodal coordinates and relative joint alignment in form of transformation matrix. All initial alignment for each

member was in the ‘scan space’ from the MRI or CT scans however all specimens were aligned in the coordinate system of the template mesh by using relative transformation matrix information. The data representing the variability in the training set is essentially reduced from the 18,564 individual variables (nodal coordinates for bones, cartilages and ligaments, and transformations) to a series of eigenvalues and eigenvectors. Based on anatomical measurements, the amount of variation existing within the training set was relatively large and visibly distinguishable between tall and short subjects. However, that was not the case for patellar dimensions (Figure 6.5).

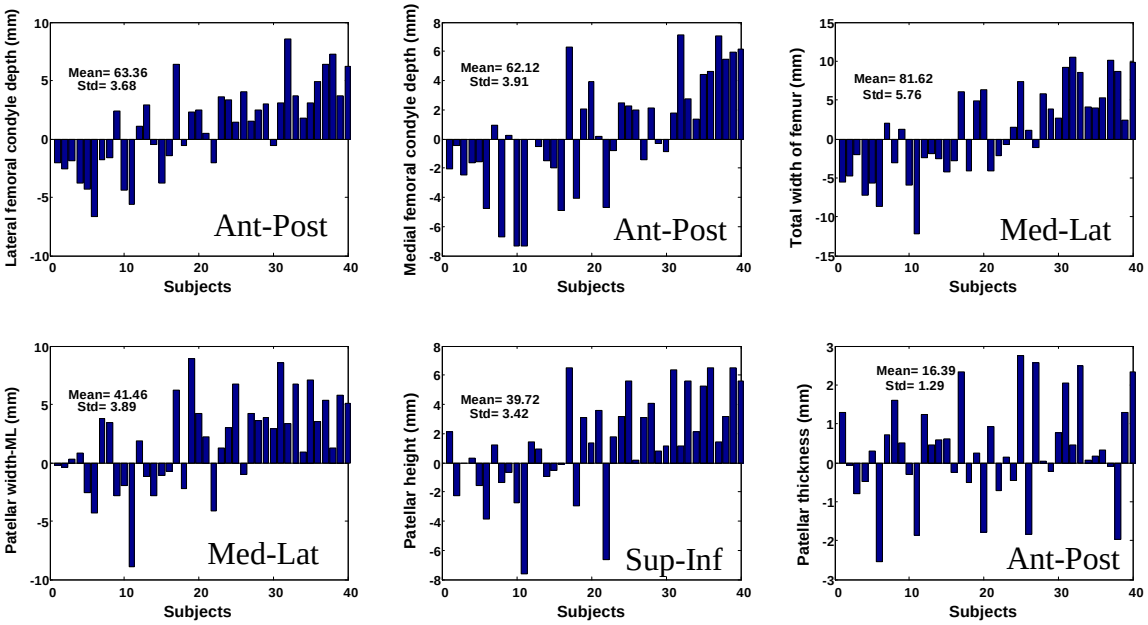

Figure 6.5 Charts show the variation in femoral and patellar bone geometries present in training set based on difference to the baseline of average femur and patella geometries. Specimens are shown with respect increasing height.

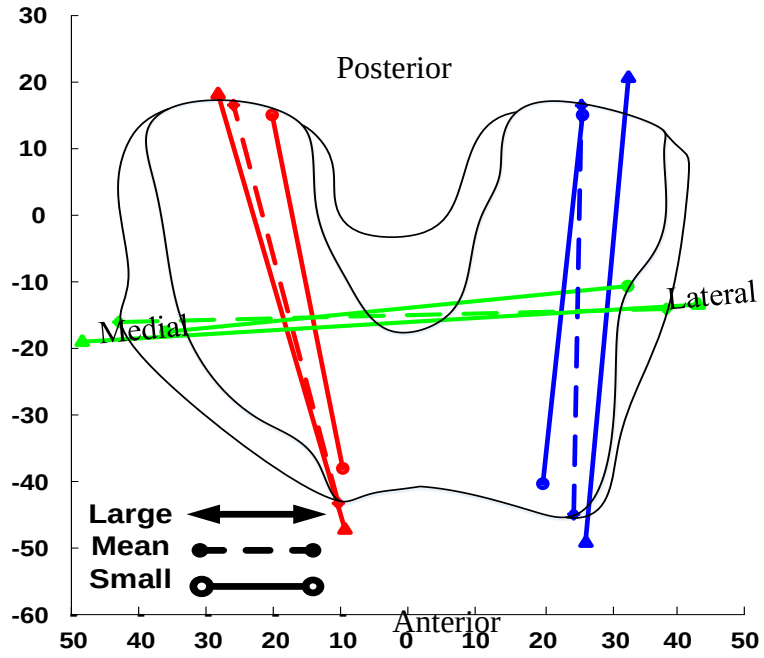

Figure 6.6 Dimensions measured from the distal femur in (mm): depth of the lateral femoral condyle (blue), depth of the medial femoral condyle (red), and femoral width (green)

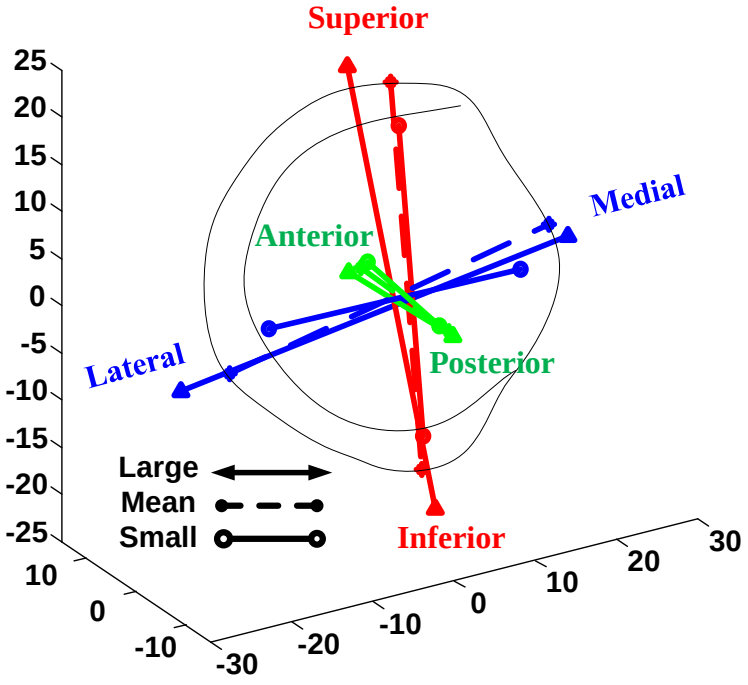

Figure 6.7 Dimensions measured from patellar bone in (mm): medial lateral width (blue), superior-inferior depth (red), and patellar thickness (green)

Table 6.2 Summary of anatomical dimensions of femoral and patellar bones of the training set

Dimension (mm)	Mean	Std	Max	Min
Lateral femoral condyle depth	63.36	3.68	71.90	56.71
Medial femoral condyle depth	62.12	3.91	69.22	54.76
Total width of femur	81.62	5.76	92.08	69.36
Patellar width	41.46	3.89	50.38	32.53
Patellar height	39.72	3.42	46.22	32.08
Patellar thickness	16.39	1.29	19.15	13.83

In Figures 6.6 and 6.7, the dimensions are in millimeters (mm) from the distal femur as reported by Mensch et al. (1975) and summarized in Table 6.2; lateral femoral condyle depth (anteroposterior length), medial femoral condyle depth, total width of femur and width, height and thickness of the patellar bone. Figure 6.5 shows the wide range of geometric variation that is present, and measurement details confirm that scaling in one anatomical dimension may not always match with another. This can be verified by visual examination all training set specimens; for instance, specimen 18 has the smallest distal femoral and patellar bone sizes in the training set but this uniformity does not apply for largest bones in the training set. Specimen 24 has the largest distal femoral bone and specimen 37 has the largest patella.

6.4.1. Shape and Size variability

The SSM model described the variability in the training set with a series of modes of variation defined by eigenvalues and eigenvectors (Figure 6.8). The PCA method allowed reduction of the numerous variables from 18,564 (nodal coordinates and transformations). The PCA result is a statistical shape model defined by a series of modes

of variation represented by the principal components or eigenvalues. The different modes of variations define the variations in size and shape of the structures and when linearly superposed represent the overall variability. This SSM study of natural knee model characterized the dominant modes of variation with the first 3 modes representing 52% of the variability (Table 6.3).

Table 6.3 Bone and ligaments: cumulative variability explained and description of characterized behavior for the most significant modes of variation.

Mode	Variability (%)		Mode Characteristics
	Variance Captured	Total Variance	
1	32.319	32.32	Uniform scaling of TF joint, Patellar thickness (AP) constant, Patella bone scaling in ML and IS Tibiofemoral ligament scaling
2	12.117	44.43	Scaling in patellar thickness, patellar Baja (+2σ) femoral intercondylar notch depth ± 3 mm femoral total width ± 5 mm from the mean TF-VV
3	7.765	52.20	Tibial bone AP scaling, scaling soft tissues, patella alta (-2σ) Soft tissues scaling

Each mode was perturbed by ± 2 standard deviation (σ) to identify the modes of variation. Mode 1 (32.3 %) captured the uniform scaling in tibiofemoral joint that showed also change in the lengths of MCL and LCL ligaments but there wasn't significant change in scaling in medial-lateral and superior-inferior patella size and patellar thickness remained constant. Mode 2 (12.13%) described the uniformity patella size in ML and IS so the perturbation by ± 2σ does not affect the width and the height of the mean in these

directions (~40 mm diameter in ML and SI). However, patellar thickness varied from the mean by ~ ± 1.4 mm.

In order to characterize shape instead of size differences, deviations from mean dimensions of main patellofemoral parameters are present in Table 6.5. Sagittal measurements showed that Mode 2 with +2σ has a patella Baja (patella infera) measurement with Insall-Salvatti Index (Insall et al., 1971), (ISI) < 0.8 whereas perturbation by -2σ did not show any abnormality in patella alignment or scaling in the soft tissue. There were a slight scaling in tibiofemoral bones and ligaments in Mode 2. Mode 3 (7.8 %) described significant scaling in joint soft tissues. This is may be due to initial alignment in scan space, not controlled, therefore this characterization needed to be verified under physiological boundary and loading conditions. Mode 3 also captured minor alterations in patella and femur shapes but scaling in tibial plateaus ±2 mm only in anteroposterior direction.

Table 6.4 Average dimensions of main patellofemoral parameters and variation from mean dimensions when shape modes are varied by ±2 standard deviations.

		Femur dimensions and size differences (mm)				Sulcus angle (deg.)	Patella shape mean and differences (mm)		
		M–L width	A–P Medial	A–P Lateral	Intercondylar notch width		M-L	S–I	A-P
Mean		81.62	59.78	62.10	21.63	144.14	41.46	39.72	17.54
PC1	+2σ	-10.47	-6.60	-4.91	+2.26	-2.44	-5.36	-4.30	-0.11
	-2σ	+11.26	+6.62	+7.55	-2.79	+3.17	+5.62	+5.10	+0.02
PC2	+2σ	-2.12	-1.16	-0.67	-0.32	-0.05	+0.15	-0.25	-0.55
	-2σ	+2.29	+0.92	+0.18	+0.10	+2.71	+0.69	+1.19	+1.36
PC3	+2σ	+1.37	-1.13	-0.27	-2.26	+0.66	+1.13	+1.83	+1.23
	-2σ	-0.84	+0.97	+0.56	+2.10	+3.11	-0.01	+0.26	+0.44

The nature of the alterations to knee joint shape observed in this study is interesting because the measurement of width, height and thickness of bones such as patellar have been shown to be important factors in bone resurfacing. However in reality, the shape of the joint bones could be a result of a number of combined modes that was not captured by this training set.

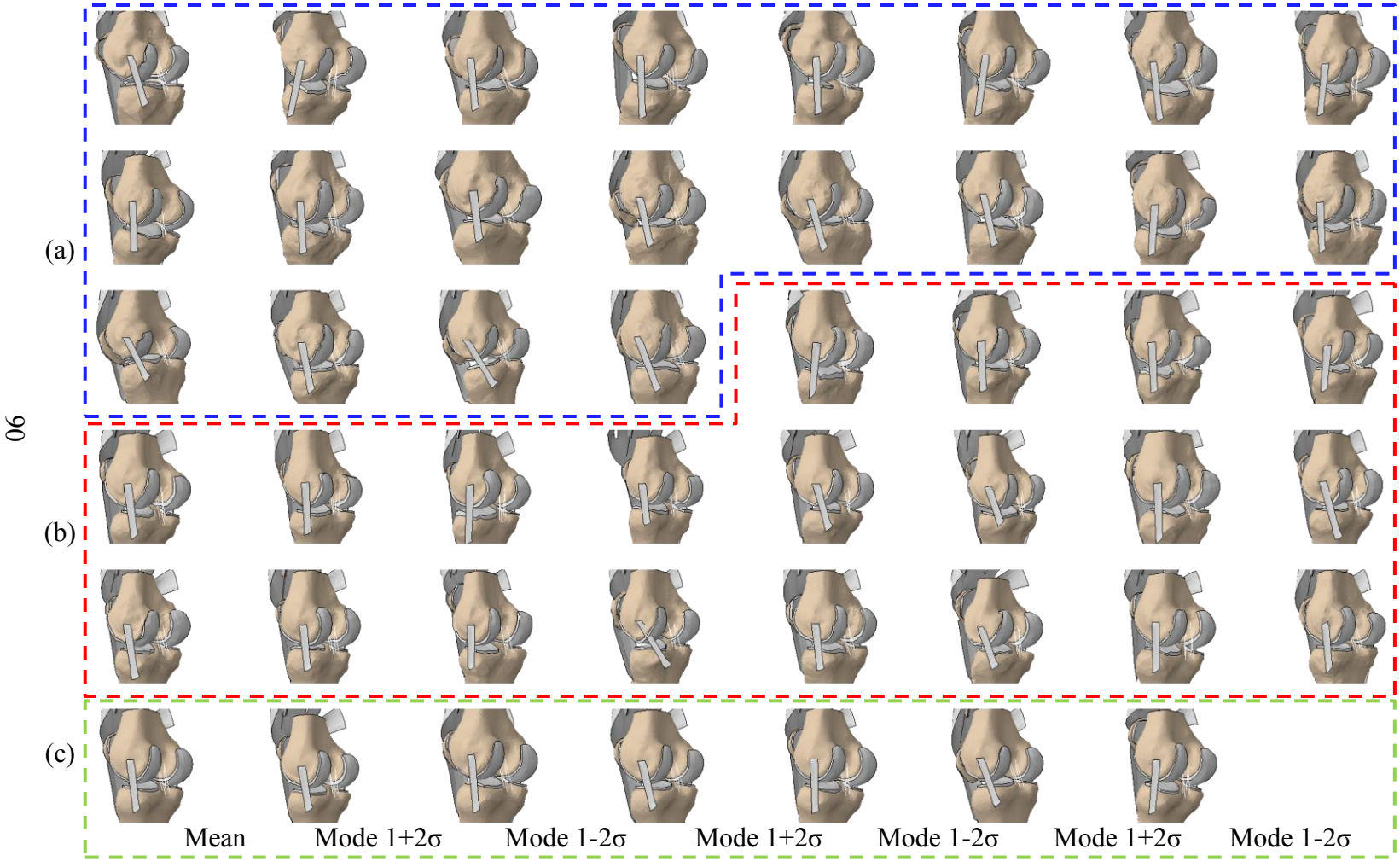

Figure 6.8 Statistical shape model showing the training set (a) males (b), female) and (c) mean and first three modes at ± 2σ

6.4.2. Finite Element Analysis on Generated SSM

One of the objectives of this study was to use the SSM to create new instances of the knee joint that include bones, cartilages, ligaments and tendons that can perfectly and directly be used in finite element analyses. FE studies have explored interactions between shape and function in the natural knee and assessed the impact of intersubject and alignment variability in the implanted knee (Laz et al., 2007). The second part of this study was to develop an FE platform to perform population-based evaluations of natural in kneeling activity and considering the impact of variability in the shape. Using a validated kneeling model, boundary and loading conditions prescribed in chapter 5 were performed on 47 specimens (training set, mean and three modes with ± 2σ) (Figure 6.7).

6.4.3. Shape Variability and Joint Mechanics

The statistical shape-function model showed relationships between joint geometry and mechanics. Using a similar predictive approach developed by Fitzpatrick et al. (2011b), to investigate the relationships between geometrical parameters and modes of variation, this study altered the values of the shape parameters in order to quantify the effect on joint kinematics and contact mechanics. Altering the first shape value by +2σ resulted in a smaller patellofemoral shape. Interestingly, PF kinematics due to knee-floor contact during kneeling has not been affected by knee joint scaling (Figure 6.11 and 6.13). However, smaller PF joint showed a considerable change in contact mechanics

(Figures 6.9, 6.12). Conversely, varying the second shape parameter by +2 standard deviations resulted in a more inferior positioned patella (patella baja), and an increase of the femoral intercondylar notch depth (+ 3 mm) caused a decrease in patella tilt with respect to the femur in sagittal plane, anterior-posterior and superior-inferior translations. There were no important contact mechanics variations in the second mode despite the variation in patellar thickness. Varying the third shape parameter by ±2 standard deviations resulted in scaling of the soft tissues causing more significant variations in contact mechanics and PF kinematics during kneeling. Altering mode 3 by (-2σ) resulted in a more superiorly positioned patella (patella alta) that caused PF contact area locations remained at superior region of the patella at 90^{o} flexion both before and after floor-patella contact (Figure 6.10, 6.11). Patellofemoral kinematics varied considerably with perturbations for mode 3 in terms of patellar spin, internal external rotation and medial lateral translations during kneeling.

6.5. Discussion

The process of generating specimen-specific FE models of knee joint with bone, cartilages and soft tissue for large populations is time-consuming. Therefore, the objective of this study was to create a framework that can be used to generate large numbers of new and unique instances with realistic variations of human knees in a finite element analysis format.

The SSM model developed in this study describes the principal modes of anatomic variation of natural knee. Three modes of variation captured 52.2 % of the variability. SSM model captured intersubject variability in anatomy including bones, cartilage and soft tissue representations. Joint dimension was the main cause of variability, describes one third of the total shape variability in the whole knee joint. Position of the patella (baja) and the depth of femoral intercondylar notch accounted for a further 12.1% of variability. TF and PF relative alignment and soft tissue dimensions accounted for 7.6% of variability. The statistical shape and function model employed a validated finite element model to characterize relationships between shape, PF kinematics and contact mechanics in high flexion activity such as kneeling using FE analysis. This study is a shape-function characterization tool to predict the relations of kinematic behavior and contact mechanics in highly dynamic activities as a function of shape parameters. The main findings in this study showed that scaling in the knee joint has minor effect on PF joint kinematics but greatly affects joint contact mechanics. However, knee soft tissue dimensions alter the kinematics.

The study predictions are based on initial alignment of knee joint in the as-scanned position. Therefore, there is some uncertainty in the actually dimensions of soft tissues. This statistical shape and function model has not included the variability in mechanical properties of soft tissues and loading conditions. Accounting for soft tissue property variability can improve the robustness of the model predictions.

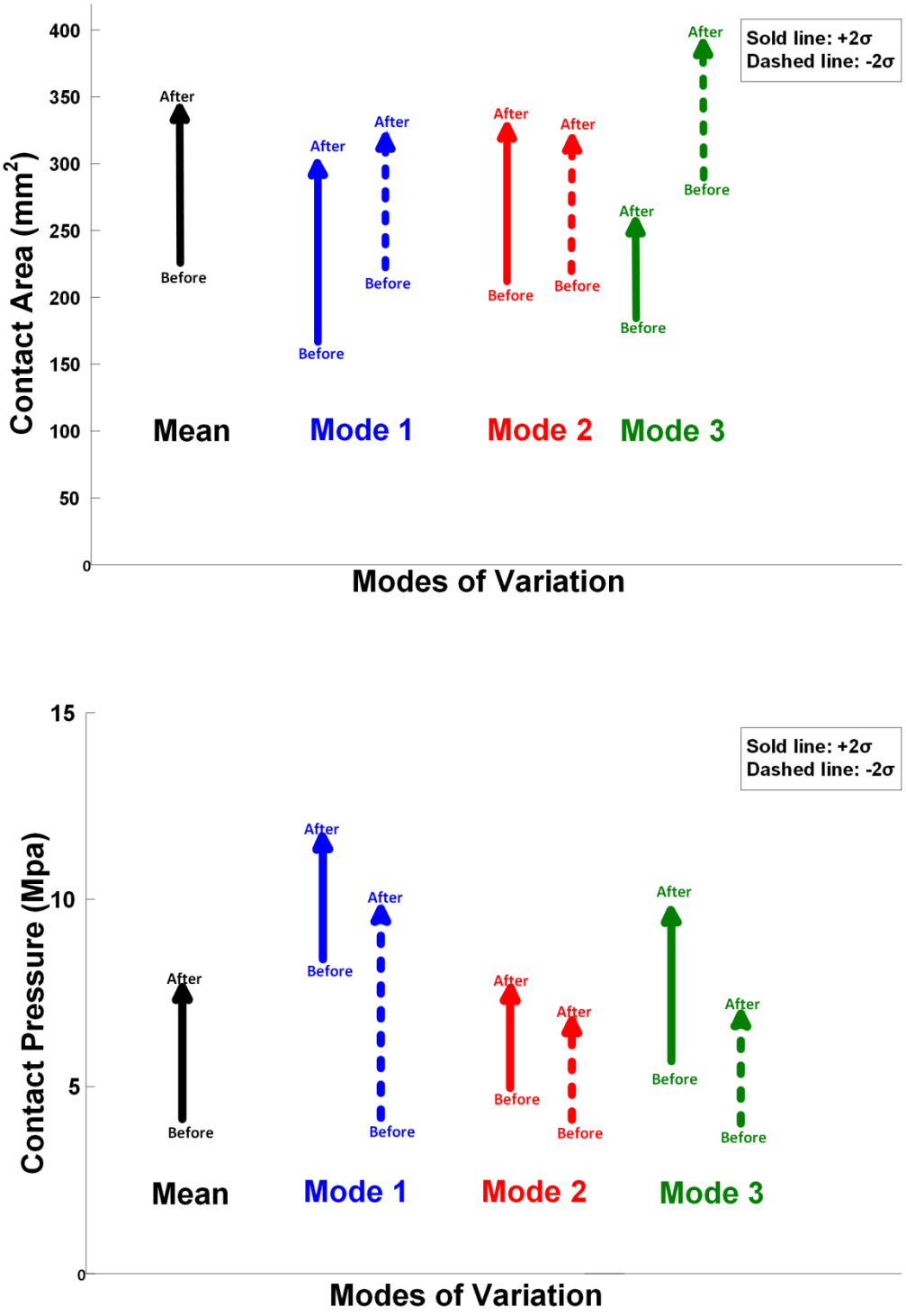

Figure 6.9 Diagram of mean and standard deviation of contact area (top) and contact pressure (bottom) before and after kneeling for 40 specimens (bar chart). Mean of training set and variation of the first three modes (arrows)

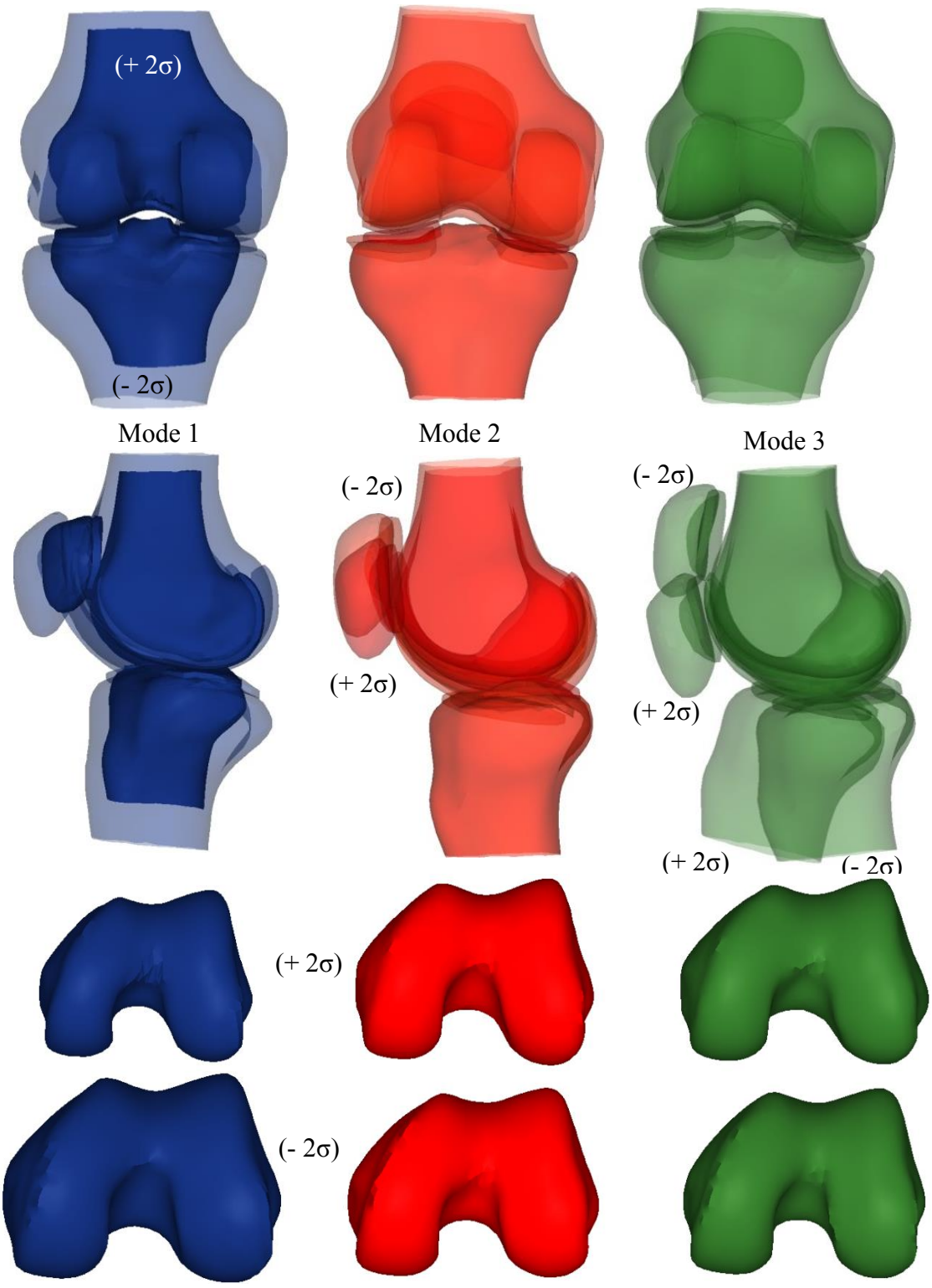

Figure 6.10 Modes of variation for the statistical shape model presented at ± 2 standard deviations.

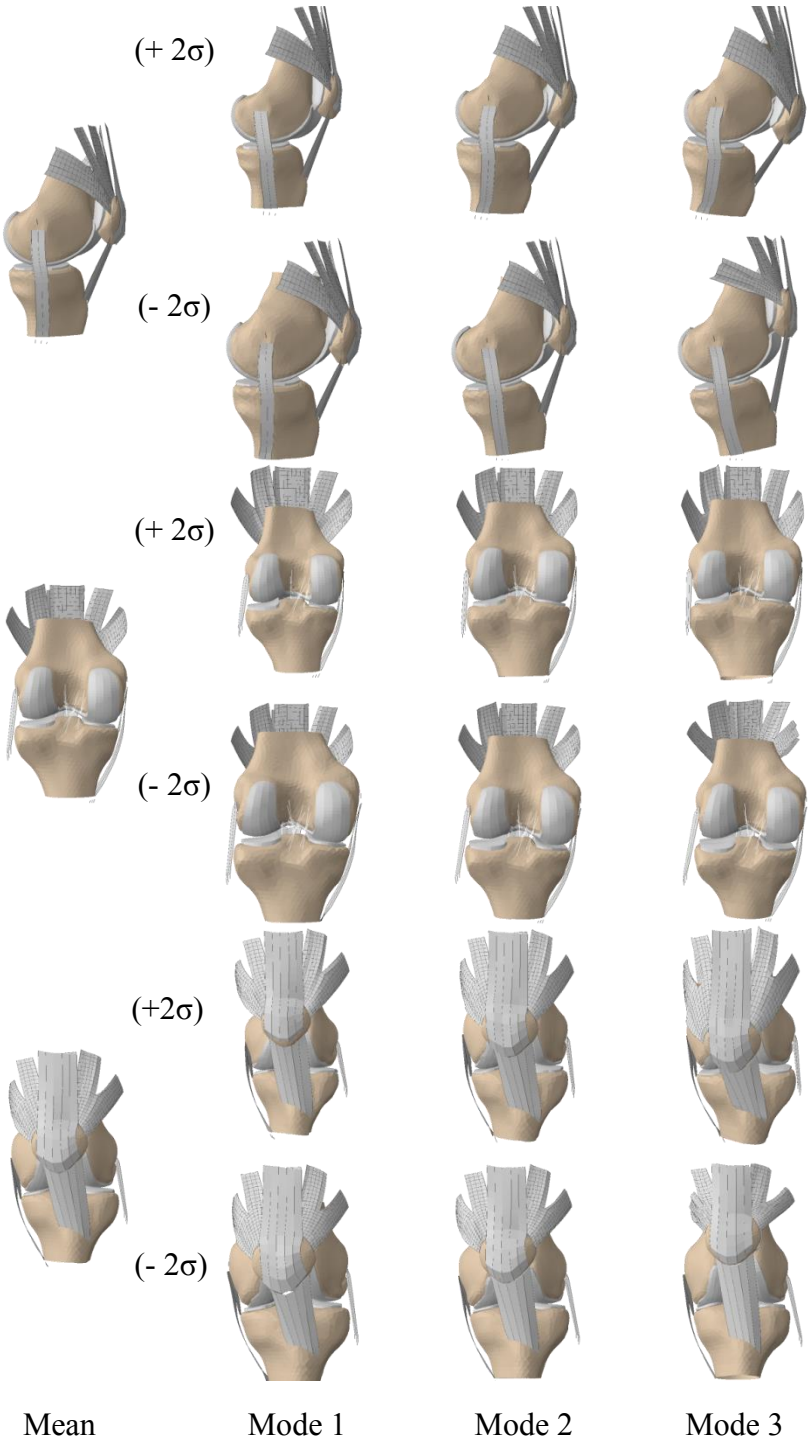

Figure 6.11 Shape variation in the first three modes with ± 2 standard deviation; (top) medial view, (center) posterior view, (bottom) frontal view

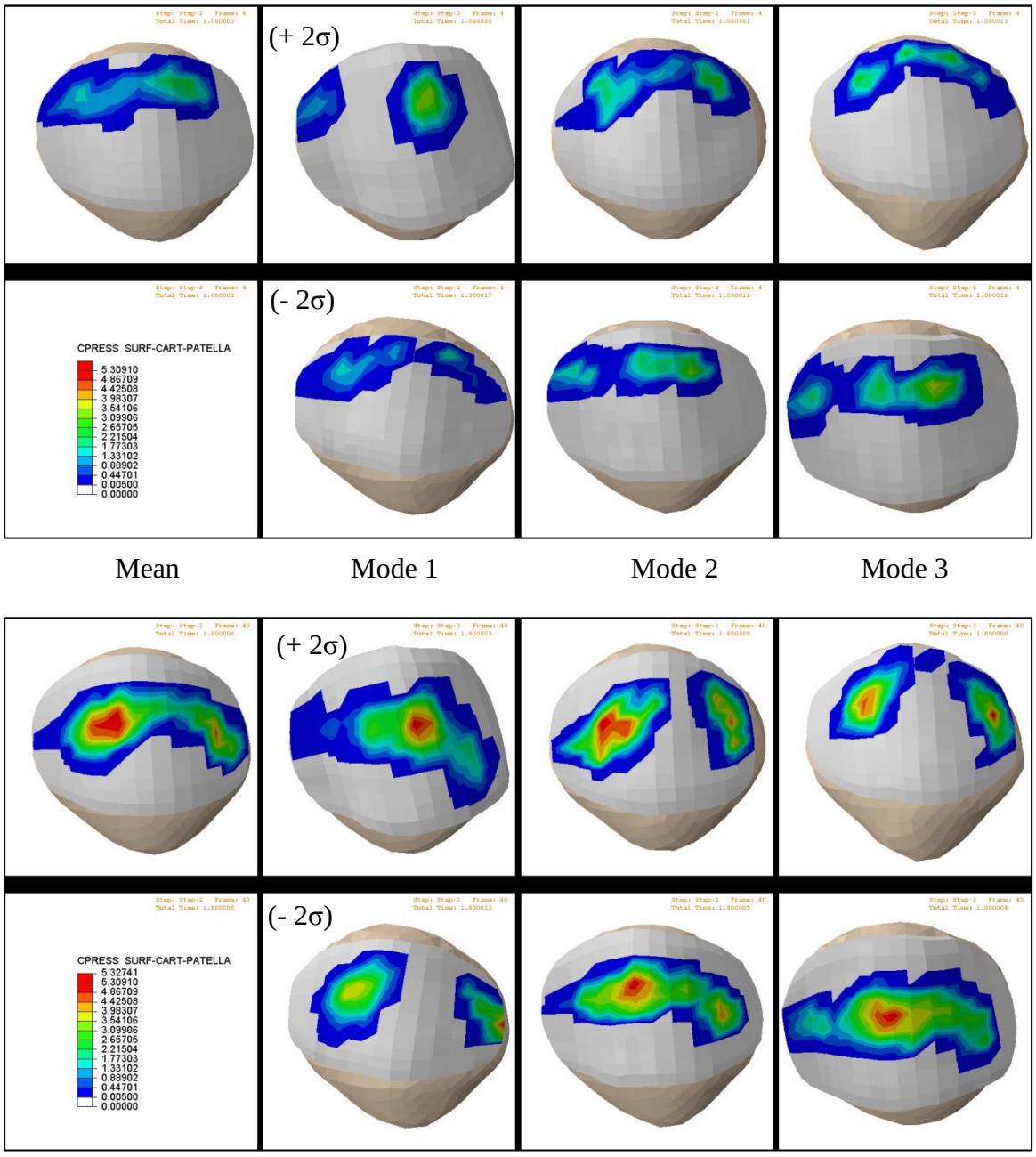

Figure 6.12 Change in patellofemoral contact mechanics shown for mean and ±2 standard deviation for the three modes of variations before (top) and after (bottom) floor-patella contact

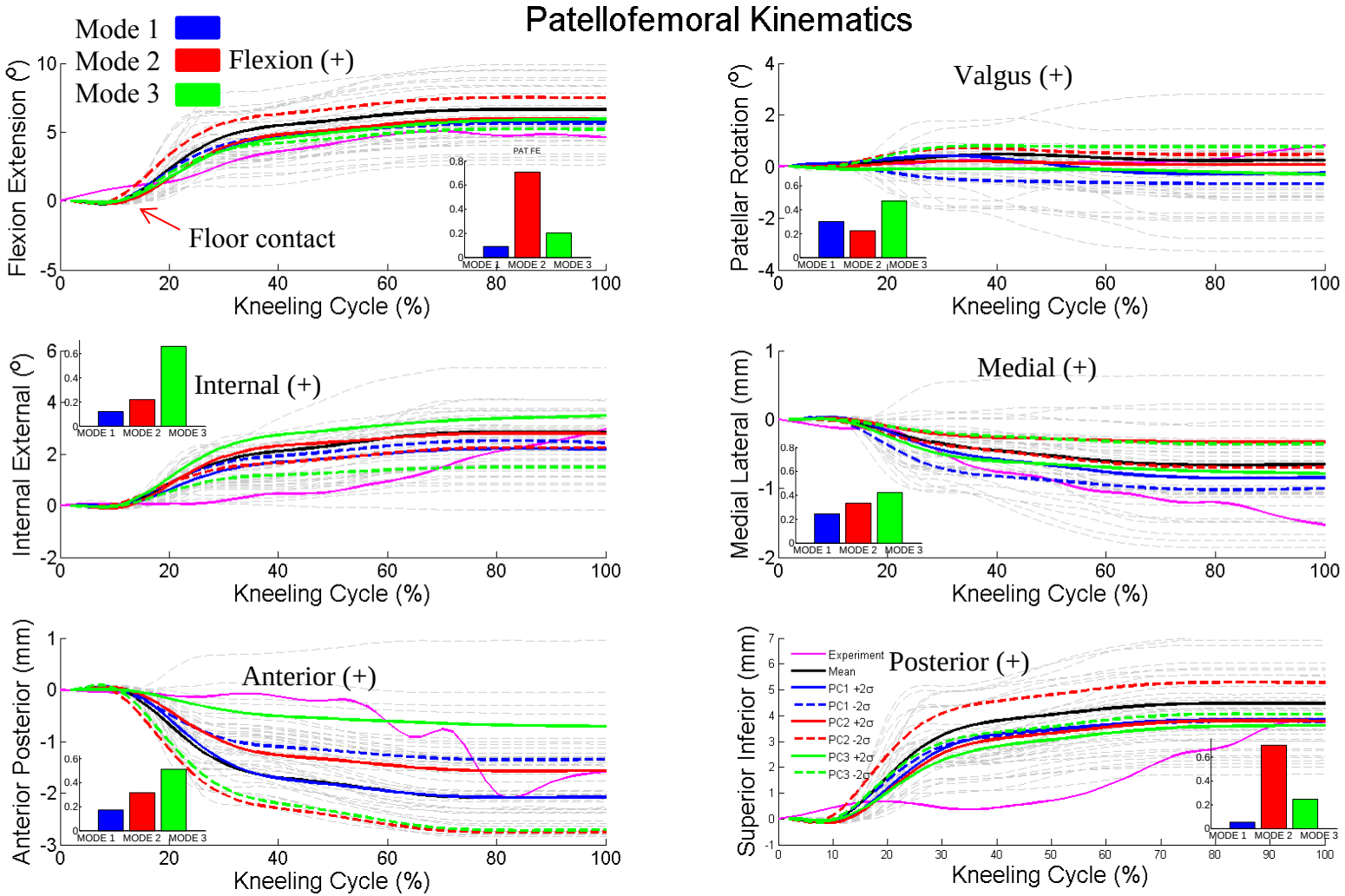

Figure 6.13 Patellofemoral kinematic during kneeling (all six dofs) shown of 40 members of the training set and the first three modes of variations for the shape-function statistical model

Chapter 7. Summary and Recommendations

7.1.Summary

Restoration of knee function and ability to perform activities of daily living is the main goal for most of TKR patients following surgery. In addition, more than half of the patients consider kneeling is the most important activity. Most implants have been designed for basic activities (squat + gait). Computational models provide additional contact mechanics, stress and strain information that is typically not available from experimental simulations. The modeling platform enables implant evaluation for a full suite of activities, including deep flexion and kneeling. The progression of work presented in this dissertation was to develop three-dimensional explicit FE models of natural and implanted to study knee joint kinematics and bone strain using different implants and to build a platform to enable population based evaluation by combining statistical model and joint function.

The FE natural and implanted kneeling models described in the first study (Chapter 4), were of PF joint developed to perform a comparative evaluation of patellofemoral joint mechanics and patellar bone strain distributions in the natural and implanted knee during simulated kneeling in multiple specimens. In the natural patella,

the cartilage and patellar cortical bone distributed the kneeling loads around the periphery of the patella with minimum principal strains centrally in the softer cancellous bone. In the implanted patella, the increased tilt in TKA specimens caused the strain distribution to shift inferiorly in both the flexed and kneeling conditions, resulting in statistically significant differences in inferior and superior highly strained bone volumes. The model predicted a strong reverse linear relationship between highly strained volume and the patellar volume in TKR cases. Unresurfaced patella approach may reduce the likelihood of patellar fracture for smaller patellae. Although this study used one type of implant, it can ultimately provide guidance related to the amount of bone resection to reduce the likelihood of patellar fracture.

The work presented in the second study (Chapter 5) specifically focused on verifying predicted kinematics directly against experimental measurements to provide adequate kinematic validation for specimen-specific knee models. A comparative evaluation among natural and three patellar designs (dome, modified dome, and anatomic) was performed to identify the relationship between joint mechanics (kinematics, contact mechanics and bone strain) and patellar component design during kneeling. The findings showed that increasing the conformity of the patellofemoral articulation reduced peak pressure on the surface of the components, but, in turn, increased strain at the patellar fixation sites. This study also predicted that the medialized dome design achieved the optimal balance between sufficient congruency between PF articular surfaces to obtain reasonable contact mechanics, while still facilitating sagittal

plane tilt to reduce isolated loading of the distal nose of the patella during kneeling. Understanding of the effect of implant design on patellar mechanics during kneeling may ultimately provide guidance to component design that may reduce the likelihood of knee pain and patellar fracture during kneeling.

Given anatomic variability present in the population, it's important to consider how implants will perform in a range of specimens. The main objective of the third study (Chapter 6) was to develop a platform to enable population based evaluation by combining statistical model and joint function. This computational model utilizes PCA to automatically generate FE ready models of whole knee joint (bones, cartilages and ligaments) that commonly requires significant manual effort. Also SSM and FE prediction can provide insight into performance in the populations Anatomy-function relations. SSM-function model characterized the variability in the training set of 40 specimens with a series of modes of variation obtained by using PCA method. 52% of variability was captured in the first three PCA modes and perturbing by $\pm 2\sigma$. This study employed a validated finite element model to characterize relationships between shape, PF kinematics and contact mechanics in high flexion activity such as kneeling. The study predicted that the size of the knee joint has minimal effect on PF joint kinematics but greatly affects joint contact mechanics during kneeling. Interestingly, knee soft tissue dimensions alter the kinematics.

There are several limitations with the work discussed in this dissertation that must be highlighted. The bone strain study although used experimentally validated model, there was consistent kneeling loading applied to each specimen. The bone strain study considered a perfect bonding between the cement-patella interfaces that might decrease the deformation at the fixing sites. All studies did not consider bone remodeling and the strain distributions are accordingly representative of conditions immediately post-operative. The members of the training set used in SSM model were developed from MR images as scanned. Although, SSM model predicted the variability inherited in joint bones and cartilages, the initial alignment of the knee may not represent a realistic soft tissue in controlled space.

7.2. Recommendations

The FE models and methods described in this dissertation have showed progresses in developing and analyzing more realistic daily life activities. To improve validation of PF joint mechanics and patellar bone strain study, Tekscan sensors can be used to measure contact area, and peak contact stress. The SSM model includes an effective generation of soft tissue structures that is able to accurately generate an entire ligament knee model based on a limited set of input parameters. Future work should not only incorporate soft tissue property variability but also the variation in loading conditions for population to improve the robustness of the model predictions.

References

Al-Hadithy, Nawfal, Rozati, Hamoun, Sewell, Mathew D, Dodds, Alex L, Brooks, Peter, & Chatoo, Minhal. (2012). Causes of a painful total knee arthroplasty. Are patients still receiving total knee arthroplasty for extrinsic pathologies? *International Orthopaedics, 36*(6), 1185-1189.

Amis, Andrew A, Senavongse, Wongwit, & Bull, Anthony MJ. (2006). Patellofemoral kinematics during knee flexion-extension: An in vitro study. *Journal of Orthopaedic Research, 24*(12), 2201-2211.

Andriacchi, Thomas P, Yoder, Douglas, Conley, Arthur, Rosenberg, Aaron, Sum, Jeffrey, & Galante, Jorge O. (1997). Patellofemoral design influences function following total knee arthroplasty. *The Journal of Arthroplasty, 12*(3), 243-249.

Atkinson, TS, Haut, RC, & Altiero, NJ. (1997). A poroelastic model that predicts some phenomenological responses of ligaments and tendons. *Journal of Biomechanical Engineering, 119*(4), 400.

Baker, PN, Van der Meulen, JH, Lewsey, J, & Gregg, PJ. (2007). The role of pain and function in determining patient satisfaction after total knee replacement DATA FROM THE NATIONAL JOINT REGISTRY FOR ENGLAND AND WALES. *Journal of Bone & Joint Surgery, British Volume, 89*(7), 893-900.

Baldwin, Mark A, Clary, Chadd, Maletsky, Lorin P, & Rullkoetter, Paul J. (2009). Verification of predicted specimen-specific natural and implanted patellofemoral kinematics during simulated deep knee bend. *Journal of Biomechanics, 42*(14), 2341-2348.

Baldwin, Mark A, Langenderfer, Joseph E, Rullkoetter, Paul J, & Laz, Peter J. (2010). Development of subject-specific and statistical shape models of the knee using an efficient segmentation and mesh-morphing approach. *Computer Methods and Programs in Biomedicine, 97*(3), 232-240.

Baldwin, Mark A, Laz, Peter J, Stowe, Joshua Q, & Rullkoetter, Paul J. (2009). Efficient probabilistic representation of tibiofemoral soft tissue constraint. *Computer Methods in Biomechanics and Biomedical Engineering, 12*(6), 651-659.

Barink, M, Malefijt, M De Waal, Celada, P, Vena, P, Van Kampen, A, & Verdonschot, N. (2008). A mechanical comparison of high-flexion and conventional total knee arthroplasty. *Proceedings of the Institution of Mechanical Engineers, Part H: Journal of Engineering in Medicine, 222*(3), 297-307.

Bayraktar, Harun H, Morgan, Elise F, Niebur, Glen L, Morris, Grayson E, Wong, Eric K, & Keaveny, Tony M. (2004). Comparison of the elastic and yield properties of human femoral trabecular and cortical bone tissue. *Journal of Biomechanics, 37*(1), 27-35.

Blankevoort, L, & Huiskes, R. (1996). Validation of a three-dimensional model of the knee. *Journal of Biomechanics, 29*(7), 955-961.

Brick, Gregory W, & Scott, Richard D. (1988). The patellofemoral component of total knee arthroplasty. *Clinical Orthopaedics and Related Research, 231*, 163-178.

Bryan, Rebecca, Surya Mohan, P, Hopkins, Andrew, Galloway, Francis, Taylor, Mark, & Nair, Prasanth B. (2010). Statistical modelling of the whole human femur

incorporating geometric and material properties. *Medical Engineering & Physics, 32*(1), 57-65.

Chalidis, Byron E, Tsiridis, Eleftherios, Tragas, Adamantios A, Stavrou, Zois, & Giannoudis, Peter V. (2007). Management of periprosthetic patellar fractures: A systematic review of literature. *Injury, 38*(6), 714-724.

Conditt, Michael A, Noble, Philip C, Bertolusso, Roberto, Woody, Joshua, & Parsley, Brian S. (2004). The PCL significantly affects the functional outcome of total knee arthroplasty. *The Journal of Arthroplasty, 19*(7), 107-112.

Conditt, Michael A, Parsley, Brian S., Hullinger, Heidi, Ismaily, Sabir K., Kulkarni, Nikhil, Devers, Branden, . . . Noble, Philip C. (2007). *What Limits Kneeling Following TKA?* Paper presented at the Presented at the Orthopaedic Research Society, ORS®, Vol.53:1860.

Conditt, Michael A, Thompson, MT, Wenk, TJ, Huang, EH, Dawson, J, Ismaily, SK, . . . Noble, PC. (2005). *Cadaveric Simulation of Kneeling.* Paper presented at the 51st Annual Meeting of the Orthopaedic Research Society.

Coughlin, Kathryn M, Incavo, Stephen J, Doohen, Robert R, Gamada, Kazuyoshi, Banks, Scott, & Beynnon, Bruce D. (2007). Kneeling kinematics after total knee arthroplasty: anterior-posterior contact position of a standard and a high-flex tibial insert design. *The Journal of Arthroplasty, 22*(2), 160-165.

Dalury, David F, & Dennis, Douglas A. (2003). Extensor mechanism problems following total knee replacement. *The Journal of Knee Surgery, 16*(2), 118.

Dennis, Douglas A, Komistek, Richard D, Mahfouz, Mohamed R, Outten, Joel T, & Sharma, Adrija. (2005). Mobile-bearing total knee arthroplasty: do the polyethylene bearings rotate? *Clinical Orthopaedics and Related Research, 440*, 88-95.

Devers, Brandon N, Conditt, Michael A, Jamieson, Miranda L, Driscoll, Matthew D, Noble, Philip C, & Parsley, Brian S. (2011). Does greater knee flexion increase patient function and satisfaction after total knee arthroplasty? *The Journal of Arthroplasty, 26*(2), 178-186.

Farahmand, Farzam, Sejiavongse, Wongwit, & Amis, Andrew A. (1998). Quantitative study of the quadriceps muscles and trochlear groove geometry related to instability of the patellofemoral joint. *Journal of Orthopaedic Research, 16*(1), 136-143.

Fitzpatrick, Clare K, Baldwin, Mark A, Ali, Azhar A, Laz, Peter J, & Rullkoetter, Paul J. (2011a). Comparison of patellar bone strain in the natural and implanted knee during simulated deep flexion. *Journal of Orthopaedic Research, 29*(2), 232-239.

Fitzpatrick, Clare K, Baldwin, Mark A, Clary, Chadd W, Wright, Abraham, Laz, Peter J, & Rullkoetter, Paul J. (2012a). Identifying alignment parameters affecting implanted patellofemoral mechanics. *Journal of Orthopaedic Research, 30*(7), 1167-1175.

Fitzpatrick, Clare K, Baldwin, Mark A, Laz, Peter J, FitzPatrick, David P, L Lerner, Amy, & Rullkoetter, Paul J. (2011b). Development of a statistical shape model of the patellofemoral joint for investigating relationships between shape and function. *Journal of Biomechanics, 44*(13), 2446-2452.

Fitzpatrick, Clare K, Kim, Raymond H, Ali, Azhar A, Smoger, Lowell M, & Rullkoetter, Paul J. (2013). Effects of resection thickness on mechanics of resurfaced patellae. *Journal of Biomechanics, 46*(9), 1568–1575.

Fitzpatrick, Clare K, & Rullkoetter, Paul J. (2012b). Influence of patellofemoral articular geometry and material on mechanics of the unresurfaced patella. *Journal of Biomechanics*.

Fukagawa, Shingo, Matsuda, Shuichi, Mizu-uchi, Hideki, Miura, Hiromasa, Okazaki, Ken, & Iwamoto, Yukihide. (2011). Changes in patellar alignment after total knee arthroplasty. *Knee Surgery, Sports Traumatology, Arthroscopy, 19*(1), 99-104.

Galloway, Francis, Seim, Heiko, Kahnt, Max, Nair, Prasanth, Worsley, Peter, & Taylor, Mark. (2012). A large scale finite element study of an osseointegrated cementless tibial tray. *Journal of Bone & Joint Surgery, British Volume, 94*(SUPP XXV), 69-69.

Ghosh, KM, Merican, AM, Iranpour, F, Deehan, DJ, & Amis, Andrew A. (2009). The effect of overstuffing the patellofemoral joint on the extensor retinaculum of the knee. *Knee Surgery, Sports Traumatology, Arthroscopy, 17*(10), 1211-1216.

Godest, AC, Beaugonin, M, Haug, E, Taylor, M, & Gregson, PJ. (2002). Simulation of a knee joint replacement during a gait cycle using explicit finite element analysis. *Journal of Biomechanics, 35*(2), 267-275.

Goldberg, Victor M, Rggie Iii, Harry E, Inglis, Allan E, Figgie, Mark P, Sobel, Mark, Kelly, Michael, & Way, Matthew. (1988). Patellar fracture type and prognosis in condylar total knee arthroplasty. *Clinical Orthopaedics and Related Research, 236*, 115-122.

Goldstein, Wayne M, Gordon, Alexander C, Branson, Jill Jasperson, Simmons, Chris, & Berland, Kimberly A. (2007). Stress over the anterior aspect of the knee with kneeling. *The Journal of Bone & Joint Surgery, 89*(suppl_3), 162-166.

Grace, James N, & Sim, Franklin H. (1988). Fracture of the patella after total knee arthroplasty. *Clinical Orthopaedics and Related Research, 230*, 168-175.

Halloran, Jason P, Easley, Sarah K, Petrella, Anthony J, & Rullkoetter, Paul J. (2005b). Comparison of deformable and elastic foundation finite element simulations for predicting knee replacement mechanics. *Journal of Biomechanical Engineering, 127*(5), 813-818.

Halloran, Jason P, Petrella, Anthony J, & Rullkoetter, Paul J. (2005a). Explicit finite element modeling of total knee replacement mechanics. *Journal of Biomechanics, 38*(2), 323-331.

Hamai, Satoshi, Miura, Hiromasa, Higaki, Hidehiko, Matsuda, Shuichi, Shimoto, Takeshi, Sasaki, Kousuke, . . . Iwamoto, Yukihide. (2008). Kinematic analysis of kneeling in cruciate-retaining and posterior-stabilized total knee arthroplasties. *Journal of Orthopaedic Research, 26*(4), 435-442.

Hanson, George R, Park, Sang E, Suggs, Jeremy F, Moynihan, Angela L, Nha, Kyung W, Freiberg, Andrew A, & Li, Guoan. (2007). In vivo kneeling biomechanics after posterior stabilized total knee arthroplasty. *Journal of Orthopaedic Science, 12*(5), 476-483.

Hassaballa, MA, Artz, Neil, Weale, Adrian, & Porteous, Andrew. (2012). Alteration in skin sensation following knee arthroplasty and its impact on kneeling ability: a comparison of three common surgical incisions. *Knee Surgery, Sports Traumatology, Arthroscopy*, *20*(10), 1983-1987.

Hassaballa, MA, Porteous, AJ, & Newman, JH. (2004). Observed kneeling ability after total, unicompartmental and patellofemoral knee arthroplasty: perception versus reality. *Knee Surgery, Sports Traumatology, Arthroscopy*, *12*(2), 136-139.

Hassaballa, MA, Porteous, AJ, Newman, JH, & Rogers, CA. (2003). Can knees kneel? Kneeling ability after total, unicompartmental and patellofemoral knee arthroplasty. *The Knee*, *10*(2), 155-160.

Hassaballa, MA, Vale, Tom, Weeg, Natalie, & Hardy, John RW. (2002). Kneeling requirements and arthroplasty surgery. *The Knee*, *9*(4), 317-319.

Hayes, WC, Swenson, LW, & Schurman, DJ. (1978). Axisymmetric finite element analysis of the lateral tibial plateau. *Journal of Biomechanics*, *11*(1), 21-33.

Healy, William L, Wasilewski, Stephen A, Takei, Robert, & Oberlander, Michael. (1995). Patellofemoral complications following total knee arthroplasty: correlation with implant design and patient risk factors. *The Journal of Arthroplasty*, *10*(2), 197-201.

Hefzy, MS, Kelly, BP, Cooke, TD, Al-Baddah, AM, & Harrison, L. (1997). Knee kinematics in-vivo of kneeling in deep flexion examined by bi-planar radiographs. *Biomedical Sciences Instrumentation*, *33*, 453.

Helmy, Naeder, Greidanus, Nelson V, & Masri, Bassam A. (2008). To resurface or not to resurface the patella in total knee arthroplasty. *Clinical Orthopaedics and Related Research*, *466*(11), 2775-2783.

Hofer, Jason K, Gejo, Ryuichi, McGarry, Michelle H, & Lee, Thay Q. (2008). Effects of Kneeling on Tibiofemoral Biomechanics in the Native Knee. Paper presented at the *The Orthopaedic Research Society*, ORS®, Vol.33, P:1267-2008.

Hofer, Jason K, Gejo, Ryuichi, McGarry, Michelle H, & Lee, Thay Q. (2011). Effects on tibiofemoral biomechanics from kneeling. *Clinical Biomechanics*, *26*(6), 605-611.

Hofmann, Aaron A, Tkach, Thomas K, Evanich, Christopher J, Camargo, Marcelo P, & Zhang, Yongde. (1997). Patellar component medialization in total knee arthroplasty. *The Journal of Arthroplasty*, *12*(2), 155-160.

Huang, Chang-Hung, Liau, Jiann-Jong, Huang, Chun-Hsiung, & Cheng, Cheng-Kung. (2006). Influence of post-cam design on stresses on posterior-stabilized tibial posts. *Clinical Orthopaedics and Related Research*, *450*, 150-156.

Incavo, Stephen J, Mullins, Eric R, Coughlin, Kathryn M, Banks, Scott, Banks, Anne, & Beynnon, Bruce D. (2004). Tibiofemoral kinematic analysis of kneeling after total knee arthroplasty. *The Journal of Arthroplasty*, *19*(7), 906-910.

Innocenti, B., Labey, L., Victor, J., Wong, P., & Bellemans, J. (2009). An in-vitro study of the human knee kinematics: Natural vs. replaced joint. *ECIFMBE 2008, IFMBE Proceedings 22*, 1867–1870.

Insall, John, & Salvati, Eduardo. (1971). Patella position in the normal knee joint. *Radiology*, *101*(1), 101-104.

Ismaily, S., Maheshwari, R., Conditt, M., Hullinger, H., Holden, C., Kulkarni, N., & Noble, P. (2006). *Kneeling Discomfort after Total Knee Arthroplasty*. Paper presented at the Orthopaedic Research Society, ORS®, Vol.31, P:0274

Jolliffe, Ian T. (2002). *Principal component analysis*: Springer verlag.

Jujo, Yasuyuki, Yasui, Tetsuro, Nagase, Yuichi, Kadono, Yuho, Oka, Hiroyuki, & Tanaka, Sakae. (2012). Patellar Fracture After Total Knee Arthroplasty for Rheumatoid Arthritis. *The Journal of Arthroplasty*.

Kallemeyn, Nicole A, Shivanna, Kiran H, DeVries, Nicole A, Kode, Swathi, Gandhi, Anup A, Fredericks, Douglas C, . . . Grosland, Nicole M. (2012). Advancements in Spine FE Mesh Development: Toward Patient-Specific Models *Patient-Specific Modeling in Tomorrow's Medicine* (pp. 75-101): Springer.

Kanekasu, Kouichi, Banks, Scott A, Honjo, Shigeru, Nakata, Osanari, & Kato, Hiromi. (2004). Fluoroscopic analysis of knee arthroplasty kinematics during deep flexion kneeling. *The Journal of Arthroplasty, 19*(8), 998-1003.

Keller, Tony S. (1994). Predicting the compressive mechanical behavior of bone. *Journal of Biomechanics, 27*(9), 1159-1168.

Keyak, JH, & Skinner, HB. (1992). Three-dimensional finite element modelling of bone: effects of element size. *Journal of Biomechanical Engineering, 14*(6), 483-489.

Kim, Tae Kyun, Kwon, Sae Kwang, Kang, Yeon Gwi, Chang, Chong Bum, & Seong, Sang Cheol. (2010). Functional disabilities and satisfaction after total knee arthroplasty in female Asian patients. *The Journal of Arthroplasty, 25*(3), 458-464. e452.

Komistek, Richard D, Dennis, Douglas A, & Mahfouz, Mohamed. (2003). In vivo fluoroscopic analysis of the normal human knee. *Clinical Orthopaedics and Related Research, 410*, 69-81.

Kopperdahl, David L, & Keaveny, Tony M. (1998). Yield strain behavior of trabecular bone. *Journal of Biomechanics, 31*(7), 601-608.

Kurtz, Steven, Ong, Kevin, Lau, Edmund, Mowat, Fionna, & Halpern, Michael. (2007). Projections of primary and revision hip and knee arthroplasty in the United States from 2005 to 2030. *The Journal of Bone & Joint Surgery, 89*(4), 780-785.

Laz, Peter J, Stowe, Joshua Q, Baldwin, Mark A, Petrella, Anthony J, & Rullkoetter, Paul J. (2007). Incorporating uncertainty in mechanical properties for finite element-based evaluation of bone mechanics. *Journal of Biomechanics, 40*(13), 2831-2836.

Le, Anh X, Cameron, HU, Otsuka, NY, Harrington, IJ, & Bhargava, M. (1999). Fracture of the patella following total knee arthroplasty. *Orthopedics, 22*(4), 395.

Lee, Jackson, & Franzino, Stephen J. (1999). Patellar fractures and extensor mechanism injuries. *Current Opinion in Orthopaedics, 10*(1), 22-26.

Li, Guoan, Zayontz, Shay, DeFrate, Louis E, Most, Ephrat, Suggs, Jeremy F, & Rubash, Harry E. (2004). Kinematics of the knee at high flexion angles: an in vitro investigation. *Journal of Orthopaedic Research, 22*(1), 90-95.

Li, Wendy, Anderson, Donald D, Goldsworthy, Jane K, Marsh, J Lawrence, & Brown, Thomas D. (2008). Patient-specific finite element analysis of chronic contact

stress exposure after intraarticular fracture of the tibial plafond. *Journal of Orthopaedic Research, 26*(8), 1039-1045.
Lie, DTT, Gloria, N, Amis, AA, Lee, BPH, Yeo, SJ, & Chou, SM. (2005). Patellar resection during total knee arthroplasty: effect on bone strain and fracture risk. *Knee Surgery, Sports Traumatology, Arthroscopy, 13*(3), 203-208.
Lin, Kun-Jhih, Huang, Chang-Hung, Liu, Yu-Liang, Chen, Wen-Chuan, Chang, Tsung-Wei, Yang, Chan-Tsung, . . . Cheng, Cheng-Kung. (2011). Influence of post-cam design of posterior stabilized knee prosthesis on tibiofemoral motion during high knee flexion. *Clinical Biomechanics, 26*(8), 847-852.
MacCollum, 3rdMS, & Karpman, RR. (1989). Complications of the PCA anatomic patella. *Orthopedics, 12*(11), 1423.
Mahfouz, MR, Fatah, EE Abdel, LS, Bowers, & Scuderi, G. (2012). Three-dimensional morphology of the knee reveals ethnic differences. *Clinical Orthopaedics and Related Research®, 470*(1), 172-185. doi: 10.1007/s11999-011-2089-2
McLain, Robert F, & Bargar, William L. (1985). Patellar Strain in Three Models of Total Knee Prothesis. *The Iowa Orthopaedic Journal, 5*, 92.
Meding, John B, Fish, Mark D, Berend, Michael E, & Ritter, Merrill A. (2008). Predicting patellar failure after total knee arthroplasty. *Clinical Orthopaedics and Related Research, 466*(11), 2769-2774.
Mensch, Joseph S, & Amstutz, HC. (1975). Knee morphology as a guide to knee replacement. *Clinical Orthopaedics and Related Research*(112), 231.
Morra, Edward A, & Greenwald, A Seth. (2005). Polymer insert stress in total knee designs during high-flexion activities: a finite element study. *The Journal of Bone & Joint Surgery, 87*(suppl_2), 120-124.
Nagura, Takeo, Otani, Toshiro, Suda, Yasunori, Matsumoto, Hideo, & Toyama, Yoshiaki. (2005). Is high flexion following total knee arthroplasty safe?: evaluation of knee joint loads in the patients during maximal flexion. *The Journal of Arthroplasty, 20*(5), 647-651.
Nakamura, Eiichi, Banks, SA, Tanaka, Azusa, Sei, Akira, & Mizuta, Hiroshi. (2009). Three-dimensional tibiofemoral kinematics during deep flexion kneeling in a mobile-bearing total knee arthroplasty. *The Journal of Arthroplasty, 24*(7), 1120-1124.
Nijs, Jo, Van Geel, Catherine, & Van de Velde, Bart. (2006). Diagnostic value of five clinical tests in patellofemoral pain syndrome. *Manual therapy, 11*(1), 69-77.
Noble, Philip C, Conditt, Michael A, Cook, Karon F, & Mathis, Kenneth B. (2006). The John Insall Award: Patient Expectations Affect Satisfaction with Total Knee Arthroplasty. *Clinical Orthopaedics & Related Research, 452*, 35-43.
Noble, Philip C, Gordon, Michael J, Weiss, Jennifer M, Reddix, Robert N, Conditt, Michael A, & Mathis, Kenneth B. (2005). Does total knee replacement restore normal knee function? *Clinical Orthopaedics and Related Research, 431*, 157-165.
Ortiguera, Cedric J, & Berry, Daniel J. (2002). Patellar fracture after total knee arthroplasty. *The Journal of Bone & Joint Surgery, 84*(4), 532-540.

Palastanga, Nigel, Field, Derek, & Soames, Roger. (2006). *Anatomy and human movement: structure and function* (Vol. 20056): Butterworth-Heinemann.

Palmer, SH, Servant, CT, Maguire, J, Parish, EN, & Cross, MJ. (2002). Ability to kneel after total knee replacement. *Journal of Bone & Joint Surgery, British Volume, 84*(2), 220-222.

Park, Kwan Kyu, Shin, Kwang Sook, Chang, Chong Bum, Kim, Sung Ju, & Kim, Tae Kyun. (2007). Functional disabilities and issues of concern in female Asian patients before TKA. *Clinical Orthopaedics and Related Research, 461*, 143-152.

Pena, E, Calvo, B, Martinez, MA, & Doblare, M. (2006). A three-dimensional finite element analysis of the combined behavior of ligaments and menisci in the healthy human knee joint. *Journal of Biomechanics, 39*(9), 1686-1701.

Peng, Liang, Bai, Jing, Zeng, Xiaoli, & Zhou, Yongxin. (2006). Comparison of isotropic and orthotropic material property assignments on femoral finite element models under two loading conditions. *Medical Engineering & Physics, 28*(3), 227-233.

Perillo-Marcone, A, ., & Taylor, M. (2007). Effect of varus/valgus malalignment on bone strains in the proximal tibia after TKR: an explicit finite element study. *Journal of Biomechanical Engineering, 129*(1), 1.

Querol, Laura Belenguer, Büchler, Philippe, Rueckert, Daniel, Nolte, Lutz P, & Ballester, Miguel Á González. (2006). Statistical finite element model for bone shape and biomechanical properties *Medical Image Computing and Computer-Assisted Intervention–MICCAI 2006* (pp. 405-411): Springer.

Ramos, A, & Simoes, JA. (2006). Tetrahedral versus hexahedral finite elements in numerical modelling of the proximal femur. *Medical Engineering & Physics, 28*(9), 916-924.

Rand, JA, & Gustilo, B. (1996). Comparison of inset and resurfacing patellar prostheses in total knee arthroplasty. *Acta orthopaedica Belgica, 62*, 154.

Rao, Chandreshwar, Fitzpatrick, Clare K, Rullkoetter, Paul J, Maletsky, Lorin P, Kim, Raymond H, & Laz, Peter J. (2013). A statistical finite element model of the knee accounting for shape and alignment variability. *Medical Engineering & Physics*.

Reuben, Jeffrey D, McDonald, Craig L, Woodard, Peggy L, & Hennington, Linda J. (1991). Effect of patella thickness on patella strain following total knee arthroplasty. *The Journal of Arthroplasty, 6*(3), 251-258.

Rhoads, Daniel D, Noble, Philip C, Reuben, Jeffrey D, Mahoney, Ormonde M, & Tullos, Hugh S. (1990). The effect of femoral component position on patellar tracking after total knee arthroplasty. *Clinical Orthopaedics and Related Research, 260*, 43-51.

Ritter, Merrill A, Pierce, Michael J, Zhou, Hongling, Meding, John B, Faris, Philip M, & Keating, E Michael. (1999). Patellar complications (total knee arthroplasty) Effect of lateral release and thickness. *Clinical Orthopaedics and Related Research, 367*, 149-157.

Schai, PA, Gibbon, AJ, & Scott, RD. (1999). Kneeling ability after total knee arthroplasty: perception and reality. *Clinical Orthopaedics and Related Research, 367*, 195-200.

Schileo, Enrico, Taddei, Fulvia, Cristofolini, Luca, & Viceconti, Marco. (2008). Subject-specific finite element models implementing a maximum principal strain criterion are able to estimate failure risk and fracture location on human femurs tested *in-vitro*. *Journal of Biomechanics, 41*(2), 356-367.

Shafi, Mohamed, Kim, Young Yul, Lee, Yeon Soo, Kim, Jin Young, & Han, Chang Whan. (2005). Patellar polyethylene peg fracture: a case report and review of the literature. *Knee Surgery, Sports Traumatology, Arthroscopy, 13*(6), 472-475.

Sharkey, Peter F, & Miller, Andrew J. (2011). Noise, numbness, and kneeling difficulties after total knee arthroplasty: is the outcome affected? *The Journal of Arthroplasty, 26*(8), 1427-1431.

Singh, Jasvinder A, Jensen, Matthew, & Lewallen, David. (2013). Predictors of periprosthetic fracture after total knee replacement: An analysis of 21,723 cases. *Acta Orthopaedica, 84*(2), 1-8.

Snyder-Macker L., & M., Lewek. (2005). "The Knee" in; Levangie P, Norkin C. "Joint Structure and Function: A Comprehensive Analysis" 4th ed. Philadelphia, PA: FA Davis Co : 393-431.

Star, Michael J, Kaufman, Kenton R, Irby, Steven E, & Colwell Jr, Clifford W. (1996). The effects of patellar thickness on patellofemoral forces after resurfacing. *Clinical Orthopaedics and Related Research, 322*, 279-284.

Stäubli, Hans U, Schatzmann, Lukas, Brunner, Peter, Rincón, Liliana, & Nolte, Lutz-P. (1999). Mechanical tensile properties of the quadriceps tendon and patellar ligament in young adults. *The American Journal of Sports Medicine, 27*(1), 27-34.

Stiehl, James B, Komistek, RD, Dennis, DA, Paxson, RD, & Hoff, WA. (1995). Fluoroscopic analysis of kinematics after posterior-cruciate-retaining knee arthroplasty. *Journal of Bone & Joint Surgery, British Volume, 77*(6), 884-889.

Stiehl, James B, Komistek, Richard D, Dennis, Douglas A, & Keblish, Peter A. (2001). Kinematics of the patellofemoral joint in total knee arthroplasty. *The Journal of Arthroplasty, 16*(6), 706-714.

Suggs, Jeremy, Wang, Conrad, & Li, Guoan. (2003). The effect of graft stiffness on knee joint biomechanics after ACL reconstruction—a 3D computational simulation. *Clinical Biomechanics, 18*(1), 35-43.

Taddei, Fulvia, Cristofolini, Luca, Martelli, Saulo, Gill, HS, & Viceconti, Marco. (2006). Subject-specific finite element models of long bones: an in vitro evaluation of the overall accuracy. *Journal of Biomechanics, 39*(13), 2457-2467.

Taddei, Fulvia, Schileo, Enrico, Helgason, Benedikt, Cristofolini, Luca, & Viceconti, Marco. (2007). The material mapping strategy influences the accuracy of CT-based finite element models of bones: an evaluation against experimental measurements. *Medical Engineering & Physics, 29*(9), 973-979.

Taylor, Mark, Bryan, Rebecca, & Galloway, Francis. (2013). Accounting for patient variability in finite element analysis of the intact and implanted hip and knee: A review. *International Journal for Numerical Methods in Biomedical Engineering, 29*(2), 273-292.

Thambyah, Ashvin, Goh, James CH, & De, Shamal Das. (2005). Contact stresses in the knee joint in deep flexion. *Medical Engineering & Physics, 27*(4), 329-335.

Theiss, Steven M, Kitziger, Kurt J, Lotke, Pamela S, & Lotke, Paul A. (1996). Component design affecting patellofemoral complications after total knee arthroplasty. *Clinical Orthopaedics and Related Research, 326*, 183-187.

Tria Jr, Alfred J, Harwood, David A, Alicea, Jose A, & Cody, Ronald P. (1994). Patellar fractures in posterior stabilized knee arthroplasties. *Clinical Orthopaedics and Related Research, 299*, 131-138.

Walker, PS, VC, Mow, & eds, Huiskes R. (2005). *"Biomechanics of total knee replacement designs". In: Mow VC, Huiskes R eds. "Basic Orthopaedic Biomechanics and Mechano-biology".* : Lippincott Williams & Wilkins.

Weiss, Jennifer M, Noble, Philip C, Conditt, Michael A, Kohl, Harold W, Roberts, Seth, Cook, Karon F, . . . Mathis, Kenneth B. (2002). What functional activities are important to patients with knee replacements? *Clinical Orthopaedics and Related Research, 404*, 172-188.

Wilkens, Kenneth J, Duong, L V, McGarry, M H, Kim, W C, Skinner, H B, & Lee, T Q. (2005). Kneeling at High Knee Flexion Angles after Total Knee Arthroplasty Does Not Affect Patellofemoral Joint Contact Area And Pressure. Paper presented at the *The Orthopaedic Research Society*, ORS®, Vol 30:1247-2005.

Wilkens, Kenneth J, Duong, Long V, McGarry, Michelle H, Kim, William C, & Lee, Thay Q. (2007). Biomechanical effects of kneeling after total knee arthroplasty. *The Journal of Bone & Joint Surgery, 89*(12), 2745-2751.

Windsor, Russell E, Scuderi, Giles R, & Insall, John N. (1989). Patellar fractures in total knee arthroplasty. *The Journal of Arthroplasty, 4*, S63-S67.

Wulff, Warren, & Incavo, Stephen J. (2000). The effect of patella preparation for total knee arthroplasty on patellar strain. *The Journal of Arthroplasty, 15*(6), 778-782.

Yang, Zhaochun, Wickwire, Alexis C, & Debski, Richard E. (2010). Development of a subject-specific model to predict the forces in the knee ligaments at high flexion angles. *Medical & Biological Engineering & Computing, 48*(11), 1077-1085.

Zelle, Jorrit, Janssen, Dennis, Van Eijden, Jolanda, De Waal Malefijt, Maarten, & Verdonschot, Nico. (2011). Does high-flexion total knee arthroplasty promote early loosening of the femoral component? *Journal of Orthopaedic Research, 29*(7), 976-983.